BUKTI KORESPONDENSI

ARTIKEL JURNAL INTERNASIONAL BEREPUTASI

Judul artikel	:	Feasibility study of nanocrystalline cellulose as adsorbent of steryl glucosides from palm-based biodiesel
Jurnal	:	Renewable Energy (Elsevier, Q1, impact factor: 9.0)
Penulis	:	Liangna Widdyaningsih (*first author*) Albert Setiawan Shella Permatasari Santoso Felycia Edi Soetaredjo Suryadi Ismadji Sandy Budi Hartono Yi-Hsu Ju Phuong Lan Tran-Nguyen Maria Yuliana (*corresponding author*)

No	Perihal	Tanggal
1	Bukti konfirmasi submit artikel dan artikel yang disubmit	16 Oktober 2019
2	Bukti konfirmasi review dan hasil review pertama	11 Januari 2020
3	Bukti konfirmasi submit revisi pertama, respon kepada reviewer, dan artikel yang diresubmit	3 Februari 2020
4	Bukti konfirmasi artikel accepted	1 Maret 2020
5	Bukti artikel published	PDF

Gmail

Maria Yuliana <mariayuliana@ukwms.ac.id>

Submission Confirmation

1 message

Renewable Energy <eesserver@eesmail.elsevier.com> Wed, Oct 16, 2019 at 2:42 PM
Reply-To: Renewable Energy <rene@elsevier.com>
To: mariayuliana@ukwms.ac.id, maria_yuliana_liauw@yahoo.com
Cc: liangna16@gmail.com, albert.st12@gmail.com, shella_p5@yahoo.com, felyciae@yahoo.com, sandy@ukwms.ac.id, tnplan@ctu.edu.vn, suryadiismadji@yahoo.com, yhju@mail.ntust.edu.tw

*** Automated email sent by the system ***

Ms. Ref. No.:
Title: FEASIBILITY STUDY OF NANOCRYSTALLINE CELLULOSE AS ADSORBENT OF STERYL GLUCOSIDES FROM PALM-BASED BIODIESEL
Article Type: Research Paper
Journal: Renewable Energy

Dear Dr. Maria Yuliana,

We have received your article "FEASIBILITY STUDY OF NANOCRYSTALLINE CELLULOSE AS ADSORBENT OF STERYL GLUCOSIDES FROM PALM-BASED BIODIESEL" for consideration for publication in Renewable Energy.

Your manuscript will be given a reference number once an editor has been assigned.

To track the status of your paper, please do the following:

1. Go to this URL: https://ees.elsevier.com/rene/

2. Enter these login details:
Your username is: mariayuliana@ukwms.ac.id
If you need to retrieve password details, please go to:
http://ees.elsevier.com/rene/automail_query.asp

3. Click [Author Login]
This takes you to the Author Main Menu.

4. Click [Submissions Being Processed]

Our reviewers will endeavour to review your paper at the earliest opportunity although it may take several weeks to let you know the outcome. Thank you for your patience.

Thank you for your interest in Renewable Energy.

Kind regards,

Elsevier Editorial System
Renewable Energy

****
Please note that the editorial process varies considerably from journal to journal. To view a sample editorial process, please click here:
http://help.elsevier.com/app/answers/detail/p/7923/a_id/160

For further assistance, please visit our customer support site at http://help.elsevier.com/app/answers/list/p/7923. Here you can search for solutions on a range of topics, find answers to frequently asked questions and learn more about EES via interactive tutorials. You will also find our 24/7 support contact details should you need any further assistance from one of

our customer support representatives.

Elsevier Editorial System(tm) for Renewable Energy

Manuscript Draft

Manuscript Number:

Title: FEASIBILITY STUDY OF NANOCRYSTALLINE CELLULOSE AS ADSORBENT OF STERYL GLUCOSIDES FROM PALM-BASED BIODIESEL

Article Type: Research Paper

Keywords: biodiesel; steryl glucosides removal; nanocrystalline cellulose; adsorption isotherm; adsorption mechanism; feasibility study

Corresponding Author: Dr. Maria Yuliana, Ph.D.

Corresponding Author's Institution: Widya Mandala Catholic University Surabaya

First Author: Liangna Widdyaningsih

Order of Authors: Liangna Widdyaningsih; Albert Setiawan; Shella P Santoso, Ph.D.; Felycia E Soetaredjo, Ph.D.; Suryadi Ismadji, Ph.D.; Sandy B Hartono, Ph.D.; Yi-Hsu Ju, Ph.D.; Phuong Lan Tran-Nguyen, Ph.D.; Maria Yuliana, Ph.D.

Abstract: Increasing the content of biodiesel in the diesel fuel mixture faces some challenges due to the presence of steryl glucosides (SG) compounds, which causes the filter clogging and the reduction of engine power. In this study, coarse filter paper-based nanocrystalline cellulose (CFP-based NCC) with the crystallinity of 65.64% is selected as a potential adsorbent to separate SG compounds in palm-based biodiesel (PO-B100). The adsorption experiments were carried out at various CFP-based NCC to PO-B100 mass ratio (1:50, 1:75, 1:100, 1:125, 1:150, 1:175, 1:200) and temperature (65, 75, 85°C). The maximum SG removal was 91.81%, obtained at 75°C for CFP-based NCC to PO-B100 mass ratio of 1:50. The adsorption treatment also improves the cold stability of PO-B100 by reducing the cloud point from 13.2°C to 11.5°C. Langmuir isotherm model is best-fitted to the equilibrium adsorption data and thermodynamic studies suggested that the adsorption of SG onto the CFP-based NCC surface is spontaneous and endothermic. The isotherm and thermodynamic study showed that the mechanism governing the adsorption process may be driven by both dipole-dipole interactions and ion exchange. The adsorption results showed that CFP-based NCC has great affinity and selectivity to SG and can be considered as a promising adsorbent of SG.

Suggested Reviewers: Lucian Lucia
lalucia@ncsu.edu

Mamata Mohapatra
mamatamohapatra@yahoo.com

Noureddine Abidi
noureddine.abidi@ttu.edu

*Title Page

FEASIBILITY STUDY OF NANOCRYSTALLINE CELLULOSE AS ADSORBENT OF STERYL GLUCOSIDES FROM PALM-BASED BIODIESEL

Liangna Widdyaningsih[a,1], Albert Setiawan[a,1], Shella Permatasari Santoso[1,2], Felycia Edi Soetaredjo[1,2], Suryadi Ismadji[1,2], Sandy Budi Hartono[1], Yi-Hsu Ju[2,3,4], Phuong Lan Tran-Nguyen[5], Maria Yuliana[1,*]

[1] Department of Chemical Engineering, Widya Mandala Catholic University Surabaya, Kalijudan 37, Surabaya 60114, Indonesia

[2] Department of Chemical Engineering, National Taiwan University of Science and Technology, 43 Keelung Road, Sec 4, Taipei, 10607, Taiwan

[3] Graduate Institute of Applied Science and Technology, National Taiwan University of Science and Technology, 43 Keelung Road, Sec 4, Taipei, 10607, Taiwan

[4] Taiwan Building Technology Center, National Taiwan University of Science and Technology, 43 Keelung Road, Sec 4, Taipei, 10607, Taiwan

[5] Department of Mechanical Engineering, Can Tho University, 3-2 Street, Can Tho City, Vietnam

*Corresponding authors: Tel. (62) 31 3891264; Fax. (62) 31 3891267; Email address: mariayuliana@ukwms.ac.id (M. Yuliana)

[a] These authors contributed equally to this work

ABSTRACT

Increasing the content of biodiesel in the diesel fuel mixture faces some challenges due to the presence of steryl glucosides (SG) compounds, which causes the filter clogging and the reduction of engine power. In this study, coarse filter paper-based nanocrystalline cellulose (CFP-based NCC) with the crystallinity of 65.64% is selected as a potential adsorbent to separate SG compounds in palm-based biodiesel (PO-B100). The adsorption experiments were carried out at various CFP-based NCC to PO-B100 mass ratio (1:50, 1:75, 1:100, 1:125, 1:150, 1:175, 1:200) and temperature (65, 75, 85°C). The maximum SG removal was 91.81%, obtained at 75°C for CFP-based NCC to PO-B100 mass ratio of 1:50. The adsorption treatment also improves the cold stability of PO-B100 by reducing the cloud point from 13.2°C to 11.5°C. Langmuir isotherm model is best-fitted to the equilibrium adsorption data and thermodynamic studies suggested that the adsorption of SG onto the CFP-based NCC surface is spontaneous and endothermic. The isotherm and thermodynamic study showed that the mechanism governing the adsorption process may be driven by both dipole-dipole interactions and ion exchange. The adsorption results showed that CFP-based NCC has great affinity and selectivity to SG and can be considered as a promising adsorbent of SG.

Keywords: biodiesel; steryl glucosides removal; nanocrystalline cellulose; adsorption isotherm; adsorption mechanism; feasibility study

1. INTRODUCTION[1]

To date, Indonesia still depends on fossil fuel as an energy source with petroleum as the most common fossil fuel. Based on the data from the Ministry of Energy and Mineral Resources, Indonesia still possesses around 9 billion barrels of crude oil reserves. Petroleum diesel is commonly used for transportation and industries, which covers up to 40% of the total fuel for transportation sector and 74% for industrial and power plant sectors. With the average production rate of 500 million barrels per year, these supplies will completely run out in the next two decades [1]. Therefore, it is necessary to develop alternative fuels that are environmentally friendly, especially as a substitute for diesel fuel.

Of the several alternative fuels available, biodiesel is an alternative diesel fuel made from renewable biological resources [2]. Biodiesel is generally derived from transesterification of agricultural or animal lipids and short-chain alcohols in the presence of a catalyst. The Indonesia government started to commercialize palm-based biodiesel (PO-B100) as B-20 in 2016, which requires mixing 20% vol. of PO-B100 with diesel fuel. While PO-B100 is currently mass-produced, the cold is still a challenge for its manufacturers. Although PO-B100 distributed around the country must conform to the fuel property specifications as controlled by ASTM D6751 and Indonesia National Standard (SNI)

---

[1] **Abbreviation**

SG	Steryl glucoside(s)
MG	Monoacylglyceride(s)
DG	Diacylglyceride(s)
TG	Triacylglyceride(s)
CFP	Coarse filter paper
NCC	Nanocrystalline cellulose
FAME	Fatty Acid Methyl Ester(s)

7182:2015, white precipitates were often detected in PO-B100 and its blends during storage [3]. Several cases even showed that suspended particles in PO-B100 have been found shortly after the production and at a rather high temperature (slightly below 60°C) [4]. The white precipitates may cause filter plugging in engine systems [4,5]. This phenomenon was also observed in many biodiesel plants and hence frequent maintenance and process modification is often essential to maintain plant effectiveness and efficiency.

The presence of steryl glucosides (SG), which is one of the plant sterols, has been identified as the major component of the white precipitates. It mostly presents in biodiesel with a concentration of 35 ppm or higher [6]. The existence of this dispersed particles of SG promotes the aggregation of other components in biodiesel, saturated monoacylglycerides (MG) and diacylglycerides (DG), and subsequently affects the cold flow stability of fuel and widespread use [7].

Several techniques have been conducted to minimize the SG content in the biodiesel product, namely enzymatic hydrolysis [8,9], adsorption using magnesium silicate and bleaching earth [7] and ultrafiltration [10]. SG removal by enzymatic hydrolysis resulted in 81% removal efficiency with the addition of a synthetic codon-optimized version of the LacS gene expressed from *E. coli* with the total operating time of 7 h [8]. Na-Ranong et al. (2015) reported that the conventional adsorption using magnesium silicate and bleaching earth in temperature of 65-80°C yielded in 81.4-82.5% removal efficiency of SG [7]. Tremblay and Montpetit (2017) stated that the highest separation for SG (86%) by ultrafiltration was obtained when the biodiesel was transesterified using 0.7% (w/w) catalyst and 4:1 methanol : soybean oil molar ratio [10]. Based on the removal efficiency and economic feasibility, the adsorption treatment is a potential method to reduce SG content as well as to improve the cold flow properties of the fuel in the industrial scale because it is found to be effective and facile, time-saving and energy-efficient.

The development of adsorbent for effective adsorption has been conducted using various types of materials. Currently, the development of cellulosic adsorbent received major interest because it is renewable, biodegradable, low cost, and non-toxic [11]. Cellulosic adsorbents have the ability to meet the requirement of being a biosorbent, as it is abundantly available as natural biopolymer. Cellulose in the form of nanocrystalline cellulose (NCC) has been widely studied due to its extensive industrial application, namely enzyme immobilization, adsorption, catalysis, drug delivery, biosensors and bio-imaging [12]. NCC, with a large specific surface area and plenty of surface hydroxyl and anionic sulfate ester group for physical and chemical reactions [13–15], can be considered as a new promising adsorbent for SG removal.

As the government plans to increase the use of PO-B100 in diesel blend to B30 in the time span of 5 years, the use of CFP-based NCC for SG removal and improvement of the cold stability is an interesting topic to be studied. The objective of this study is to observe the feasibility of CFP-based NCC as the adsorption agent for SG. Various operating parameters, namely temperature, and the mass ratio of CFP-based NCC to PO-B100 will be monitored. The adsorption mechanism was also proposed based on the isotherm and thermodynamics study.

2. MATERIALS AND METHODS

2.1 Materials

PO-B100 was collected from a local palm oil manufacturer in Gresik, Indonesia, and stored for 3 days at room temperature prior to adsorption experiment. Coarse filter paper (CFP) as the cellulosic material was obtained from a local supplier in Surabaya, Indonesia. Sulphuric acid, sodium hydroxide, ethyl acetate, and n-hexane were purchased from Merck, Germany. FAMEs standard 47885 U contains 37 components FAME mix and SG standard

1117 were procured from Supelco (Bellefonte, PA, USA) and Matreya (State College, PA, USA), respectively. Nitrogen gas (99.9% purity) was purchased from Aneka Gas Industry Pty. Ltd., Surabaya. All reagents were of analytical grade and required no further purification.

2.2 Preparation of NCC

CFP was ground into fibrous powder before use. The non-cellulosic material of CFP was subsequently removed to obtain purified cellulose using the following method: 12 grams of the CFP powder was delignified using 0.1 g/ml sodium hydroxide aqueous solution. The delignified product was washed with distilled water and filtrated three times before being dried under vacuum at 80°C for 12 hours.

CFP-based NCC was prepared by using acid hydrolysis following the modified method of Putro et al. (2017) [16]. 1 gram of delignified cellulose was hydrolyzed with 20 ml sulphuric acid 64% at 45°C for 75 min under constant agitation. The reaction time was selected to ensure high reaction efficiency. After the specified duration, the reaction was immediately quenched using 20-fold of cold distilled water. The suspension was centrifuged at 4500 rpm for 10 min to remove the excess acid solution. The resulting precipitates were dialyzed against distilled water until neutral pH was achieved. The colloidal suspension was subjected to sonication treatment for 30 min in a cooling bath to avoid overheating and subsequently subjected to vacuum drying at 80°C for 6 h to obtain CFP-based NCC powder.

2.3 Characterization of CFP-based NCC

The surface morphologies of the CFP-based NCC particles were analyzed on a field emission scanning electron microscope (FESEM) JEOL JSM-6500F (Jeol Ltd., Japan), with an accelerating voltage of 5 – 10 kV and 9.5 – 9.6 mm working distance. The CFP-based NCC powder was attached to a stub, sputtered and coated with gold prior to analysis. Fourier

Transform Infrared (FTIR) analysis was performed by an FTIR-8400S spectrophotometer (Shimadzu, Japan) in the range of 400 – 4000 cm^{-1} at a 4 cm^{-1} scanning resolution. XRD analysis was conducted by an X'PERT Panalytical Pro X-Ray diffractometer (Philips-FEI, Netherlands) with monochromatic Cu $K\alpha_1$ radiation at wavelength (λ) = 0.154 nm, 40 kV of voltage and 30 mA of tube current. The diffraction pattern was acquired in the range of 5° to 60° (2θ angle). The crystallinity index (CrI) was expressed according to the following equation, as proposed by Segal et al. (1959) [17].

$$\mathrm{CrI}\ (\%) = \frac{(I_{200} - I_{am})}{I_{200}} x100 \qquad (1)$$

Where I_{200} is the maximum intensity of the crystalline region at 2θ = 22 – 23°, I_{am} is the maximum intensity of the amorphous region at 2θ = 15 – 17°. The crystallite size (nm) was calculated using the Scherrer analysis.

2.4 Compositional study of SG in PO-B100 using GC-FID analysis

The analysis of SG composition in PO-B100 was carried out using GC-17A (Shimadzu, Japan), completely equipped with a split/splitless injector and a flame ionization detector (FID). The separation was performed using nonpolar capillary column DB-5HT (5%-phenyl)-methylpolysiloxane (15m x 0.32 mm ID, Agilent Technology, CA). The column temperature was initially set at 80°C, then subsequently ramped to 365°C at the rate of 15°C/min, and held constant for 19 min. The temperature of the injector and detector were adjusted constant at 370°C. 100 mg of SG was dissolved in 1 ml ethyl acetate and subjected to filtration using polyvinylidene difluoride (PVDF) filter prior analysis. The prepared sample (1 μl) was injected into the GC with a split ratio of 1:50. The velocity of nitrogen (N_2, 99.9%) as the carrier gas was fixed at 30 cm/s at 80°C.

2.5 Removal of SG using adsorption

The adsorption of SG from PO-B100 was conducted in a batch mode. A various mass ratio of CFP-based NCC to PO-B100 (1:50, 1:75, 1:100, 1:125, 1:150, 1:175, 1:200) was introduced into a series of beaker glass, where the mixture will be subjected to a 1-hour adsorption process at constant temperature and agitation speed (250 rpm). The selection of adsorption duration was based on the preliminary experiment conducted to find the equilibrium time. Several adsorption temperatures (65, 75 and 85°C) were used to study the effect of temperature on the adsorption of SG. The solution was separated from the adsorbent by using centrifugation at the rotational speed of 4900 rpm for 10 min. The SG contents in PO-B100 before and after adsorption were analyzed using UV-mini 1240 spectrophotometer (Shimadzu, Japan) at 240 nm, and the percentage of SG removal was determined by using the following equation.

$$SG\ removal\ (\%) = \frac{C_i - C_f}{C_i} x100 \qquad (2)$$

Where C_i is the concentration of SG in untreated PO-B100 (mg/kg) and C_f is the concentration of SG in treated (after adsorption) PO-B100 (mg/kg).

2.6 Isotherm study of the SG adsorption

The adsorption isotherm was conducted at the temperature of 65, 75 and 85°C with various CFP-based NCC to PO-B100 mass ratio (1:50, 1:75, 1:100, 1:125, 1:150, 1:175, 1:200). It was conducted using a similar procedure as previously mentioned in subsection 2.5. At the equilibrium condition, the amount of adsorbed SG per unit mass of CFP-based NCC as the adsorbent (Q_e) was calculated by the equation below.

$$Q_e\left(\frac{mg}{g}\right) = \frac{C_o - C_e}{m} x\ V \qquad (3)$$

Where C_o and C_e are the initial and final (equilibrium) concentration of SG in PO-B100 (mg/L), respectively, m is the mass of adsorbent (g) and V is the volume of PO-B100 (L).

3. RESULTS AND DISCUSSIONS

3.1 Characterization of CFP-based NCC

The X-ray diffraction pattern of the CFP and its NCC are shown in Figure 1, and the corresponding crystallinity index is presented in Table 1. The characteristic peaks of CFP are at 15.44° and 22.63°, while the diffraction peaks of CFP-based NCC are found at 16.52° and 22.60°. The crystal plane of 200 at around 22.60° - 22.63° represents the crystalline part of cellulose and the broad peak at 15.44° - 16.52° indicates the crystal plane of 110, which is the characteristic of typical amorphous structure of cellulose I [16,18]. The crystallinity of CFP and its NCC were calculated to be 36.35% and 65.64%, respectively. The change of crystallinity index is apparently occurred because of the progressive removal of amorphous hemicellulose and lignin during acid hydrolysis. The highly crystalline product is more efficient to improve the mechanical properties of the composite material, particularly as an adsorbent, since crystallinity positively corresponds to the tensile strength of the material [19].

Figure 1

Table 1

The scanning electron micrograph in Figure 2 shows the shape and size of the CFP-based NCC. The distribution of NCC products derived from CFP was estimated to have approximately 200-400 nm in length (Figure 2). The prepared CFP-based NCC has a homogenous needle-shaped with average crystallite size of 2 – 4 nm, obtained from the combination of X-ray diffraction data and Scherrer analysis. The homogenous CFP-based NCC particles are likely caused by the swollen of cellulose fibers due to NaOH delignification pretreatment [16].

Figure 2

191 Figure 3 illustrated the FTIR spectra of CFP and its NCC. Several peaks representing
192 certain functional groups in CFP-based NCC were found in the spectra. The broad bands in
193 the range of 3008 – 3459 cm^{-1} represents the O-H stretching vibrations, while the peaks in the
194 range of 2802 – 2925 cm^{-1} correspond to C-H stretching vibrations. The absorption at 936 –
195 1137 cm^{-1} is related to the functional group of C-O-C, and the peak at 1640 cm^{-1} indicates the
196 presence of abundant hydrophilic hydroxide group in the cellulose [20]. A peak at 1382 cm^{-1}
197 represents the C-H asymmetric deformations [21]

198 **Figure 3**

199

200 *3.2 Properties of PO-B100*

201 The properties of PO-B100 have been analyzed according to the standard method of
202 ASTM for its content of FAME, acid value (AV), MG, DG and triglycerides (TG). As
203 reported in Table 2, the purity of FAME in PO-B100 is 98.7%, while the AV, MG, DG, and
204 TG values are 0.12 mg KOH/g, 0.23%, 0.09%, and 0.06%, respectively. Furthermore, PO-
205 B100 feedstock contained 194.1 mg/kg of SG with the cloud point of 13.2°C and clear initial
206 appearance. Based on the GC-FID analysis, the SG profile in PO-B100 consists of 34.79% of
207 campesteryl glucoside, 23.73% of stigmasteryl glucoside and 41.48% of β-sitosteryl
208 glucoside. The results met the requirements of ASTM D6751 and SNI 7182:2015. However,
209 white precipitates could be found within few hours after production.

210 **Table 2**

211 After the adsorption using the parameters giving the highest SG removal (1:50, 75°C,
212 1 h), the sample of treated PO-B100 was collected for the properties measurement in order to
213 monitor the effect of adsorbent. According to the results, the treated PO-B100 contained
214 FAME with a purity of 98.8% and AV value of 0.11 mg KOH/g. The concentration of SG

reduced significantly to 15.9 mg/kg with the composition of 24.81% campesteryl glucoside, 25.07% stigmasteryl glucoside and 50.12% β-sitosteryl glucoside, while the other glycerides components, MG, DG, and TG, were slightly decreased to 0.22%, 0.09%, 0.05%, respectively. The cloud point of the treated PO-B100 was also found to be decreased to 11.5°C. These results indicated that CFP-based NCC has selectivity to adsorb SG, particularly campesteryl glucoside and stigmasteryl glucoside, as compared to the other minor components, such as MG, DG, and TG. It also subsequently lowered the cloud point significantly, which is advantageous for storage and transportation purposes [22].

3.3 Adsorption of SG using CFP-based NCC

The effect of CFP-based NCC loading on the SG removal was investigated for the treatment of PO-B100 (Figure 4). Based on the results provided in Figure 4, the lowest removal rate of SG in every adsorption temperature was seen at 1:200 of CFP-based NCC to PO-B100 mass ratio. It was likely due to insufficient binding and active adsorption sites and the adsorption required more time to reach the equilibrium stage. The removal percentage of SG was observed to have amplified with the increase of CFP-based NCC to PO-B100 mass ratio from 1:200 to 1:50 at all temperatures in the tested range. Greater amounts of CFP-based NCC provide greater adsorption surface area and active sites in CFP-based NCC, leading to an adequate SG binding area and certainly, higher percentage of SG removal [23]. It was also monitored that the SG removal rate exponentially increased when the CFP-based NCC to PO-B100 mass ratio was increased from 1:100 to 1:50 in the all adsorption temperature**.** The phenomenon indicated the good dispersion ability of CFP-based NCC in PO-B100, where constant diffusion path length of SG binding to CFP-based NCC surface was found regardless the amount of adsorbent [24].

Figure 4

240 As presented in Figure 4, temperature remarkably affected the SG reduction. A
241 temperature elevation from 65°C to 75°C greatly improves the reduction of SG, regardless of
242 CFP-based NCC to PO-B100 mass ratio. Chowdhury et al. (2011) stated that the adsorption
243 enhancement along with the temperature increase may be associated with the increase of the
244 number of active sites available for adsorption. The diffusion rate of the adsorbate across the
245 external boundary layer also escalates with rise in temperature, due to lower solution
246 viscosity and enhancement in the mobility and kinetic energy of the adsorbate [25]. Therefore,
247 the collision between particles intensifies with the temperature elevation so that the activation
248 energy of adsorption process is easier to achieve. As a result, the amount of the adsorbed SG
249 enhances along with the temperature increase. However, it was also observed that the SG
250 removal rate decreased when the temperature was further escalated from 75°C to 85°C. More
251 (2018) mentioned that after reaching certain temperature, excessive particle collision causes
252 the removal of adsorbates from the adsorbent, leading to lower adsorption capacity [26]. Lee
253 et al. (2019) also stated that the NCC surface binding generally weakens along with the
254 temperature enhancement [24]. The fluctuations of the SG uptake observed with the change
255 in temperature suggests that the SG adsorption is governed by both physical attraction and
256 chemical bonding, indicating that the sorption of SG by CFP-based NCC is both driven by
257 physical and chemical sorption [25,27].
258
259 *3.4 Study of adsorption isotherm and thermodynamic parameters*
260 In this study, three isotherm equations were fitted to the experimental equilibrium
261 data for SG at three temperature points (65°C, 75°C and 85°C). The results are presented in
262 Table 3 and the isotherm models are plotted in Figure 5. The Langmuir isotherm constant, K_L
263 and maximum absorption capacity, $Q_{m(L)}$ were calculated from the nonlinear curve fitting
264 between Q_e and C_e. The value of $Q_{m(L)}$ was found to be increased from 12.50 mg/g at 65°C to

12.93 mg/g at 75°C before declining to 11.24 mg/g at the highest tested temperature (85°C). The $Q_{m(L)}$ results are quite comparable to the adsorption capacity of magnesium silicate and bleaching earth on the SG (~13 mg/g) [7]. The Langmuir constant (K_L) also increases along with the temperature, from 0.11 L/mg at the lowest temperature (65°C) to 0.26 L/mg at the highest temperature point (85°C), indicating that the adsorption of SG to CFP-based NCC is an endothermic process.

Table 3

Figure 5

The isotherm data were further analyzed by Freundlich model. The Freundlich constant K_F and 1/n were obtained from the non-linear regression analysis. Table 3 showed that the values of 1/n are all under unity, ranging from 0.03 at 75°C to 0.16 at 65°C. The extent of 1/n represents the favorability degree of adsorption. The value of 1/n less than unity corresponds to favorable sorption. It was also observed that the Freundlich constant greatly escalates along with the temperature, implying that the adsorption was favorable at high temperature and the process is certainly endothermic. de Sá et al. (2017) mentioned that 1/n value between 0 and 1 is associated with a chemisorption process [28].

Another isotherm equation, the Dubinin-Radushkevich (D-R) model, was further applied to analyze the equilibrium data, particularly to determine the nature of SG adsorption onto CFP-based NCC surface. The D-R constant (β) gives an idea about the mean sorption energy, E, and their correlation can be expressed by the following equation:

$$E = \frac{1}{\sqrt{2\beta}} \quad (4)$$

where E represents sorption energy (kJ/mol) and β is the D-R constant ($mmol^2/J^2$). The value of sorption energy provides information to determine the type of adsorption mechanism, as chemical ion exchange or physical adsorption. Li et al. (2009) and Zhu et al. (2009) stated that if the sorption energy ranges from 8 to 16 kJ/mol, the sorption process is supposed to be

chemisorption, while for energy value lower than 8 kJ/mol, the sorption is of physical nature [29,30]. Based on the results provided in Table 3, the adsorption mechanism is physical attraction since the E values for all tested temperatures are lower than 8 kJ/mol. The highest $Q_{m(D-R)}$ was found at 75°C with a value of 12.13 mg/g, which was similar to the result obtained using Langmuir isotherm. The effect of temperature previously studied also provides similar results where temperature of 75°C gives highest SG removal rate compared to the other tested temperatures.

The correlation coefficient (r^2) and chi-square (χ^2) values of the three isotherms are also listed in Table 3. It could be concluded that the adsorption of SG onto the CFP-based NCC surface is best fitted to the Langmuir isotherm equation under the temperature range studied. Based on the three isotherm models studied, the adsorption mechanism is predicted to be driven by both physical and chemical sorption due to its sorption energy value and endothermic nature, respectively. The overall results of this study showed that NCC has a particular affinity for SG and is an effective adsorbent for SG removal from PO-B100.

Table 4 listed the thermodynamics parameters of the SG adsorption onto the surface of NCC, such as Gibbs free energy change (ΔG°), enthalpy (ΔH°) and entropy (ΔS°). The three thermodynamics parameters were determined using equation (5) and (6).

$$\Delta G° = -RTln(K_L.M_{SG}.10^3.C^o) \quad (5)$$

$$\Delta G° = \Delta H° - T\Delta S° \quad (6)$$

Where R is the gas constant with the value of 8.314 J/mol.K, T is the absolute temperature in Kelvin, K_L is Langmuir equilibrium constant in L/mg, M_{SG} is the molecular weight of SG in g/mol and C^o is the reference concentration in standard state with the value of 1 mol/L.

The values of Gibbs free energy (ΔG°) for the adsorption of SG were negative at all tested temperatures. These values confirm the spontaneous nature of SG adsorption onto the CFP-based NCC. Enhancement of the ΔG° value along with the increasing temperature

implies that the affinity of SG on CFP-based NCC was higher at high temperature. Positive ΔH° value (42.90 kJ/mol) verifies that the adsorption is indeed an endothermic process, while absolute value of ΔS° (219.80 J/mol.K) reflects the increased randomness at the solid-solution interface during the adsorption process [25,31].

Table 4

3.6 Adsorption mechanism study

The study of the adsorption mechanism was used to further illustrate the interaction between SG and CFP-based NCC surface. Two important points have to be considered to understand the mechanism, namely the surface properties of the adsorbent and the structure of adsorbate. The NCC molecule was constructed by substantial number of hydrogen bonds between glucose units or glucose chains inside the molecule to form a very stable structure [32,33]. NCC contains majority of oxygen functional groups such as hydroxyl, ether, and sulfonate. While the hydroxyl and ether groups are originally present in the cellulosic material, the sulfonate group existed due to the acid hydrolysis to produce NCC. On the other hand, SG was built by a steryl cation (SC^{+}) and a glucose unit, with a positive charge on the cationic steryl part.

In this study, the removal of SG from PO-B100 by adsorption using CFP-based NCC was found to be greatly increased when the temperature raised from 65°C to 75°C and then declined when the temperature further escalated to 85°C, indicating that the adsorption was strongly temperature-dependent. It was also observed that the isotherm modeling showed equal contribution of physical attraction and chemical binding. According to the findings of this study, the mechanism of SG removal by adsorption on the CFP-based NCC surface may be presumed to involve these following steps:

- Migration of SG from the bulk of PO-B100 to the CFP-based NCC surface

340 • Diffusion of SG through the boundary layer to the CFP-based NCC surface

341 • Adsorption of SG on the surface of CFP-based NCC, which may be caused by physical
342 interaction of dipole-dipole coupling between the positively charged SC^+ and the
343 negatively charged NCC surface as suggested in Figure 6; and through a possible
344 chemical binding mechanism of ion exchange as shown below:

$$NCC - OH \leftrightarrow NCC - O^- + H^+$$

$$NCC - SO_3^- \leftrightarrow NCC - SO_3^-$$

$$NCC - O^- + SC^+ \leftrightarrow NCC - O - SC$$

$$NCC - SO_3^- + SC^+ \leftrightarrow NCC - O - SO_3$$

345 • Intraparticle diffusion of SG into the pores of CFP-based NCC

346 **Figure 6**

347

348 **4. CONCLUSIONS**

349 CFP-based NCC was successfully used as adsorbent for reducing SG in PO-B100. The
350 content of SG was able to be reduced from 194.1 mg/kg to as low as 15.9 mg/kg (91.81%
351 removal rate) within 1 hour at the temperature of 75°C using CFP-based NCC to PO-B100
352 mass ratio of 1:50. The study proved that CFP-based NCC has great affinity and selectivity to
353 SG, particularly on the campesteryl glucoside and stigmasteryl glucoside. The adsorption
354 treatment greatly improves the cold stability of PO-B100 by reducing the cloud point from
355 13.2°C to 11.5°C, while slightly affected the purity of FAME, AV and other minor
356 components, such as MG, DG, and TG, which were still in the acceptable range according to
357 ASTM D6751. The adsorption process was endothermic and may be driven by both physical
358 attraction and chemical ion exchange. The adsorption treatment using CFP-based NCC
359 should be a prospective method used to remove SG from PO-B100 since it possesses high
360 efficiency, time-saving and energy-efficient.

ACKNOWLEDGMENT

This research did not receive any specific grant from funding agencies in the public, commercial or not-for-profit sectors.

REFERENCES

[1] Indonesian Palm Oil Association, Perkembangan Biodiesel di Indonesia dan Terbesar di Asia, (2017). https://gapki.id/news/3250/perkembangan-biodiesel-di-indonesia-dan-terbesar-di-asia (accessed September 30, 2018).

[2] A.C. Pinto, L.L.N. Guarieiro, M.J.C. Rezende, N.M. Ribeiro, A. Ednildo, Biodiesel : An Overview, 16 (2005) 1313–1330.

[3] I. Lee, L.M. Pfalzgraf, G.B. Poppe, E. Powers, T. Haines, The role of sterol glucosides on filter plugging, Biodiesel Mag. 4. (2007) 105–112.

[4] V. Van Hoed, N. Zyaykina, W. De Greyt, J. Maes, R. Verhé, K. Demeestere, Identification and occurrence of steryl glucosides in palm and soy biodiesel, JAOCS, J. Am. Oil Chem. Soc. 85 (2008) 701–709. doi:10.1007/s11746-008-1263-5.

[5] R.A. Moreau, K.M. Scott, M.J. Haas, The identification and quantification of steryl glucosides in precipitates from commercial biodiesel, JAOCS, J. Am. Oil Chem. Soc. 85 (2008) 761–770. doi:10.1007/s11746-008-1264-4.

[6] H. Tang, S.O. Salley, K.Y. Simon Ng, Fuel properties and precipitate formation at low temperature in soy-, cottonseed-, and poultry fat-based biodiesel blends, Fuel. 87 (2008) 3006–3017. doi:10.1016/j.fuel.2008.04.030.

383 [7] D. Na-Ranong, P. Laungthaleongpong, S. Khambung, Removal of steryl glucosides in
384 palm oil based biodiesel using magnesium silicate and bleaching earth, Fuel. 143
385 (2015) 229–235. doi:10.1016/j.fuel.2014.11.049.

386 [8] A. Aguirre, S. Peiru, F. Eberhardt, L. Vetcher, R. Cabrera, H.G. Menzella, Enzymatic
387 hydrolysis of steryl glucosides, major contaminants of vegetable oil-derived biodiesel,
388 Appl. Microbiol. Biotechnol. 98 (2014) 4033–4040. doi:10.1007/s00253-013-5345-4.

389 [9] S. Peiru, A. Aguirre, F. Eberhardt, M. Braia, R. Cabrera, H.G. Menzella, An industrial
390 scale process for the enzymatic removal of steryl glucosides from biodiesel,
391 Biotechnol. Biofuels. 8 (2015). doi:10.1186/s13068-015-0405-x.

392 [10] A.Y. Tremblay, A. Montpetit, The in-process removal of sterol glycosides by
393 ultrafiltration in biodiesel production, Biofuel Res. J. 4 (2017) 559–564.
394 doi:10.18331/brj2017.4.1.6.

395 [11] M.Y. Chang, R.S. Juang, Adsorption of tannic acid, humic acid, and dyes from water
396 using the composite of chitosan and activated clay, J. Colloid Interface Sci. 278 (2004)
397 18–25. doi:10.1016/j.jcis.2004.05.029.

398 [12] A.G. Varghese, S.A. Paul, M.S. Latha, Green Adsorbents for Pollutant Removal, 2018.
399 doi:10.1007/978-3-319-92111-2.

400 [13] M. Börjesson, G. Westman, Crystalline Nanocellulose — Preparation, Modification,
401 and Properties, Cellul. - Fundam. Asp. Curr. Trends. (2015). doi:10.5772/61899.

402 [14] H. Voisin, L. Bergström, P. Liu, A. Mathew, Nanocellulose-Based Materials for Water
403 Purification, Nanomaterials. 7 (2017) 57. doi:10.3390/nano7030057.

404 [15] H. Liang, X. Hu, A quick review of the applications of nano crystalline cellulose in
405 wastewater treatment, J. Bioresour. Bioprod. 2016 (2016) 199–204.

www.Bioresources-Bioproducts.com.

[16] J.N. Putro, S.P. Santoso, S. Ismadji, Y.H. Ju, Investigation of heavy metal adsorption in binary system by nanocrystalline cellulose – Bentonite nanocomposite: Improvement on extended Langmuir isotherm model, Microporous Mesoporous Mater. 246 (2017) 166–177. doi:10.1016/j.micromeso.2017.03.032.

[17] L. Segal, J.J. Creely, A.E. Martin, C.M. Conrad, An Empirical Method for Estimating the Degree of Crystallinity of Native Cellulose Using the X-Ray Diffractometer, Text. Res. J. 29 (1959) 786–794. doi:10.1177/004051755902901003.

[18] M. Wada, L. Heux, J. Sugiyama, Polymorphism of cellulose I family: Reinvestigation of cellulose IVl, Biomacromolecules. 5 (2004) 1385–1391. doi:10.1021/bm0345357.

[19] Y. Hu, L. Tang, Q. Lu, S. Wang, X. Chen, B. Huang, Preparation of cellulose nanocrystals and carboxylated cellulose nanocrystals from borer powder of bamboo, Cellulose. 21 (2014) 1611–1618. doi:10.1007/s10570-014-0236-0.

[20] A. Alemdar, M. Sain, Isolation and characterization of nanofibers from agricultural residues - Wheat straw and soy hulls, Bioresour. Technol. 99 (2008) 1664–1671. doi:10.1016/j.biortech.2007.04.029.

[21] X.F. Sun, F. Xu, R.C. Sun, P. Fowler, M.S. Baird, Characteristics of degraded cellulose obtained from steam-exploded wheat straw, Carbohydr. Res. 340 (2005) 97–106. doi:10.1016/j.carres.2004.10.022.

[22] N.A. Negm, M.T.H. Abou Kana, M.A. Youssif, M.Y. Mohamed, Biofuels from vegetable oils as alternative fuels: Advantages and disadvantages, 2017. doi:10.1201/b20780.

[23] A. Khodabandehloo, A. Rahbar-Kelishami, H. Shayesteh, Methylene blue removal

429 using Salix babylonica (Weeping willow) leaves powder as a low-cost biosorbent in
430 batch mode: Kinetic, equilibrium, and thermodynamic studies, J. Mol. Liq. 244 (2017)
431 540–548. doi:10.1016/j.molliq.2017.08.108.

432 [24] H.J. Lee, H.S. Lee, J. Seo, Y.H. Kang, W. Kim, T.H.K. Kang, State-of-the-art of
433 cellulose nanocrystals and optimal method for their dispersion for construction-related
434 applications, Appl. Sci. 9 (2019) 1–14. doi:10.3390/app9030426.

435 [25] S. Chowdhury, R. Mishra, P. Saha, P. Kushwaha, Adsorption thermodynamics,
436 kinetics and isosteric heat of adsorption of malachite green onto chemically modified
437 rice husk, Desalination. 265 (2011) 159–168. doi:10.1016/j.desal.2010.07.047.

438 [26] H. More, Factors Affecting Adsorption, (2018).
439 https://hemantmore.org.in/science/chemistry/factors-affecting-adsorption/13094/
440 (accessed May 5, 2019).

441 [27] M. Mohapatra, S. Khatun, S. Anand, Kinetics and thermodynamics of lead (II)
442 adsorption on lateritic nickel ores of Indian origin, Chem. Eng. J. 155 (2009) 184–190.
443 doi:10.1016/j.cej.2009.07.035.

444 [28] A. de Sá, A.S. Abreu, I. Moura, A.V. Machado, Polymeric materials for metal sorption
445 from hydric resources, Elsevier Inc., 2017. doi:10.1016/b978-0-12-804300-4.00008-3.

446 [29] C.S. Zhu, L.P. Wang, W. bin Chen, Removal of Cu(II) from aqueous solution by
447 agricultural by-product: Peanut hull, J. Hazard. Mater. 168 (2009) 739–746.
448 doi:10.1016/j.jhazmat.2009.02.085.

449 [30] Q. Li, L. Chai, Z. Yang, Q. Wang, Kinetics and thermodynamics of Pb(II) adsorption
450 onto modified spent grain from aqueous solutions, Appl. Surf. Sci. 255 (2009) 4298–
451 4303. doi:10.1016/j.apsusc.2008.11.024.

[31] Y. Liu, Y.J. Liu, Biosorption isotherms, kinetics and thermodynamics, Sep. Purif. Technol. 61 (2008) 229–242. doi:10.1016/j.seppur.2007.10.002.

[32] Y. Habibi, L.A. Lucia, O.J. Rojas, Cellulose nanocrystals: Chemistry, self-assembly, and applications, Chem. Rev. 110 (2010) 3479–3500. doi:10.1021/cr900339w.

[33] Y. Liu, D. Ying, L. Sanguansri, Y. Cai, X. Le, Adsorption of catechin onto cellulose and its mechanism study: Kinetic models, characterization and molecular simulation, Food Res. Int. 112 (2018) 225–232. doi:10.1016/j.foodres.2018.06.044.

461 **Figure captions.**

462 **Figure 1.** X-Ray Diffraction Patterns of (a) CFP, (b) CFP-based NCC

463 **Figure 2.** SEM image of the rod-like CFP-based NCC particles

464 **Figure 3.** FTIR spectrum of CFP-based NCC

465 **Figure 4.** SG removal rate varied with the mass ratio of CFP-based NCC to PO-B100 at three
466 different temperatures

467 **Figure 5.** The modelled isotherm profiles for the adsorption of SG to CFP-based NCC
468 surface (temperature = 75°C, mass ratio of CFP-based NCC to PO-B100 = 1:50, time = 1 h,
469 agitation speed = 250 rpm)

470 **Figure 6.** Schematic representation of the proposed adsorption mechanism of SG onto CFP-
471 based NCC surface

472

473

474

475

476

477 **Table 1. The crystallinity index of CFP and CFP-based NCC**

Samples	2-theta (°)		Crystallinity (%)
	110 crystal plane	200 crystal plane	
CFP	15.44	22.63	36.35
CFP-based NCC	16.52	22.60	65.64

478

479

480 **Table 2. The properties of untreated and treated PO-B100 (1:50, 75°C, 1 h), and the**
481 **comparison with ASTM D6751 and SNI 7182:2015**

Parameters	ASTM D6751	SNI 7182:2015	Untreated PO-B100	Treated PO-B100 (1:50, 75°C, 1 h)
FAME (%)	≥ 96.5	≥ 96.5	98.7	98.8
AV (mg KOH/g)	≤ 0.50	≤ 0.50	0.12	0.11
MG (%)	≤ 0.80	≤ 0.80	0.23	0.22
DG (%)	≤ 0.20	-	0.09	0.09
TG (%)	≤ 0.20	-	0.06	0.05
SG (mg/kg)	N/A*	N/A*	194.1	15.9
Cloud point (°C)	-	18.0	13.2	11.5

482 * Not available

483

484 **Table 3. Isotherm parameters of SG adsorption onto CFP-based NCC surface**

Isotherm	Parameters	Temperature (K)		
		338	348	358
Langmuir	$Q_{m(L)}$ (mg/g)	12.50	12.93	11.24
	K_L (L/mg)	0.11	0.16	0.26
	r^2	0.8587	0.8580	0.7039
	χ^2	0.2329	0.2865	0.2487
Freundlich	K_F ((mg/g) $(L/mg)^{1/n}$)	5.59	6.48	7.31
	1/n	0.16	0.03	0.09
	r^2	0.8408	0.7986	0.6079
	χ^2	0.2624	0.4064	0.3293
Dubinin-Radushkevich	$Q_{m(D-R)}$ (mg/g)	11.58	12.13	10.86
	E (kJ/mol)	0.18	0.25	0.29
	r^2	0.8094	0.8387	0.7555
	χ^2	0.3147	0.3254	0.2053

485

486

Table 4. Thermodynamics parameters of adsorption of SG onto CFP-based NCC surface

Temperature (K)	Thermodynamic parameters		
	ΔG° (kJ/mol)	ΔH° (kJ/mol)	ΔS° (J/mol.K)
338	-31.44	42.90	219.80
348	-33.46		
358	-35.84		

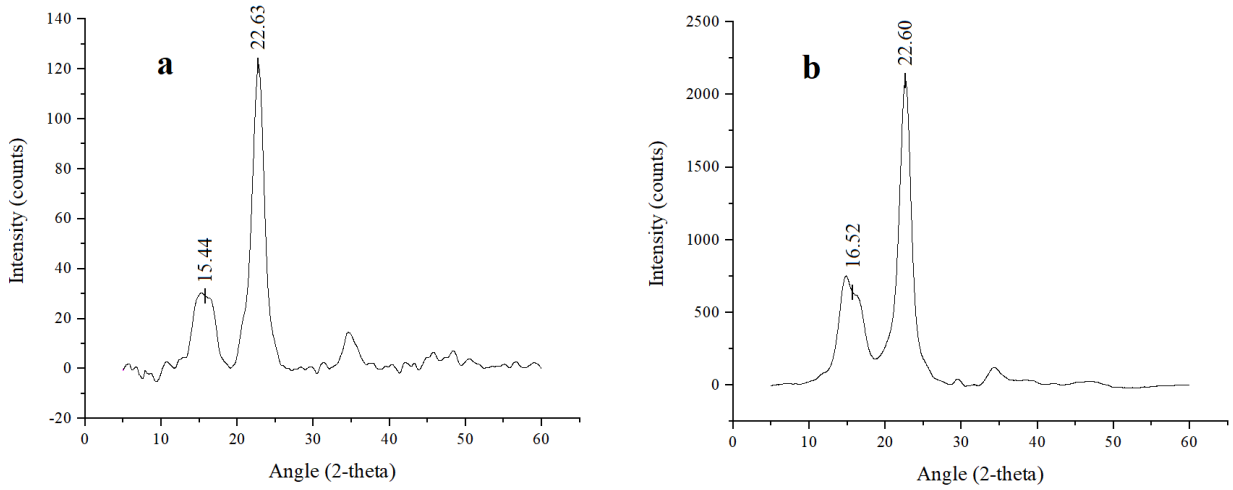
a
22.63
15.44
Intensity (counts)
Angle (2-theta)
b
22.60
16.52
Intensity (counts)
Angle (2-theta)

Figure 1

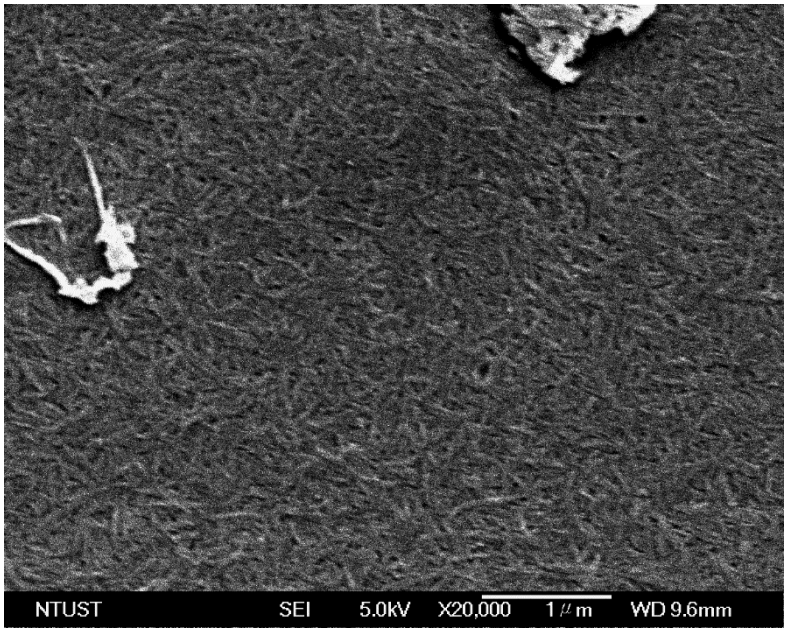

Figure 2

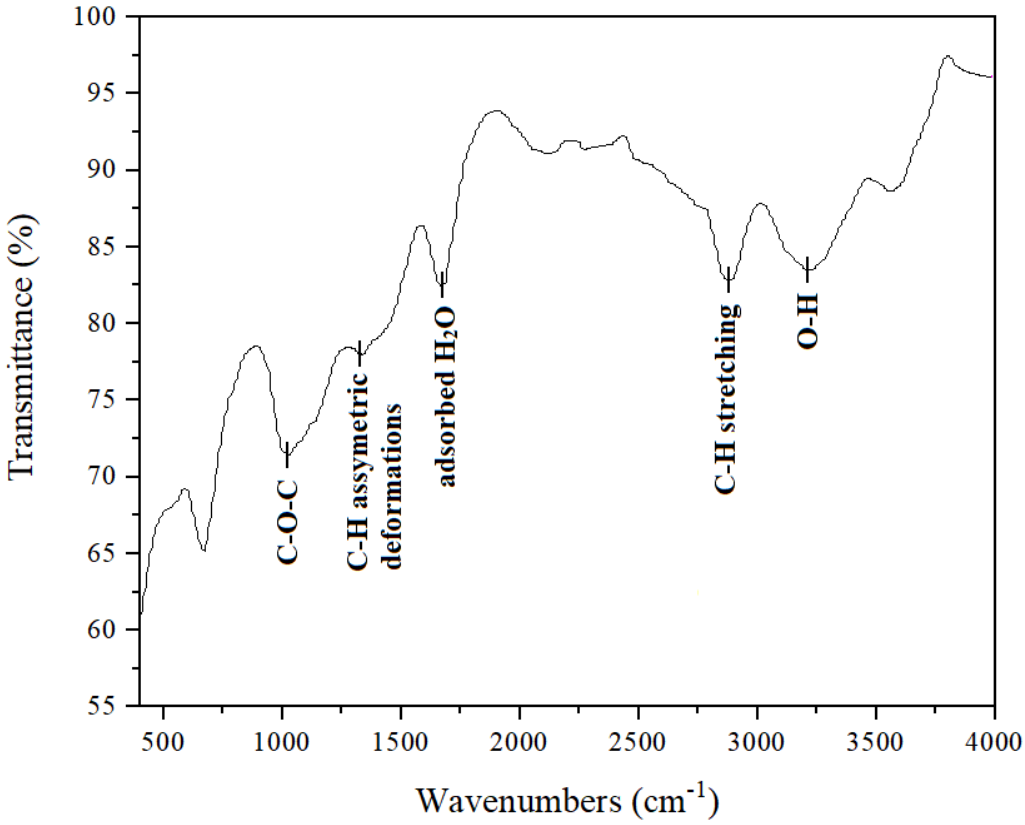
Transmittance (%)
Wavenumbers (cm-1)
C-O-C
C-H assymetric deformations
adsorbed H2O
C-H stretching
O-H
100
95
90
85
80
75
70
65
60
55
500
1000
1500
2000
2500
3000
3500
4000

Figure 3

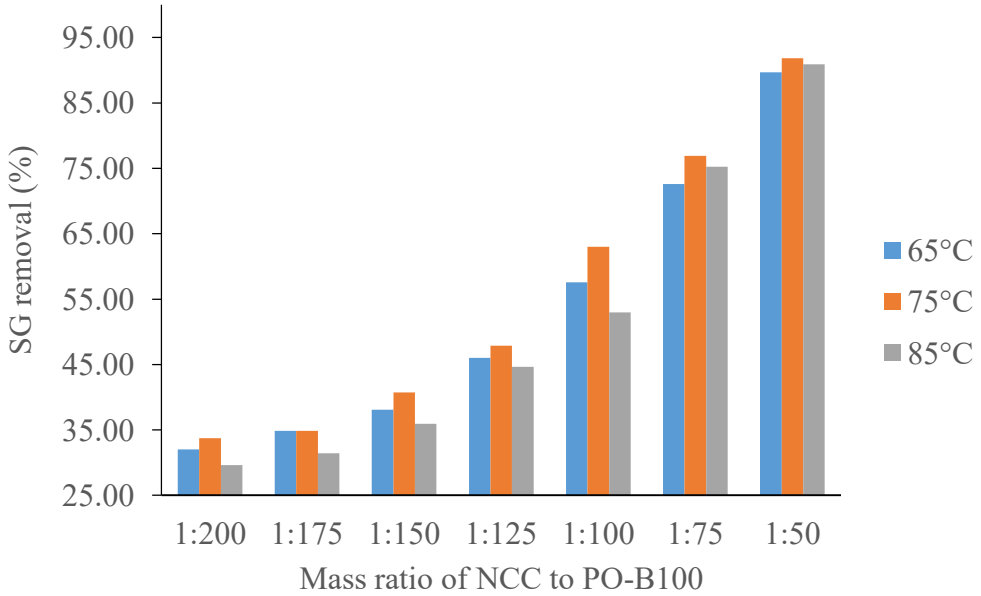
95.00
85.00
75.00
65.00
55.00
45.00
35.00
25.00
SG removal (%)
1:200
1:175
1:150
1:125
1:100
1:75
1:50
Mass ratio of NCC to PO-B100
65°C
75°C
85°C

Figure 4

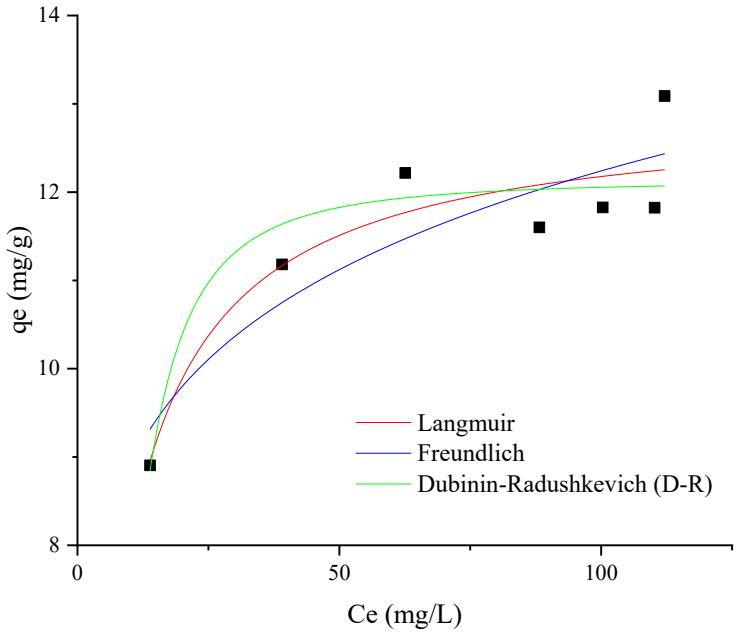
14
12
10
8
qe (mg/g)
0
50
100
Ce (mg/L)
Langmuir
Freundlich
Dubinin-Radushkevich (D-R)

Figure 5

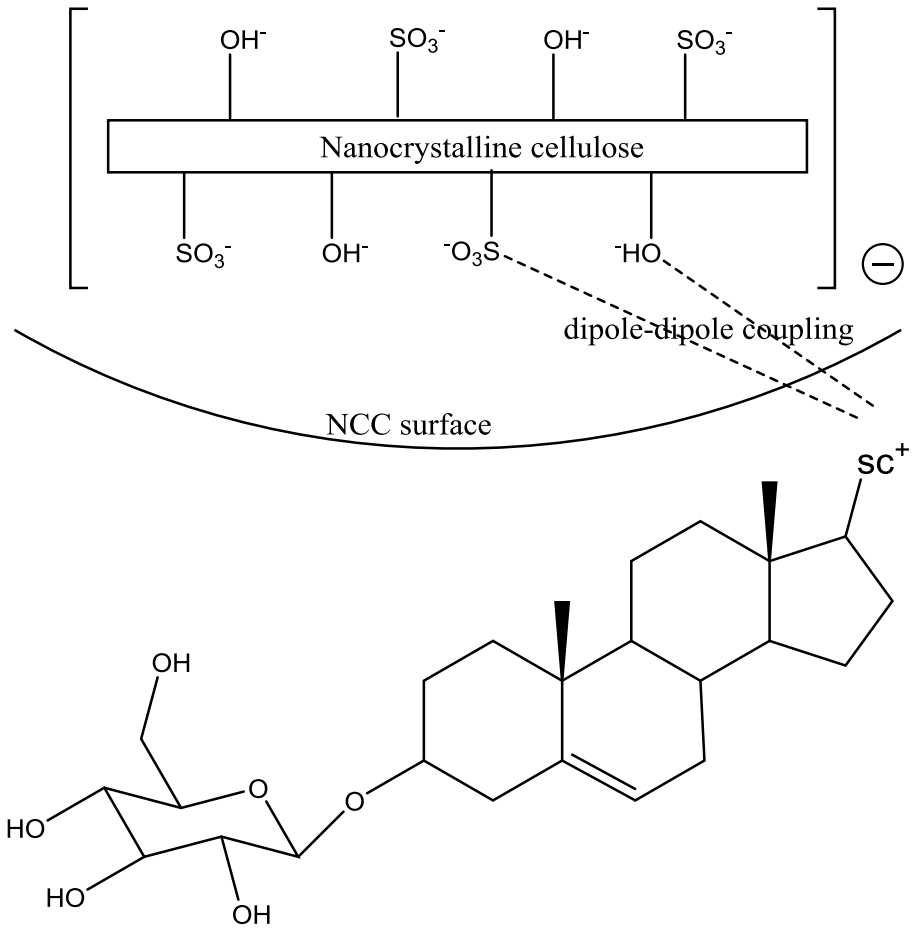
OH-
SO3-
OH-
SO3-
Nanocrystalline cellulose
SO3-
OH-
-O3S
-HO
dipole-dipole coupling
NCC surface
SC+
OH
O
O
HO
HO
OH

Figure 6

*Declaration of Interest Statement

Declaration of interests

☒ The authors declare that they have no known competing financial interests or personal relationships that could have appeared to influence the work reported in this paper.

☐The authors declare the following financial interests/personal relationships which may be considered as potential competing interests:

Gmail

Maria Yuliana <mariayuliana@ukwms.ac.id>

Your Submission RENE-D-19-04543

1 message

Renewable Energy <eesserver@eesmail.elsevier.com> Sat, Jan 11, 2020 at 4:28 PM
Reply-To: Renewable Energy <rene@elsevier.com>
To: mariayuliana@ukwms.ac.id, maria_yuliana_liauw@yahoo.com
Cc: liangna16@gmail.com, albert.st12@gmail.com, shella_p5@yahoo.com, felyciae@yahoo.com, sandy@ukwms.ac.id, tnplan@ctu.edu.vn, suryadiismadji@yahoo.com, yhju@mail.ntust.edu.tw

Ms. Ref. No.: RENE-D-19-04543
Title: FEASIBILITY STUDY OF NANOCRYSTALLINE CELLULOSE AS ADSORBENT OF STERYL GLUCOSIDES FROM PALM-BASED BIODIESEL
Renewable Energy

Dear Dr. Yuliana,

The review of your paper is now complete; the Reviewers' reports are below. As you can see, the Reviewers present important points of criticism and a series of recommendations. We kindly ask you to consider all comments and revise the paper accordingly in order to respond fully and in detail to the Reviewers' recommendations. If this process is completed thoroughly, the paper will be acceptable for a second review.

Once you have revised the paper accordingly, please submit it together with a detailed description of your response to these comments. Please, also include a separate copy of the revised paper in which you have marked the revisions made.

The revision will be due by: 10/02/2020

To submit a revision, please go to https://ees.elsevier.com/rene/ and login as an Author.

Your username is: mariayuliana@ukwms.ac.id
If you need to retrieve password details, please go to: http://ees.elsevier.com/rene/automail_query.asp .

NOTE: Upon submitting your revised manuscript, please upload the source files for your article. For additional details regarding acceptable file formats, please refer to the Guide for Authors at: http://www.elsevier.com/journals/renewable-energy/0960-1481/guide-for-authors

When submitting your revised paper, we ask that you include the following items:

Manuscript, Marked manuscript and Figure Source Files (mandatory)

We cannot accommodate PDF manuscript files for production purposes. We also ask that when submitting your revision you follow the journal formatting guidelines. Figures and tables may be embedded within the source file for the submission as long as they are of sufficient resolution for Production.For any figure that cannot be embedded within the source file (such as *.PSD Photoshop files), the original figure needs to be uploaded separately. Refer to the Guide for Authors for additional information.
http://www.elsevier.com/journals/renewable-energy/0960-1481/guide-for-authors

Highlights (mandatory)

Highlights consist of a short collection of bullet points that convey the core findings of the article and should be submitted in a separate file in the online submission system. Please use 'Highlights' in the file name and include 3 to 5 bullet points (maximum 85 characters, including spaces, per bullet point). See the following website for more information
http://www.elsevier.com/highlights

On your Main Menu page, you will find a folder entitled "Submissions Needing Revision". Your submission record will be presented here.

Please note that this journal offers a new, free service called AudioSlides: brief, webcast-style presentations that are shown next to published articles on ScienceDirect (see also http://www.elsevier.com/audioslides). If your paper is

accepted for publication, you will automatically receive an invitation to create an AudioSlides presentation.

Effective peer review is essential to uphold the quality and validity of individual articles, but also the overall integrity of the journal. We would like to remind you that for every article considered for publication, there are usually at least 2 reviews required for each review round, and it is critical that scientists wishing to publish their research also be willing to provide reviews to similarly enable the peer review of papers by other authors. Please accept any review assignment within your expertise area(s) we may address to you and undertake reviewing in the manner in which you would hope your own paper to be reviewed.
MethodsX file (optional)

If you have customized (a) research method(s) for the project presented in your Renewable Energy article, you are invited to submit this part of your work as MethodsX article alongside your revised research article. MethodsX is an independent journal that publishes the work you have done to develop research methods to your specific needs or setting. This is an opportunity to get full credit for the time and money you may have spent on developing research methods, and to increase the visibility and impact of your work.

How does it work?
1) Fill in the MethodsX article template: https://www.elsevier.com/MethodsX-template
2) Place all MethodsX files (including graphical abstract, figures and other relevant files) into a .zip file and upload this as a 'Method Details (MethodsX) ' item alongside your revised Renewable Energy manuscript. Please ensure all of your relevant MethodsX documents are zipped into a single file.
3) If your Renewable Energy research article is accepted, your MethodsX article will automatically be transferred to MethodsX, where it will be reviewed and published as a separate article upon acceptance. MethodsX is a fully Open Access journal, the publication fee is only 520 US$.

Questions? Please contact the MethodsX team at methodsx@elsevier.com. Example MethodsX articles can be found here: http://www.sciencedirect.com/science/journal/22150161

Include interactive data visualizations in your publication and let your readers interact and engage more closely with your research. Follow the instructions here: https://www.elsevier.com/authors/author-services/data-visualization to find out about available data visualization options and how to include them with your article.

Thank you very much for expressing your interest in RENEWABLE ENERGY.
MethodsX file (optional)
We invite you to submit a method article alongside your research article. This is an opportunity to get full credit for the time and money you have spent on developing research methods, and to increase the visibility and impact of your work. If your research article is accepted, your method article will be automatically transferred over to the open access journal, MethodsX, where it will be editorially reviewed and published as a separate method article upon acceptance. Both articles will be linked on ScienceDirect. Please use the MethodsX template available here when preparing your article: https://www.elsevier.com/MethodsX-template. Open access fees apply.

Sincerely,

Soteris Kalogirou, D.Sc.
Editor-in-Chief
Renewable Energy

Data in Brief (optional):

We invite you to convert your supplementary data (or a part of it) into an additional journal publication in Data in Brief, a multi-disciplinary open access journal. Data in Brief articles are a fantastic way to describe supplementary data and associated metadata, or full raw datasets deposited in an external repository, which are otherwise unnoticed. A Data in Brief article (which will be reviewed, formatted, indexed, and given a DOI) will make your data easier to find, reproduce, and cite.

You can submit to Data in Brief via the Renewable Energy submission system when you upload your revised Renewable Energy manuscript. To do so, complete the template and follow the co-submission instructions found here: www.elsevier.com/dib-template. If your Renewable Energy manuscript is accepted, your Data in Brief submission will automatically be transferred to Data in Brief for editorial review and publication.

Please note: an open access Article Publication Charge (APC) is payable by the author or research funder to cover the costs associated with publication in Data in Brief and ensure your data article is immediately and permanently free to access by all. For the current APC see: www.elsevier.com/journals/data-in-brief/2352-3409/open-access-journal

Please contact the Data in Brief editorial office at dib-me@elsevier.com or visit the Data in Brief homepage

(www.journals.elsevier.com/data-in-brief/) if you have questions or need further information.

.....
Note: While submitting the revised manuscript, please double check the author names provided in the submission so that authorship related changes are made in the revision stage. If your manuscript is accepted, any authorship change will involve approval from co-authors and respective editor handling the submission and this may cause a significant delay in publishing your manuscript.
.....
Reviewers' comments:

Please note that editors and/or reviewers have uploaded files related to this submission. To access these file(s) while you are not logged into the system, please click on the link below. (Note: this link will expire after 5 clicks or 30 days.) Alternatively, you may log in to the system and click the 'View Review Attachments' link in the Action column.

Reviewer #1: Review (recommended major revision)

In manuscript, authors describe sustainable biomass-derived successfully-applied coarse filter paper-based nano-crystalline cellulose material as an adsorbent in biodiesel purification process. Manuscript is appropriate for selected research journal; however, major article revision is required before acceptance as a rule.

uploaded reviewer attachment

Reviewer #2: The authors presented the removal of SG from biodiesel. However, this work lacks in novelty in general. In addition, following comments need to be addressed prior further consideration.

1. First highlight is not from this work
2. Indonesia related background information is unnecessary in Introduction section
3. How did the experiment conditions were selected, need further justification/reference
4. Line 99, delignification method need justification/reference
5. Line 149, SG measurement method need more detail/reference
6. Figures need error bars and statistical analysis to identify the significance between treatments

Editor: You may include the papers cited by the reviewer/s only if these are relevant and improve the understanding of the paper.

For further assistance, please visit our customer support site at http://help.elsevier.com/app/answers/list/p/7923 Here you can search for solutions on a range of topics, find answers to frequently asked questions and learn more about EES via interactive tutorials. You will also find our 24/7 support contact details should you need any further assistance from one of our customer support representatives.

Gmail

Maria Yuliana <mariayuliana@ukwms.ac.id>

Submission Confirmation for RENE-D-19-04543R1

1 message

Renewable Energy <eesserver@eesmail.elsevier.com> Mon, Feb 3, 2020 at 11:38 AM
Reply-To: Renewable Energy <rene@elsevier.com>
To: mariayuliana@ukwms.ac.id, maria_yuliana_liauw@yahoo.com
Cc: liangna16@gmail.com, albert.st12@gmail.com, shella_p5@yahoo.com, felyciae@yahoo.com, sandy@ukwms.ac.id, tnplan@ctu.edu.vn, suryadiismadji@yahoo.com, yhju@mail.ntust.edu.tw

*** Automated email sent by the system ***

Ms. Ref. No.: RENE-D-19-04543R1
Title: FEASIBILITY STUDY OF NANOCRYSTALLINE CELLULOSE AS ADSORBENT OF STERYL GLUCOSIDES FROM PALM-BASED BIODIESEL
Article Type: Research Paper
Journal: Renewable Energy

Dear Dr. Maria Yuliana,

This message is to acknowledge that we have received your revised manuscript for reconsideration for publication in Renewable Energy.

You may check the status of your manuscript by logging into the Elsevier Editorial System as an author at https://ees.elsevier.com/rene/.

Thank you for submitting your work to Renewable Energy.

Kind regards,

Elsevier Editorial System
Renewable Energy

****
For further assistance, please visit our customer support site at http://help.elsevier.com/app/answers/list/p/7923. Here you can search for solutions on a range of topics, find answers to frequently asked questions and learn more about EES via interactive tutorials. You will also find our 24/7 support contact details should you need any further assistance from one of our customer support representatives.

Elsevier Editorial System(tm) for Renewable Energy

Manuscript Draft

Manuscript Number: RENE-D-19-04543R1

Title: FEASIBILITY STUDY OF NANOCRYSTALLINE CELLULOSE AS ADSORBENT OF STERYL GLUCOSIDES FROM PALM-BASED BIODIESEL

Article Type: Research Paper

Keywords: biodiesel; steryl glucosides removal; nanocrystalline cellulose; adsorption isotherm; adsorption mechanism; feasibility study

Corresponding Author: Dr. Maria Yuliana, Ph.D.

Corresponding Author's Institution: Widya Mandala Catholic University Surabaya

First Author: Liangna Widdyaningsih

Order of Authors: Liangna Widdyaningsih; Albert Setiawan; Shella P Santoso, Ph.D.; Felycia E Soetaredjo, Ph.D.; Suryadi Ismadji, Ph.D.; Sandy B Hartono, Ph.D.; Yi-Hsu Ju, Ph.D.; Phuong Lan Tran-Nguyen, Ph.D.; Maria Yuliana, Ph.D.

Abstract: Increasing the content of biodiesel in the diesel fuel mixture faces some challenges due to the presence of steryl glucosides (SG) compounds, which causes the filter clogging and the reduction of engine power. In this study, coarse filter paper-based nanocrystalline cellulose (CFP-based NCC) with the crystallinity of 85.73% is selected as a potential adsorbent to separate SG compounds in palm-based biodiesel (PO-B100). The adsorption experiments were carried out at various CFP-based NCC to PO-B100 mass ratio (1:50, 1:75, 1:100, 1:125, 1:150, 1:175, 1:200) and temperature (65, 75, 85°C). The maximum SG removal was 91.81%, obtained at 75°C for CFP-based NCC to PO-B100 mass ratio of 1:50. The adsorption treatment also improves the cold stability of PO-B100 by reducing the cloud point from 13.2°C to 11.5°C. Langmuir isotherm model is best-fitted to the equilibrium adsorption data and thermodynamic studies suggested that the adsorption of SG onto the CFP-based NCC surface is spontaneous and endothermic. The isotherm and thermodynamic study showed that the mechanism governing the adsorption process may be driven by both dipole-dipole interactions and ion exchange. The adsorption results showed that CFP-based NCC has great affinity and selectivity to SG and can be considered as a promising adsorbent of SG.

FEASIBILITY STUDY OF NANOCRYSTALLINE CELLULOSE AS ADSORBENT OF STERYL GLUCOSIDES FROM PALM-BASED BIODIESEL

Liangna Widdyaningsih[a,1], Albert Setiawan[a,1], Shella Permatasari Santoso[1,2], Felycia Edi Soetaredjo[1,2], Suryadi Ismadji[1,2], Sandy Budi Hartono[1], Yi-Hsu Ju[2,3,4], Phuong Lan Tran-Nguyen[5], Maria Yuliana[1,*]

[1] Department of Chemical Engineering, Widya Mandala Catholic University Surabaya, Kalijudan 37, Surabaya 60114, Indonesia

[2] Department of Chemical Engineering, National Taiwan University of Science and Technology, 43 Keelung Road, Sec 4, Taipei, 10607, Taiwan

[3] Graduate Institute of Applied Science and Technology, National Taiwan University of Science and Technology, 43 Keelung Road, Sec 4, Taipei, 10607, Taiwan

[4] Taiwan Building Technology Center, National Taiwan University of Science and Technology, 43 Keelung Road, Sec 4, Taipei, 10607, Taiwan

[5] Department of Mechanical Engineering, Can Tho University, 3-2 Street, Can Tho City, Vietnam

*Corresponding authors: Tel. (62) 31 3891264; Fax. (62) 31 3891267; Email address: mariayuliana@ukwms.ac.id (M. Yuliana)

[a] These authors contributed equally to this work

*Cover Letter

Widya Mandala Catholic University Surabaya
Engineering Department
CHEMICAL ENGINEERING
Jl. Kalijudan 37 Surabaya 60114; Phone: +62 313893933 Fax: +62 31 3891267
Website: http://www.widyamandala.org, http://www.eng.wima.ac.id

February 3, 2020

Professor Soteris Kalogirou
Editor-in-Chief
Renewable Energy

Dear Professor Kalogirou,

On behalf of my co-author, I am writing to submit the revised manuscript for publication consideration in *Renewable Energy*. The details of the manuscript are as follows:

Title of Manuscript: **FEASIBILITY STUDY OF NANOCRYSTALLINE CELLULOSE AS ADSORBENT OF STERYL GLUCOSIDES FROM PALM-BASED BIODIESEL**

Authors: Liangna Widdyaningsih (liangna16@gmail.com), Albert Setiawan (albert.st12@gmail.com), Shella Permatasari Santoso (shella_p5@yahoo.com), Felycia Edi Soetaredjo (felyciae@yahoo.com), Suryadi Ismadji (suryadiismadji@yahoo.com), Sandy Budi Hartono (sandy@ukwms.ac.id), Yi-Hsu Ju (yhju@mail.ntust.edu.tw), Phuong Lan Tran-Nguyen (tnplan@ctu.edu.vn), Maria Yuliana

Corresponding author:
Maria Yuliana; Department of Chemical Engineering; Widya Mandala Catholic University Surabaya; Kalijudan 37, Surabaya 60114, Indonesia
Tel: (62) 31 3891264; Fax. (62) 31 3891267;
E-mail: mariayuliana@ukwms.ac.id

Keywords: *biodiesel; steryl glucosides removal; nanocrystalline cellulose; adsorption isotherm; adsorption mechanism; feasibility study*

We greatly appreciate the constructive comments and suggestions given by the editor and reviewers. We have addressed the major concerns of the reviewers and revised the manuscript accordingly. We also know of no conflicts of interest associated with this publication and there has been no significant financial support for this work that could have influenced its outcome. Furthermore, we have strictly prepared the manuscript in accordance with the journal and ethical guidelines.

Widya Mandala Catholic University Surabaya
Engineering Department
CHEMICAL ENGINEERING
Jl. Kalijudan 37 Surabaya 60114; Phone: +62 313893933 Fax: +62 31 3891267
Website: http://www.widyamandala.org, http://www.eng.wima.ac.id

Thank you for your consideration. I am looking forward to your positive response.

Sincerely yours,

Maria Yuliana

*Detailed Response to Reviewers

Widya Mandala Catholic University Surabaya
Engineering Department
CHEMICAL ENGINEERING
Jl. Kalijudan 37 Surabaya 60114; Phone: +62 313893933 Fax: +62 31 3891267
Website: http://www.widyamandala.org, http://www.eng.wima.ac.id

Journal: *Renewable Energy*
Title: **Feasibility study of nanocrystalline cellulose as adsorbent of steryl glucosides from palm-based biodiesel**

Dear Editor,

We appreciate your useful comments and suggestions on our manuscript. We have modified the manuscript accordingly, and detailed corrections are listed below:

Editor

1) You may include the papers cited by the reviewer/s only if these are relevant and improve the understanding of the paper
   Response: We have added only the relevant papers in the introduction section (p.2-3 line 34-44).

Reviewer #1

1) In manuscript, entitled "Feasibility study of nanocrystalline cellulose as adsorbent of steryl glucosides from palm-based biodiesel", authors describe sustainable biomass-derived successfully-applied coarse filter paper-based nano-crystalline cellulose material as an adsorbent in biodiesel purification process. Manuscript is appropriate for selected research journal; however, major article revision is required before acceptance.
   Response: We are grateful for the reviews provided by the reviewer. The comments are especially encouraging for the authors. The detailed responses to the comments are provided below.
2) General: space between number and unit is required (i.e. 60 °C, 15 m)
   Response: We have added space between the number and unit throughout the manuscript.
3) Introduction, page 2, line 35: "Biodiesel is generally derived from transesterification of agricultural or animal lipids and short-chain alcohols in the presence of a catalyst." – A bit more should be explained about biodiesel production operation, economics and optimisation, noting some relevant works available. Some relevant articles include Fuel Processing Technology. 2016, 142,

326, Fuel Processing Technology. 2014, 122, 30, and Bioresource technology. 2010, 101(10), 3333, but others should be found, expanding present literature review.

Response: We have added relevant articles to extend our literature review about biodiesel in p.2-3 line 34-44.

4) Introduction, page 2, line 39: What is considered ''cold''?

Response: Based on the authors' decision, we have replaced the term of "cold" to "white precipitates" in p.3 line 46, since this term is directly related to the problem/challenge encountered by the biodiesel manufacturers.

Meanwhile, regarding the question enquired by the reviewer, the cold temperature of biodiesel is actually location-dependent and not limited to a certain value, as stated in ASTM D6751. While it is one of the causes, the cold temperature is not the only trigger for precipitation, since in several cases, white precipitates have been also found at the temperature of slightly below 60 °C.

5) Materials and Methods, Preparation of NCC, page 5, line 100: What kind of filter material and pores size was used for filtration process?

Response: We have mentioned the type and pore size of the filter used for the filtration process of the delignified product in p.5 line 108.

6) Materials and Methods, Removal of SG using adsorption, page 7. Was the experiment done in parallels and how many repetitions were done?

Response: The adsorption experiments were carried out in parallel, with the various mass ratios of CFP-based NCC to PO-B100 introduced into a series of beakers for every temperature. The final results of SG removal shown in Figure 4 (p.32) were the average values of three independent experiments conducted in the same condition. We have also added the error bars of SG removal in Figure 4 (p.32).

7) Materials and Methods, Removal of SG using adsorption, page 7, line 144: Series of beaker glass should be corrected to series of beakers.

Response: We have corrected the phrase to a series of beakers in p.7 line 153.

8) Materials and Methods, Characterization of CFP-based NCC, page 6, lines 126: The maximum intensity of amorphous region is not at 2θ = 15 – 17°. This is peak for crystal plane 110. Moreover, authors calculated the CrI based on the Segal et al., which indeed used the same formula, however, the parameters used in the equation were not determined accurately. The amorphous region according to Segal, the

equation should include maximum intensity of crystalline region and maximum of amorphous (2θ = 18°) region, which is between 110 and 200 peaks.

Response: We have corrected the parameters in the equation and thoroughly revised the results and discussions according to the reviewer's comment in p.6 line 133-134 and p.9 line 193-196.

9) Results and discussion, page 8, line 177: the change of crystallinity has occurred

Response: We have revised the sentence according to the suggestion in p.9 line 196-197.

10) Results and discussion, page 8: How was crystallinity index calculated?. It is not clear.

Response: The crystallinity index was calculated using Equation 1 (p.6 line 132). We have also mentioned this equation in the results and discussions section (p.9 line 195-196)

11) Results and discussion, Characterization of CFP-based NCC, page 8, lines 186: Whatis the exact average and what is standard deviation? Or rephrase to '' The prepared CFP-based NCC has a homogenous needle-shaped with crystallite size in range of 2 – 4 nm''.

Response: We have rephrased the sentence according to the suggestion in p.9 line 205-206.

12) Results and discussion, FTIR – What does this spectra by itself explain? What can beconcluded from it? Adding spectra of CFP-NCC after adsorption might be helpful.

Response: The FTIR spectra presented in Figure 3 (a) depicted the functional groups of CFP-based NCC. In addition, we have also enclosed the spectra of CFP-based NCC after adsorption in Figure 3 (b) to verify the adsorption of SG onto the surface area of CFP-based NCC (p.31). The discussions for Figure 3 (b) have also been added in p.10 line 219-226.

13) Results and discussion Page 9, lines 211 & 212: A cross reference to section 3.3 would point out why these parameters (1:50, 75 °C, 1 h) were used.

Response: We have added a cross-reference to section 3.3 to further address why the parameters stated in p.11, line 240-241 were used.

14) Results and discussion, Study of adsorption isotherm and thermodynamic parameters:Equations and explanation of how were results calculated should be in materials and methods.

Response: We agree with the reviewer that all equations and descriptions of every calculation should be in the materials and methods section. Therefore, the

equations for thermodynamics study have been moved to p.8 line 184-185 in the section of materials and methods (equations 4 and 5). However, we still placed the equation describing the correlation between energy and Dubinin-Radushkevich constant (equation 6) in section 3.4 (p.14 line 323) since it is essential to explain the nature of the adsorption mechanism.

15) Results and discussion, Adsorption mechanism study, page 14, lines 332-336:Repeating what was already written in a section before.
Response: The repeated sentences have been removed from the paragraph and we have rewritten the sentence in p.16 line 364-366.
16) Correct the numbering of Section since 3.5 is missing.
Response: We have corrected the numbering of section 3.5 in p.15 line 353.
17) Figure 5: Use subscripts (C_e and Q_e) for the axis titles.
Response: We have used subscripts for the axis titles of Figure 6 (p.34).
18) Revision from a native speaker is suggested.
Response: The paper has been carefully revised by a native English speaker to improve the grammar and readability.

Reviewer #2

1) The authors presented the removal of SG from biodiesel. However, this work lacks in novelty in general. In addition, following comments need to be addressed prior further consideration.
Response: We greatly appreciated the constructive comments given by the reviewer. We have addressed the major concerns of the reviewer with the detailed responses provided below.
2) First highlight is not from this work
Response: We have removed the first highlight and added the new highlight in the third bullet point
3) Indonesia related background information is unnecessary in Introduction section.
Response: The Indonesia-related background has been removed from the introductory section, leaving only the commercial composition data of biodiesel blend. The introduction section has been also rewritten accordingly in p.2 line 25-30.
4) How did the experiment conditions were selected, need further justification/reference.
Response: We have added the reference for the selection of experimental

Widya Mandala Catholic University Surabaya
Engineering Department
CHEMICAL ENGINEERING
Jl. Kalijudan 37 Surabaya 60114; Phone: +62 313893933 Fax: +62 31 3891267
Website: http://www.widyamandala.org, http://www.eng.wima.ac.id

conditions in p.7 line 150-151.

5) Line 99, delignification method need justification/reference.
   Response: We have added the reference for the delignification method in p.5 line 104-106.
6) Line 149, SG measurement method need more detail/reference.
   Response: We have added the references for the measurement method in p.7 line 160-161. The results were also verified by the GC-FID analysis.
7) Figures need error bars and statistical analysis to identify the significance between treatment
   Response: We have added the error bars in Figure 4 (p.32) and the Pareto chart in Figure 5 (p.33) to identify the significance order of the adsorption parameter. The results and discussions section has been rewritten to include the brief statistical analysis result (p.13 line 289-294).

The manuscript has been resubmitted to your journal. We look forward to your positive response.

Sincerely yours,

Maria Yuliana

***Highlights**

Highlights:

- CFP-based NCC has been successfully applied to remove 91.81 % SG from PO-B100
- Highest SG removal rate obtained at 75 °C and NCC to PO-B100 mass ratio 1:50
- The cloud point of PO-B100 is reduced from 13.2 °C to 11.5 °C after adsorption
- The adsorption mechanism may be driven by dipole-dipole coupling and ion exchange
- CFP-based NCC has been found to have a great affinity and selectivity to SG

ABSTRACT

Increasing the content of biodiesel in the diesel fuel mixture faces some challenges due to the presence of steryl glucosides (SG) compounds, which causes the filter clogging and the reduction of engine power. In this study, coarse filter paper-based nanocrystalline cellulose (CFP-based NCC) with the crystallinity of 85.73 % is selected as a potential adsorbent to separate SG compounds in palm-based biodiesel (PO-B100). The adsorption experiments were carried out at various CFP-based NCC to PO-B100 mass ratio (1:50, 1:75, 1:100, 1:125, 1:150, 1:175, 1:200) and temperature (65, 75, 85 °C). The maximum SG removal was 91.81 %, obtained at 75 °C for CFP-based NCC to PO-B100 mass ratio of 1:50. The adsorption treatment also improves the cold stability of PO-B100 by reducing the cloud point from 13.2 °C to 11.5 °C. Langmuir isotherm model is best-fitted to the equilibrium adsorption data and thermodynamic studies suggested that the adsorption of SG onto the CFP-based NCC surface is spontaneous and endothermic. The isotherm and thermodynamic study showed that the mechanism governing the adsorption process may be driven by both dipole-dipole interactions and ion exchange. The adsorption results showed that CFP-based NCC has great affinity and selectivity to SG and can be considered as a promising adsorbent of SG.

Keywords: biodiesel; steryl glucosides removal; nanocrystalline cellulose; adsorption isotherm; adsorption mechanism; feasibility study

1. INTRODUCTION[1]

To date, petroleum diesel is used worldwide for transportation, manufacturing, power generation, construction and farming industries. However, disruption in crude market price and the long-term availability along with the nature deterioration due to its gas emission have become the major concerns for environmental sustainability [1]. Therefore, it is necessary to develop alternative fuels that are environmentally friendly, especially as a substitute for diesel fuel.

Of the several alternative fuels available, biodiesel is an alternative diesel fuel made from renewable biological resources [2]. Biodiesel is generally derived from transesterification of agricultural or animal lipids and short-chain alcohols in the presence of a catalyst. Conventional base-catalyzed transesterification in a batch stirred-tank reactor is the most common technique used to produce the commercially available biodiesel [3]. Several modifications on the conversion route as well as the reactor configuration and design have been performed in order to create, optimize and intensify the continuous production of biodiesel. The transesterification using catalyst-free subcritical [4–6] or supercritical alcohol [7,8], as well as heterogeneous [9] or enzymatic catalyst [9,10], gain wide attention in

[1] **Abbreviation**

SG	Steryl glucoside(s)
MG	Monoacylglyceride(s)
DG	Diacylglyceride(s)
TG	Triacylglyceride(s)
CFP	Coarse filter paper
NCC	Nanocrystalline cellulose
FAME	Fatty Acid Methyl Ester(s)
PO-B100	Palm-based biodiesel

improving the continuity of biodiesel production. Likozar et al. (2016) also introduced a simple and robust design of a tubular reactor with a static mixer to intensify the mass transfer rate between the reactants and increase the biodiesel conversion rate. Their work also studied the chemical equilibrium and reaction kinetics at different operating parameters to optimize the product yield [11].

While biodiesel is currently mass-produced and a large number of studies have been carried out to improve its performance in various aspects, the white precipitates are still a challenge for its manufacturers. Although biodiesel distributed around the country must conform to the fuel property specifications as controlled by ASTM D6751, white precipitates were often detected in biodiesel and its blends during storage [12]. Several cases even showed that suspended particles in biodiesel have been found shortly after the production and at a rather high temperature (slightly below 60 °C) [13]. The white precipitates may cause filter plugging in engine systems [13,14]. This phenomenon was also observed in many biodiesel plants and hence frequent maintenance and process modification are often essential to maintain plant effectiveness and efficiency.

The presence of steryl glucosides (SG), which is one of the plant sterols, has been identified as the major component of the white precipitates. It mostly presents in biodiesel with a concentration of 35 ppm or higher [15]. The existence of this dispersed particles of SG promotes the aggregation of other components in biodiesel, saturated monoacylglycerides (MG) and diacylglycerides (DG), and subsequently affects the cold flow stability of fuel and widespread use [16].

Several techniques have been conducted to minimize the SG content in the biodiesel product, namely enzymatic hydrolysis [17,18], adsorption using magnesium silicate and bleaching earth [16] and ultrafiltration [19]. SG removal by enzymatic hydrolysis resulted in 81 % removal efficiency with the addition of a synthetic codon-optimized version of the LacS

gene expressed from *E. coli* with the total operating time of 7 h [17]. Na-Ranong et al. (2015) reported that the conventional adsorption using magnesium silicate and bleaching earth in temperature of 65-80 °C yielded in 81.4-82.5 % removal efficiency of SG [16]. Tremblay and Montpetit (2017) stated that the highest separation for SG (86 %) by ultrafiltration was obtained when the biodiesel was transesterified using 0.7 % (w/w) catalyst and 4:1 methanol:soybean oil molar ratio [19]. Based on the removal efficiency and economic feasibility, the adsorption treatment is a potential method to reduce SG content as well as to improve the cold flow properties of the fuel in the industrial scale because it is found to be effective and facile, time-saving and energy-efficient.

The development of adsorbent for effective adsorption has been conducted using various types of materials. Currently, the development of cellulosic adsorbent received major interest because it is renewable, biodegradable, low cost, and non-toxic [20]. Cellulosic adsorbents have the ability to meet the requirement of being a biosorbent, as it is abundantly available as a natural biopolymer. Cellulose in the form of nanocrystalline cellulose (NCC) has been widely studied due to its extensive industrial application, namely enzyme immobilization, adsorption, catalysis, drug delivery, biosensors and bio-imaging [21]. NCC, with a large specific surface area and plenty of surface hydroxyl and anionic sulfate ester group for physical and chemical reactions [22–24], can be considered as a new promising adsorbent for SG removal.

As the Indonesian government plans to increase the use of biodiesel in diesel blend from B20 to B30 in the time span of 5 years, the use of NCC for SG removal and improvement of the cold stability is an interesting topic to be studied. The objective of this study is to observe the feasibility of coarse filter paper-based NCC (CFP-based NCC) as the adsorption agent for SG. Various operating parameters, namely temperature, and the mass

ratio of CFP-based NCC to palm-based biodiesel (PO-B100) will be monitored. The adsorption mechanism was also proposed based on the isotherm and thermodynamics study.

2. MATERIALS AND METHODS

2.1 Materials

PO-B100 was collected from a local palm oil manufacturer in Gresik, Indonesia, and stored for 3 days at room temperature prior to the adsorption experiment. Coarse filter paper (CFP) as the cellulosic material was obtained from a local supplier in Surabaya, Indonesia. Sulphuric acid, sodium hydroxide, ethyl acetate, and n-hexane were purchased from Merck, Germany. FAMEs standard 47885 U contains 37 components FAME mix and SG standard 1117 were procured from Supelco (Bellefonte, PA, USA) and Matreya (State College, PA, USA), respectively. Nitrogen gas (99.9 % purity) was purchased from Aneka Gas Industry Pty. Ltd., Surabaya. All reagents were of analytical grade and required no further purification.

2.2 Preparation of NCC

CFP was ground into fibrous powder before use. The non-cellulosic material of CFP was subsequently removed to obtain purified cellulose using the modified method of Putro et al. (2017) [25]: 12 grams of the CFP powder was delignified using 0.1 g/ml sodium hydroxide aqueous solution (40 ml). The delignified product was washed with distilled water and filtrated three times through a Whatman 1 (11 μm pore size) filter paper before being dried under vacuum at 80 °C for 12 hours.

CFP-based NCC was prepared by using acid hydrolysis following the procedure conducted by Putro et al. (2017) [25]. 1 gram of delignified cellulose was hydrolyzed with 20 ml sulphuric acid 64 % at 45 °C for 75 min under constant agitation. The reaction time was selected to ensure high reaction efficiency. After the specified duration, the reaction was

immediately quenched using 20-fold of cold distilled water. The suspension was centrifuged at 4500 rpm for 10 min to remove the excess acid solution. The resulting precipitates were dialyzed against distilled water until neutral pH was achieved. The colloidal suspension was subjected to sonication treatment for 30 min in a cooling bath to avoid overheating and subsequently subjected to vacuum drying at 80 °C for 6 h to obtain CFP-based NCC powder.

2.3 Characterization of CFP-based NCC

The surface morphologies of the CFP-based NCC particles were analyzed on a field emission scanning electron microscope (FESEM) JEOL JSM-6500F (Jeol Ltd., Japan), with an accelerating voltage of 5 – 10 kV and 9.5 – 9.6 mm working distance. The CFP-based NCC powder was attached to a stub, sputtered and coated with gold prior to analysis. Fourier Transform Infrared (FTIR) analysis was performed by an FTIR-8400S spectrophotometer (Shimadzu, Japan) in the range of 400 – 4000 cm^{-1} at a 4 cm^{-1} scanning resolution. XRD analysis was conducted by an X'PERT Panalytical Pro X-Ray diffractometer (Philips-FEI, Netherlands) with monochromatic Cu $K\alpha_1$ radiation at wavelength (λ) = 0.154 nm, 40 kV of voltage and 30 mA of tube current. The diffraction pattern was acquired in the range of 5° to 60° (2θ angle). The crystallinity index (CrI) was expressed according to the following equation, as proposed by Segal et al. (1959) [26].

$$\mathrm{CrI}\ (\%) = \frac{(I_{200} - I_{am})}{I_{200}} x100 \quad (1)$$

Where I_{200} is the maximum intensity of the 200 lattice diffraction at 2θ around 22°, I_{am} is the maximum intensity of the amorphous region at 2θ = 18°. The crystallite size (nm) was calculated using the Scherrer analysis.

2.4 Compositional study of SG in PO-B100 using GC-FID analysis

The analysis of SG composition in PO-B100 was carried out using GC-17A (Shimadzu, Japan), completely equipped with a split/splitless injector and a flame ionization detector (FID). The separation was performed using nonpolar capillary column DB-5HT (5 %-phenyl)-methylpolysiloxane (15 m x 0.32 mm ID, Agilent Technology, CA). The column temperature was initially set at 80 °C, then subsequently ramped to 365 °C at the rate of 15 °C/min, and held constant for 19 min. The temperature of the injector and detector were adjusted constant at 370 °C. 100 mg of SG was dissolved in 1 ml ethyl acetate and subjected to filtration using polyvinylidene difluoride (PVDF) filter prior analysis. The prepared sample (1 µl) was injected into the GC with a split ratio of 1:50. The velocity of nitrogen (N_2, 99.9 %) as the carrier gas was fixed at 30 cm/s at 80 °C.

2.5 Removal of SG using adsorption

The adsorption of SG from PO-B100 was conducted in a batch mode according to the study conducted by Na-Ranong et al. (2015) with a few modifications [16]. A various mass ratio of CFP-based NCC to PO-B100 (1:50, 1:75, 1:100, 1:125, 1:150, 1:175, 1:200) was introduced into a series of beakers, where the mixture will be subjected to a 1-hour adsorption process at constant temperature and agitation speed (250 rpm). The selection of adsorption duration was based on the preliminary experiment conducted to find the equilibrium time. Several adsorption temperatures (65, 75 and 85 °C) were used to study the effect of temperature on the adsorption of SG. The solution was separated from the adsorbent by using centrifugation at the rotational speed of 4900 rpm for 10 min. The SG contents in PO-B100 before and after adsorption were analyzed using UV-mini 1240 spectrophotometer (Shimadzu, Japan) at 240 nm, according to the modified technique conducted by Moreau et al. (2008), Nyström (2007) and Araújo et al. (2013) [14,27,28]. The percentage of SG removal was determined by using the following equation.

$$SG\ removal\ (\%) = \frac{C_i - C_f}{C_i} x100 \quad (2)$$

Where C_i is the concentration of SG in untreated PO-B100 (mg/kg) and C_f is the concentration of SG in treated (after adsorption) PO-B100 (mg/kg). The results of SG removal were verified by using GC-FID analysis (see section 2.4) and its statistical approach was performed using Minitab software (version 18.1) to identify the significance order of the parameters affecting the adsorption.

2.6 Isotherm and thermodynamics study of the SG adsorption

The adsorption isotherm was conducted at the temperature of 65, 75 and 85 °C with various CFP-based NCC to PO-B100 mass ratio (1:50, 1:75, 1:100, 1:125, 1:150, 1:175, 1:200). It was performed using a similar procedure as previously mentioned in subsection 2.5. At the equilibrium condition, the amount of adsorbed SG per unit mass of CFP-based NCC as the adsorbent (Q_e) was calculated by the equation below.

$$Q_e\left(\frac{mg}{g}\right) = \frac{C_o - C_e}{m} x\ V \quad (3)$$

Where C_o and C_e are the initial and final (equilibrium) concentration of SG in PO-B100 (mg/L), respectively, m is the mass of adsorbent (g) and V is the volume of PO-B100 (L).

The equilibrium data obtained at various temperature were fitted to the three isotherm models, namely Langmuir, Freundlich and Dubinin-Radushkevich (D-R). Meanwhile, the thermodynamic parameters such as Gibbs free energy change (ΔG°), enthalpy (ΔH°) and entropy (ΔS°) were further determined from the results of isotherm study using equation (4) and (5).

$$\Delta G° = -RTln(K_L.M_{SG}.10^3.C^o) \quad (4)$$

$$\Delta G° = \Delta H° - T\Delta S° \quad (5)$$

188 Where R is the gas constant with the value of 8.314 J/mol.K, T is the absolute temperature in
189 Kelvin, K_L is Langmuir equilibrium constant in L/mg, M_{SG} is the molecular weight of SG in
190 g/mol and C^o is the reference concentration in standard state with the value of 1 mol/L.
191

192 **3. RESULTS AND DISCUSSIONS**

193 *3.1 Characterization of CFP-based NCC*

194 The X-ray diffraction pattern of the CFP and its NCC are shown in Figure 1, and the
195 corresponding crystallinity index is presented in Table 1. Both XRD patterns showed the
196 cellulose I characteristic peaks at 2θ around 15 – 17° (110 crystal plane) and 22 – 23° (200
197 crystal plane) [26,29]. The crystallinity index of CFP and its NCC were calculated using
198 equation (1) and recorded to have the corresponding value of 57.60 % and 85.73 %. The
199 change of crystallinity has occurred because of the progressive removal of amorphous
200 hemicellulose and lignin during acid hydrolysis. The highly crystalline product is more
201 efficient to improve the mechanical properties of the composite material, particularly as an
202 adsorbent, since crystallinity positively corresponds to the tensile strength of the material [30].

203 **Figure 1**

204 **Table 1**

205 The scanning electron micrograph in Figure 2 shows the shape and size of the CFP-
206 based NCC. The distribution of NCC products derived from CFP was estimated to have
207 approximately 200-400 nm in length (Figure 2). The prepared CFP-based NCC has a
208 homogenous needle-shaped with crystallite size in the range of 2 – 4 nm, obtained from the
209 combination of X-ray diffraction data and Scherrer analysis. The homogenous CFP-based
210 NCC particles are likely caused by the swollen of cellulose fibers due to NaOH
211 delignification pretreatment [25].

212 **Figure 2**

213 Figure 3 (a) – (b) illustrated the FTIR spectra of CFP-based NCC before and after
214 adsorption. As shown in Figure 3 (a), several peaks representing certain functional groups in
215 CFP-based NCC were found in the spectra. The broad band in the range of 3008 – 3459 cm^{-1}
216 represents the O-H stretching vibrations, while the peaks in the range of 2802 – 2925 cm^{-1}
217 correspond to C-H stretching vibrations. The absorption at 936 – 1137 cm^{-1} is related to the
218 functional group of C-O-C, and the peak at 1640 cm^{-1} indicates the presence of abundant
219 hydrophilic hydroxide group in the cellulose [31]. A peak at 1382 cm^{-1} represents the C-H
220 asymmetric deformations [32].

221 Meanwhile, Figure 3 (b) showed strong peaks in the wavenumbers of around 1019 –
222 1376 cm^{-1} and 2602 – 3160 cm^{-1}, which represent the C-O moiety, and CH_2 and CH_3
223 stretching vibrations. These two specific peaks are known as the fingerprint areas for SG.
224 Another peak at 1750 cm^{-1} corresponds to the typical C=O stretching band of the methyl ester,
225 while an O-H band around 3110 - 3700 cm^{-1} indicates the presence of hydroxyl groups in SG
226 and CFP-based NCC [33]. Therefore, based on the FTIR spectra, it can be concluded that SG
227 is the major component of the adsorbate on the surface of CFP-based NCC, which is
228 consistent with the GC-FID results discussed in section 3.2.

229 **Figure 3**

230

231 *3.2 Properties of PO-B100*

232 The properties of PO-B100 have been analyzed according to the standard method of
233 ASTM for its content of FAME, acid value (AV), MG, DG and triglycerides (TG). As
234 reported in Table 2, the purity of FAME in PO-B100 is 98.7 %, while the AV, MG, DG, and
235 TG values are 0.12 mg KOH/g, 0.23 %, 0.09 %, and 0.06 %, respectively. Furthermore, PO-

236 B100 feedstock contained 194.1 mg/kg of SG with the cloud point of 13.2 °C and a clear
237 initial appearance. Based on the GC-FID analysis, the SG profile in PO-B100 consists of
238 34.79 % of campesteryl glucoside, 23.73 % of stigmasteryl glucoside and 41.48 % of β-
239 sitosteryl glucoside. The results met the requirements of ASTM D6751 and SNI 7182:2015.
240 However, white precipitates could be found within a few hours after production.

241 **Table 2**

242 After the adsorption using the parameters giving the highest SG removal (1:50, 75 °C,
243 1 h; see section 3.3), the sample of treated PO-B100 was collected for the properties
244 measurement in order to monitor the effect of the adsorbent. According to the results, the
245 treated PO-B100 contained FAME with a purity of 98.8 % and AV value of 0.11 mg KOH/g.
246 The concentration of SG reduced significantly to 15.9 mg/kg with the composition of 24.81 %
247 campesteryl glucoside, 25.07 % stigmasteryl glucoside and 50.12 % β-sitosteryl glucoside,
248 while the other glycerides components, MG, DG, and TG, were slightly decreased to 0.22 %,
249 0.09 %, 0.05 %, respectively. The cloud point of the treated PO-B100 was also found to be
250 decreased to 11.5 °C. These results indicated that CFP-based NCC has selectivity to adsorb
251 SG, particularly campesteryl glucoside and stigmasteryl glucoside, as compared to the other
252 minor components, such as MG, DG, and TG. It also subsequently lowered the cloud point
253 significantly, which is advantageous for storage and transportation purposes [34].

254

255 *3.3 Adsorption of SG using CFP-based NCC*

256 Figure 4 summarized the SG removal rate at the various temperature and mass ratios
257 of CFP-based NCC to PO-B100. The highest value of the SG removal rate (91.81 %) was
258 obtained at the following conditions: 75 °C, CFP-based NCC to PO-B100 mass ratio of 1:50,
259 and 1 h adsorption time. Based on the results shown in Figure 4, the lowest removal rate of
260 SG in every adsorption temperature was seen at 1:200 of CFP-based NCC to PO-B100 mass

ratio. It was likely due to insufficient binding and active adsorption sites and the adsorption required more time to reach the equilibrium stage. The removal percentage of SG was observed to have amplified with the increase of CFP-based NCC to PO-B100 mass ratio from 1:200 to 1:50 at all temperatures in the tested range. Greater amounts of CFP-based NCC provide greater adsorption surface area and active sites in CFP-based NCC, leading to an adequate SG binding area and certainly, a higher percentage of SG removal [35]. It was also monitored that the SG removal rate exponentially increased when the CFP-based NCC to PO-B100 mass ratio was increased from 1:100 to 1:50 in the all adsorption temperature**.** The phenomenon indicated the good dispersion ability of CFP-based NCC in PO-B100, where constant diffusion path length of SG binding to CFP-based NCC surface was found regardless of the amount of adsorbent [36].

Figure 4

As depicted in Figure 4, temperature also remarkably affected the SG reduction. A temperature elevation from 65 °C to 75 °C improves the reduction of SG, regardless of CFP-based NCC to PO-B100 mass ratio. Chowdhury et al. (2011) stated that the adsorption enhancement along with the temperature increase may be associated with the increase of the number of active sites available for adsorption. The diffusion rate of the adsorbate across the external boundary layer also escalates with the rise in temperature, due to lower solution viscosity and enhancement in the mobility and kinetic energy of the adsorbate [37]. Therefore, the collision between particles intensifies with the temperature elevation so that the activation energy of the adsorption process is easier to achieve. As a result, the amount of the adsorbed SG enhances along with the temperature increase. However, it was also observed that the SG removal rate decreased when the temperature was further escalated from 75 °C to 85 °C. More (2018) mentioned that after reaching a certain temperature, excessive particle collision causes the removal of adsorbates from the adsorbent, leading to lower adsorption capacity

[38]. Lee et al. (2019) also stated that the NCC surface binding generally weakens along with the temperature enhancement [36]. The fluctuations of the SG uptake observed with the change in temperature suggests that the SG adsorption is governed by both physical attraction and chemical bonding, indicating that the sorption of SG by CFP-based NCC is both driven by physical and chemical sorption [37,39].

Figure 5 presented the Pareto chart of the standardized effect generated using statistical analysis (Minitab version 18.1). The figure showed that both independent parameters (temperature and the mass ratio of CFP-based NCC to PO-B100) were found to be prominent with the significance order of the mass ratio of CFP-based NCC to PO-B100 > temperature. The other quadratic and two-way interaction terms were also found to significantly affect the SG removal rate.

Figure 5

3.4 Study of adsorption isotherm and thermodynamic parameters

In this study, three isotherm equations were fitted to the experimental equilibrium data for SG at three temperature points (65 °C, 75 °C and 85 °C). The results are presented in Table 3 and the isotherm models are plotted in Figure 6. The Langmuir isotherm constant, K_L and maximum absorption capacity, $Q_{m(L)}$ were calculated from the nonlinear curve fitting between Q_e and C_e. The value of $Q_{m(L)}$ was found to be increased from 12.50 mg/g at 65 °C to 12.93 mg/g at 75 °C before declining to 11.24 mg/g at the highest tested temperature (85 °C). The $Q_{m(L)}$ results are quite comparable to the adsorption capacity of magnesium silicate and bleaching earth on the SG (~13 mg/g) [16]. The Langmuir constant (K_L) also increases along with the temperature, from 0.11 L/mg at the lowest temperature (65 °C) to 0.26 L/mg at the highest temperature point (85 °C), indicating that the adsorption of SG to CFP-based NCC is an endothermic process.

Table 3

Figure 6

The isotherm data were further analyzed by the Freundlich model. The Freundlich constant K_F and 1/n were obtained from the non-linear regression analysis. Table 3 showed that the values of 1/n are all under unity, ranging from 0.03 at 75 °C to 0.16 at 65 °C. The extent of 1/n represents the favorability degree of adsorption. The value of 1/n less than unity corresponds to favorable sorption. It was also observed that the Freundlich constant greatly escalates along with the temperature, implying that the adsorption was favorable at high temperature and the process is certainly endothermic. de Sá et al. (2017) mentioned that 1/n value between 0 and 1 is associated with a chemisorption process [40].

Another isotherm equation, the Dubinin-Radushkevich (D-R) model, was further applied to analyze the equilibrium data, particularly to determine the nature of SG adsorption onto CFP-based NCC surface. The D-R constant (β) gives an idea about the mean sorption energy, E, and their correlation can be expressed by the following equation:

$$E = \frac{1}{\sqrt{2\beta}} \quad (6)$$

where E represents sorption energy (kJ/mol) and β is the D-R constant ($mmol^2/J^2$). The value of sorption energy provides information to determine the type of adsorption mechanism, as chemical ion exchange or physical adsorption. Li et al. (2009) and Zhu et al. (2009) stated that if the sorption energy ranges from 8 to 16 kJ/mol, the sorption process is supposed to be chemisorption, while for energy value lower than 8 kJ/mol, the sorption is of physical nature [41,42]. Based on the results provided in Table 3, the adsorption mechanism is physical attraction since the E values for all tested temperatures are lower than 8 kJ/mol. The highest $Q_{m(D\text{-}R)}$ was found at 75 °C with a value of 12.13 mg/g, which was similar to the result obtained using Langmuir isotherm. The effect of temperature previously studied also

335 provides similar results where the temperature of 75 °C gives the highest SG removal rate
336 compared to the other tested temperatures.

337 The correlation coefficient (r^2) and chi-square (χ^2) values of the three isotherms are
338 also listed in Table 3. It could be concluded that the adsorption of SG onto the CFP-based
339 NCC surface is best fitted to the Langmuir isotherm equation under the temperature range
340 studied. Based on the three isotherm models studied, the adsorption mechanism is predicted
341 to be driven by both physical and chemical sorption due to its sorption energy value and
342 endothermic nature, respectively. The overall results of this study showed that NCC has a
343 particular affinity for SG and is an effective adsorbent for SG removal from PO-B100.

344 Table 4 listed the thermodynamics parameters of the SG adsorption onto the surface
345 of NCC, such as Gibbs free energy change (ΔG°), enthalpy (ΔH°) and entropy (ΔS°). The
346 values of Gibbs free energy (ΔG°) for the adsorption of SG were negative at all tested
347 temperatures. These values confirm the spontaneous nature of SG adsorption onto the CFP-
348 based NCC. Enhancement of the ΔG° value along with the increasing temperature implies
349 that the affinity of SG on CFP-based NCC was higher at high temperature. Positive ΔH°
350 value (42.90 kJ/mol) verifies that the adsorption is indeed an endothermic process, while the
351 absolute value of ΔS° (219.80 J/mol.K) reflects the increased randomness at the solid-
352 solution interface during the adsorption process [37,43].

353 **Table 4**

354

355 *3.5 Adsorption mechanism study*

356 The study of the adsorption mechanism was used to further illustrate the interaction
357 between SG and CFP-based NCC surface. Two important points have to be considered to
358 understand the mechanism, namely the surface properties of the adsorbent and the structure
359 of adsorbate. The NCC molecule was constructed by a substantial number of hydrogen bonds

between glucose units or glucose chains inside the molecule to form a very stable structure [44,45]. NCC contains the majority of oxygen functional groups such as hydroxyl, ether, and sulfonate. While the hydroxyl and ether groups are originally present in the cellulosic material, the sulfonate group existed due to the acid hydrolysis to produce NCC. On the other hand, SG was built by a steryl cation (SC^+) and a glucose unit, with a positive charge on the cationic steryl part.

According to the findings of this study, the adsorption was temperature-dependent and the isotherm modeling showed an equal contribution of physical attraction and chemical binding. Therefore, the mechanism of SG removal by adsorption on the CFP-based NCC surface may be presumed to involve these following steps:

- Migration of SG from the bulk of PO-B100 to the CFP-based NCC surface
- Diffusion of SG through the boundary layer to the CFP-based NCC surface
- Adsorption of SG on the surface of CFP-based NCC, which may be caused by physical interaction of dipole-dipole coupling between the positively charged SC^+ and the negatively charged NCC surface as suggested in Figure 7; and through a possible chemical binding mechanism of ion exchange as shown below:

  $$NCC - OH \leftrightarrow NCC - O^- + H^+$$

  $$NCC - SO_3^- \leftrightarrow NCC - SO_3^-$$

  $$NCC - O^- + SC^+ \leftrightarrow NCC - O - SC$$

  $$NCC - SO_3^- + SC^+ \leftrightarrow NCC - O - SO_3$$

- Intraparticle diffusion of SG into the pores of CFP-based NCC

Figure 7

4. CONCLUSIONS

CFP-based NCC was successfully used as an adsorbent for reducing SG in PO-B100. The content of SG was able to be reduced from 194.1 mg/kg to as low as 15.9 mg/kg (91.81 % removal rate) within 1 hour at the temperature of 75 °C using CFP-based NCC to PO-B100 mass ratio of 1:50. The study proved that CFP-based NCC has great affinity and selectivity to SG, particularly on the campesteryl glucoside and stigmasteryl glucoside. The adsorption treatment greatly improves the cold stability of PO-B100 by reducing the cloud point from 13.2 °C to 11.5 °C, while slightly affected the purity of FAME, AV and other minor components, such as MG, DG, and TG, which were still in the acceptable range according to ASTM D6751. The adsorption process was endothermic and may be driven by both physical attraction and chemical ion exchange. The adsorption treatment using CFP-based NCC should be a prospective method used to remove SG from PO-B100 since it possesses high efficiency, time-saving and energy-efficient.

ACKNOWLEDGMENT

This research did not receive any specific grant from funding agencies in the public, commercial or not-for-profit sectors.

REFERENCES

[1] N. Kumar, A. Sonthalia, H. S. Pali, Sidharth, Alternative Fuels for Diesel Engines: New Frontiers, Diesel Engines [Working Title]. (2018) 1–27. doi:10.5772/intechopen.80614.

[2] A.C. Pinto, L.L.N. Guarieiro, M.J.C. Rezende, N.M. Ribeiro, A. Ednildo, Biodiesel : An Overview, 16 (2005) 1313–1330.

[3] Z. Qiu, L. Zhao, L. Weatherley, Process intensification technologies in continuous biodiesel production, Chem. Eng. Process. Process Intensif. 49 (2010) 323–330. doi:10.1016/j.cep.2010.03.005.

[4] Y.H. Ju, L.H. Huynh, Y.A. Tsigie, Q.P. Ho, Synthesis of biodiesel in subcritical water and methanol, Fuel. 105 (2013) 266–271. doi:10.1016/j.fuel.2012.05.061.

[5] S. Thiruvenkadam, S. Izhar, Y. Hiroyuki, R. Harun, One-step microalgal biodiesel production from Chlorella pyrenoidosa using subcritical methanol extraction (SCM) technology, Biomass and Bioenergy. 120 (2019) 265–272. doi:10.1016/j.biombioe.2018.11.037.

[6] F.H. Santosa, L. Laysandra, F.E. Soetaredjo, S.P. Santoso, S. Ismadji, M. Yuliana, A facile noncatalytic methyl ester production from waste chicken tallow using single step subcritical methanol: Optimization study, Int. J. Energy Res. 43 (2019) 8852–8863. doi:10.1002/er.4844.

[7] M. Aghilinategh, M. Barati, M. Hamadanian, Supercritical methanol for one put biodiesel production from chlorella vulgaris microalgae in the presence of CaO/TiO 2 nano-photocatalyst and subcritical water, Biomass and Bioenergy. 123 (2019) 34–40. doi:10.1016/j.biombioe.2019.02.011.

[8] L.K. Ong, C. Effendi, A. Kurniawan, C.X. Lin, X.S. Zhao, S. Ismadji, Optimization of catalyst-free production of biodiesel from Ceiba pentandra (kapok) oil with high free fatty acid contents, Energy. 57 (2013) 615–623. doi:10.1016/j.energy.2013.05.069.

[9] M.K. Lam, K.T. Lee, A.R. Mohamed, Homogeneous, heterogeneous and enzymatic catalysis for transesterification of high free fatty acid oil (waste cooking oil) to biodiesel: A review, Biotechnol. Adv. 28 (2010) 500–518. doi:10.1016/j.biotechadv.2010.03.002.

[10] L.P. Christopher, Hemanathan Kumar, V.P. Zambare, Enzymatic biodiesel: Challenges and opportunities, Appl. Energy. 119 (2014) 497–520. doi:10.1016/j.apenergy.2014.01.017.

[11] B. Likozar, A. Pohar, J. Levec, Transesterification of oil to biodiesel in a continuous tubular reactor with static mixers: Modelling reaction kinetics, mass transfer, scale-up and optimization considering fatty acid composition, Fuel Process. Technol. 142 (2016) 326–336. doi:10.1016/j.fuproc.2015.10.035.

[12] I. Lee, L.M. Pfalzgraf, G.B. Poppe, E. Powers, T. Haines, The role of sterol glucosides on filter plugging, Biodiesel Mag. 4. (2007) 105–112.

[13] V. Van Hoed, N. Zyaykina, W. De Greyt, J. Maes, R. Verhé, K. Demeestere, Identification and occurrence of steryl glucosides in palm and soy biodiesel, JAOCS, J. Am. Oil Chem. Soc. 85 (2008) 701–709. doi:10.1007/s11746-008-1263-5.

[14] R.A. Moreau, K.M. Scott, M.J. Haas, The identification and quantification of steryl glucosides in precipitates from commercial biodiesel, JAOCS, J. Am. Oil Chem. Soc. 85 (2008) 761–770. doi:10.1007/s11746-008-1264-4.

[15] H. Tang, S.O. Salley, K.Y. Simon Ng, Fuel properties and precipitate formation at low temperature in soy-, cottonseed-, and poultry fat-based biodiesel blends, Fuel. 87 (2008) 3006–3017. doi:10.1016/j.fuel.2008.04.030.

[16] D. Na-Ranong, P. Laungthaleongpong, S. Khambung, Removal of steryl glucosides in palm oil based biodiesel using magnesium silicate and bleaching earth, Fuel. 143 (2015) 229–235. doi:10.1016/j.fuel.2014.11.049.

[17] A. Aguirre, S. Peiru, F. Eberhardt, L. Vetcher, R. Cabrera, H.G. Menzella, Enzymatic hydrolysis of steryl glucosides, major contaminants of vegetable oil-derived biodiesel,

450 Appl. Microbiol. Biotechnol. 98 (2014) 4033–4040. doi:10.1007/s00253-013-5345-4.

451 [18] S. Peiru, A. Aguirre, F. Eberhardt, M. Braia, R. Cabrera, H.G. Menzella, An industrial
452 scale process for the enzymatic removal of steryl glucosides from biodiesel,
453 Biotechnol. Biofuels. 8 (2015). doi:10.1186/s13068-015-0405-x.

454 [19] A.Y. Tremblay, A. Montpetit, The in-process removal of sterol glycosides by
455 ultrafiltration in biodiesel production, Biofuel Res. J. 4 (2017) 559–564.
456 doi:10.18331/brj2017.4.1.6.

457 [20] M.Y. Chang, R.S. Juang, Adsorption of tannic acid, humic acid, and dyes from water
458 using the composite of chitosan and activated clay, J. Colloid Interface Sci. 278 (2004)
459 18–25. doi:10.1016/j.jcis.2004.05.029.

460 [21] A.G. Varghese, S.A. Paul, M.S. Latha, Green Adsorbents for Pollutant Removal, 2018.
461 doi:10.1007/978-3-319-92111-2.

462 [22] M. Börjesson, G. Westman, Crystalline Nanocellulose — Preparation, Modification,
463 and Properties, Cellul. - Fundam. Asp. Curr. Trends. (2015). doi:10.5772/61899.

464 [23] H. Voisin, L. Bergström, P. Liu, A. Mathew, Nanocellulose-Based Materials for Water
465 Purification, Nanomaterials. 7 (2017) 57. doi:10.3390/nano7030057.

466 [24] H. Liang, X. Hu, A quick review of the applications of nano crystalline cellulose in
467 wastewater treatment, J. Bioresour. Bioprod. 2016 (2016) 199–204.
468 www.Bioresources-Bioproducts.com.

469 [25] J.N. Putro, S.P. Santoso, S. Ismadji, Y.H. Ju, Investigation of heavy metal adsorption
470 in binary system by nanocrystalline cellulose – Bentonite nanocomposite:
471 Improvement on extended Langmuir isotherm model, Microporous Mesoporous Mater.
472 246 (2017) 166–177. doi:10.1016/j.micromeso.2017.03.032.

473 [26] L. Segal, J.J. Creely, A.E. Martin, C.M. Conrad, An Empirical Method for Estimating
474 the Degree of Crystallinity of Native Cellulose Using the X-Ray Diffractometer, Text.
475 Res. J. 29 (1959) 786–794. doi:10.1177/004051755902901003.

476 [27] L. Nyström, Occurrence and properties of steryl ferulates and glycosides in wheat and
477 rye, University of Helsinki, 2007.

478 [28] L.B.D.C. Araújo, S.L. Silva, M.A.M. Galvão, M.R.A. Ferreira, E.L. Araújo, K.P.
479 Randau, L.A.L. Soares, Total phytosterol content in drug materials and extracts from
480 roots of Acanthospermum hispidum by UV-VIS spectrophotometry, Brazilian J.
481 Pharmacogn. 23 (2013) 736–742. doi:10.1590/S0102-695X2013000500004.

482 [29] M.N.A.M. Taib, W.A. Yehye, N.M. Julkapli, Influence of Crosslinking Density on
483 Antioxidant Nanocellulose in Bio-degradation and Mechanical Properties of Nitrile
484 Rubber Composites, Fibers Polym. 20 (2019) 165–176. doi:10.1007/s12221-019-8575-
485 y.

486 [30] Y. Hu, L. Tang, Q. Lu, S. Wang, X. Chen, B. Huang, Preparation of cellulose
487 nanocrystals and carboxylated cellulose nanocrystals from borer powder of bamboo,
488 Cellulose. 21 (2014) 1611–1618. doi:10.1007/s10570-014-0236-0.

489 [31] A. Alemdar, M. Sain, Isolation and characterization of nanofibers from agricultural
490 residues - Wheat straw and soy hulls, Bioresour. Technol. 99 (2008) 1664–1671.
491 doi:10.1016/j.biortech.2007.04.029.

492 [32] X.F. Sun, F. Xu, R.C. Sun, P. Fowler, M.S. Baird, Characteristics of degraded
493 cellulose obtained from steam-exploded wheat straw, Carbohydr. Res. 340 (2005) 97–
494 106. doi:10.1016/j.carres.2004.10.022.

495 [33] H. Wang, H. Tang, S. Salley, K.Y. Simon Ng, Analysis of sterol glycosides in

496 biodiesel and biodiesel precipitates, JAOCS, J. Am. Oil Chem. Soc. 87 (2010) 215–
497 221. doi:10.1007/s11746-009-1489-x.

498 [34] N.A. Negm, M.T.H. Abou Kana, M.A. Youssif, M.Y. Mohamed, Biofuels from
499 vegetable oils as alternative fuels: Advantages and disadvantages, 2017.
500 doi:10.1201/b20780.

501 [35] A. Khodabandehloo, A. Rahbar-Kelishami, H. Shayesteh, Methylene blue removal
502 using Salix babylonica (Weeping willow) leaves powder as a low-cost biosorbent in
503 batch mode: Kinetic, equilibrium, and thermodynamic studies, J. Mol. Liq. 244 (2017)
504 540–548. doi:10.1016/j.molliq.2017.08.108.

505 [36] H.J. Lee, H.S. Lee, J. Seo, Y.H. Kang, W. Kim, T.H.K. Kang, State-of-the-art of
506 cellulose nanocrystals and optimal method for their dispersion for construction-related
507 applications, Appl. Sci. 9 (2019) 1–14. doi:10.3390/app9030426.

508 [37] S. Chowdhury, R. Mishra, P. Saha, P. Kushwaha, Adsorption thermodynamics,
509 kinetics and isosteric heat of adsorption of malachite green onto chemically modified
510 rice husk, Desalination. 265 (2011) 159–168. doi:10.1016/j.desal.2010.07.047.

511 [38] H. More, Factors Affecting Adsorption, (2018).
512 https://hemantmore.org.in/science/chemistry/factors-affecting-adsorption/13094/
513 (accessed May 5, 2019).

514 [39] M. Mohapatra, S. Khatun, S. Anand, Kinetics and thermodynamics of lead (II)
515 adsorption on lateritic nickel ores of Indian origin, Chem. Eng. J. 155 (2009) 184–190.
516 doi:10.1016/j.cej.2009.07.035.

517 [40] A. de Sá, A.S. Abreu, I. Moura, A.V. Machado, Polymeric materials for metal sorption
518 from hydric resources, Elsevier Inc., 2017. doi:10.1016/b978-0-12-804300-4.00008-3.

[41] C.S. Zhu, L.P. Wang, W. bin Chen, Removal of Cu(II) from aqueous solution by agricultural by-product: Peanut hull, J. Hazard. Mater. 168 (2009) 739–746. doi:10.1016/j.jhazmat.2009.02.085.

[42] Q. Li, L. Chai, Z. Yang, Q. Wang, Kinetics and thermodynamics of Pb(II) adsorption onto modified spent grain from aqueous solutions, Appl. Surf. Sci. 255 (2009) 4298–4303. doi:10.1016/j.apsusc.2008.11.024.

[43] Y. Liu, Y.J. Liu, Biosorption isotherms, kinetics and thermodynamics, Sep. Purif. Technol. 61 (2008) 229–242. doi:10.1016/j.seppur.2007.10.002.

[44] Y. Habibi, L.A. Lucia, O.J. Rojas, Cellulose nanocrystals: Chemistry, self-assembly, and applications, Chem. Rev. 110 (2010) 3479–3500. doi:10.1021/cr900339w.

[45] Y. Liu, D. Ying, L. Sanguansri, Y. Cai, X. Le, Adsorption of catechin onto cellulose and its mechanism study: Kinetic models, characterization and molecular simulation, Food Res. Int. 112 (2018) 225–232. doi:10.1016/j.foodres.2018.06.044.

534 **Figure captions.**

535 **Figure 1.** X-Ray Diffraction Patterns of (a) CFP, (b) CFP-based NCC

536 **Figure 2.** SEM image of the rod-like CFP-based NCC particles

537 **Figure 3.** FTIR spectrum of (a) CFP-based NCC before adsorption and (b) CFP-based NCC
538 after adsorption

539 **Figure 4.** SG removal rate varied with the mass ratio of CFP-based NCC to PO-B100 at three
540 different temperatures

541 **Figure 5.** The Pareto chart of the standardized effect showing the significance order of the
542 two independent variables (temperature and mass ratio of NCC to PO-B100) on the SG
543 removal, generated by ANOVA

544 **Figure 6.** The modelled isotherm profiles for the adsorption of SG to CFP-based NCC
545 surface (temperature = 75 °C, mass ratio of CFP-based NCC to PO-B100 = 1:50, time = 1 h,
546 agitation speed = 250 rpm)

547 **Figure 7.** Schematic representation of the proposed adsorption mechanism of SG onto CFP-
548 based NCC surface

549

550

551

552

553

554 **Table 1. The crystallinity index of CFP and CFP-based NCC**

Samples	2-theta (°)		Crystallinity (%)
	110 crystal plane	200 crystal plane	
CFP	15.44	22.63	57.60
CFP-based NCC	16.52	22.60	85.73

555

556

557 **Table 2. The properties of untreated and treated PO-B100 (1:50, 75 °C, 1 h), and the**
558 **comparison with ASTM D6751 and SNI 7182:2015**

Parameters	ASTM D6751	SNI 7182:2015	Untreated PO-B100	Treated PO-B100 (1:50, 75 °C, 1 h)
FAME (%)	≥ 96.5	≥ 96.5	98.7	98.8
AV (mg KOH/g)	≤ 0.50	≤ 0.50	0.12	0.11
MG (%)	≤ 0.80	≤ 0.80	0.23	0.22
DG (%)	≤ 0.20	-	0.09	0.09
TG (%)	≤ 0.20	-	0.06	0.05
SG (mg/kg)	N/A*	N/A*	194.1	15.9
Cloud point (°C)	-	18.0	13.2	11.5

559 * Not available

560

Table 3. Isotherm parameters of SG adsorption onto CFP-based NCC surface

Isotherm	Parameters	Temperature (K)		
		338	348	358
Langmuir	$Q_{m(L)}$ (mg/g)	12.50	12.93	11.24
	K_L (L/mg)	0.11	0.16	0.26
	r^2	0.8587	0.8580	0.7039
	χ^2	0.2329	0.2865	0.2487
Freundlich	K_F ((mg/g) $(L/mg)^{1/n}$)	5.59	6.48	7.31
	1/n	0.16	0.03	0.09
	r^2	0.8408	0.7986	0.6079
	χ^2	0.2624	0.4064	0.3293
Dubinin-Radushkevich	$Q_{m(D-R)}$ (mg/g)	11.58	12.13	10.86
	E (kJ/mol)	0.18	0.25	0.29
	r^2	0.8094	0.8387	0.7555
	χ^2	0.3147	0.3254	0.2053

564 **Table 4. Thermodynamic parameters of adsorption of SG onto CFP-based NCC surface**

Temperature (K)	Thermodynamic parameters		
	ΔG° (kJ/mol)	ΔH° (kJ/mol)	ΔS° (J/mol.K)
338	-31.44	42.90	219.80
348	-33.46		
358	-35.84		

565

566

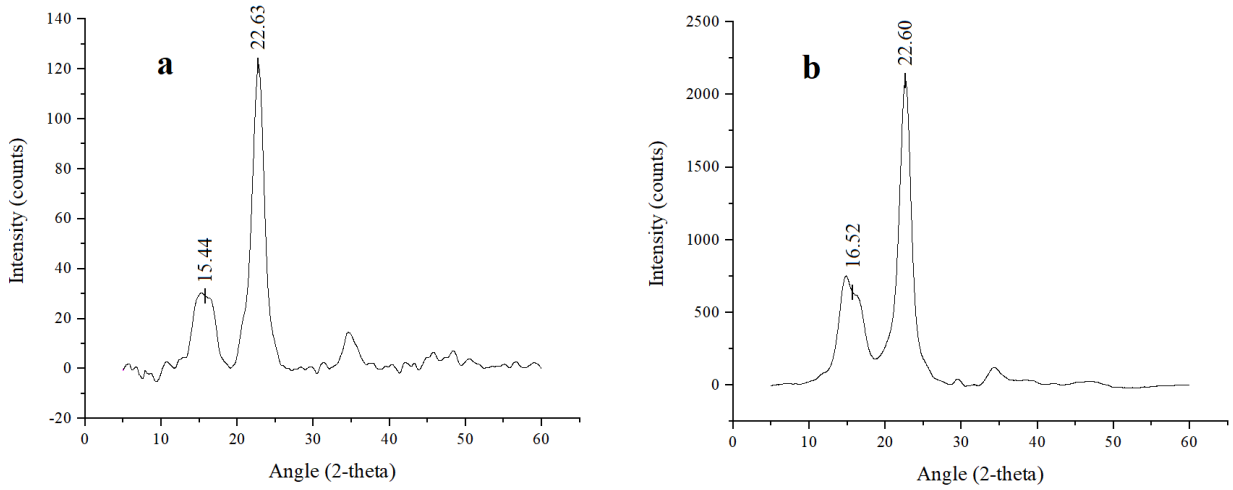
a
22.63
15.44
Intensity (counts)
Angle (2-theta)
b
22.60
16.52
Intensity (counts)
Angle (2-theta)

Figure 1

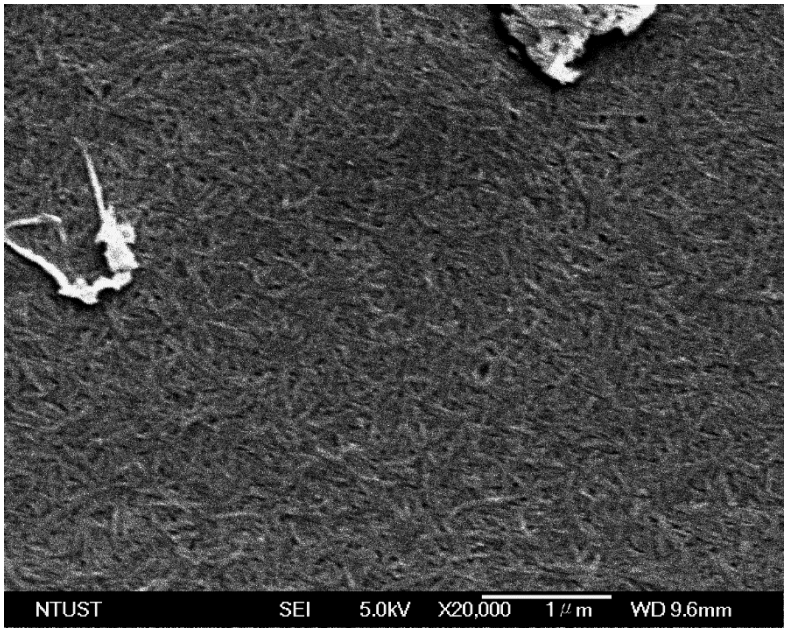

Figure 2

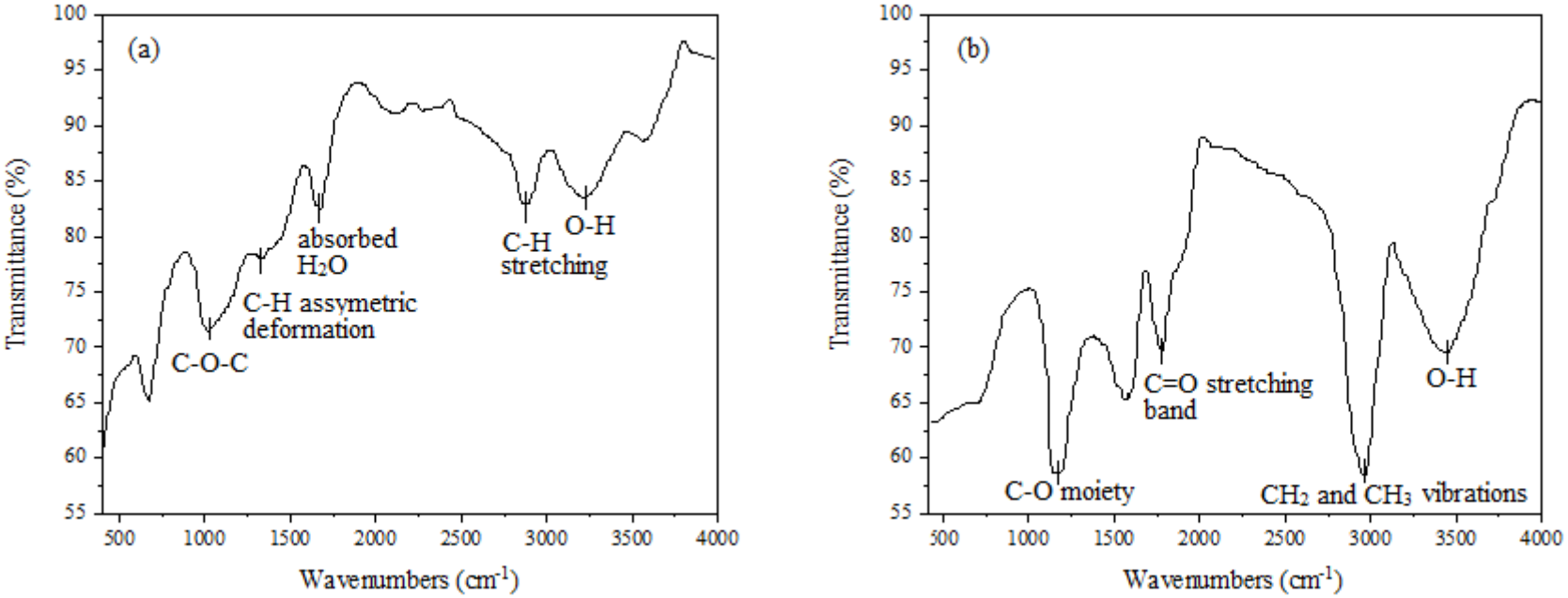
(a)
Transmittance (%)
Wavenumbers (cm-1)
C-O-C
C-H assymetric deformation
absorbed H2O
C-H stretching
O-H
(b)
Transmittance (%)
Wavenumbers (cm-1)
C-O moiety
C=O stretching band
CH2 and CH3 vibrations
O-H

Figure 3

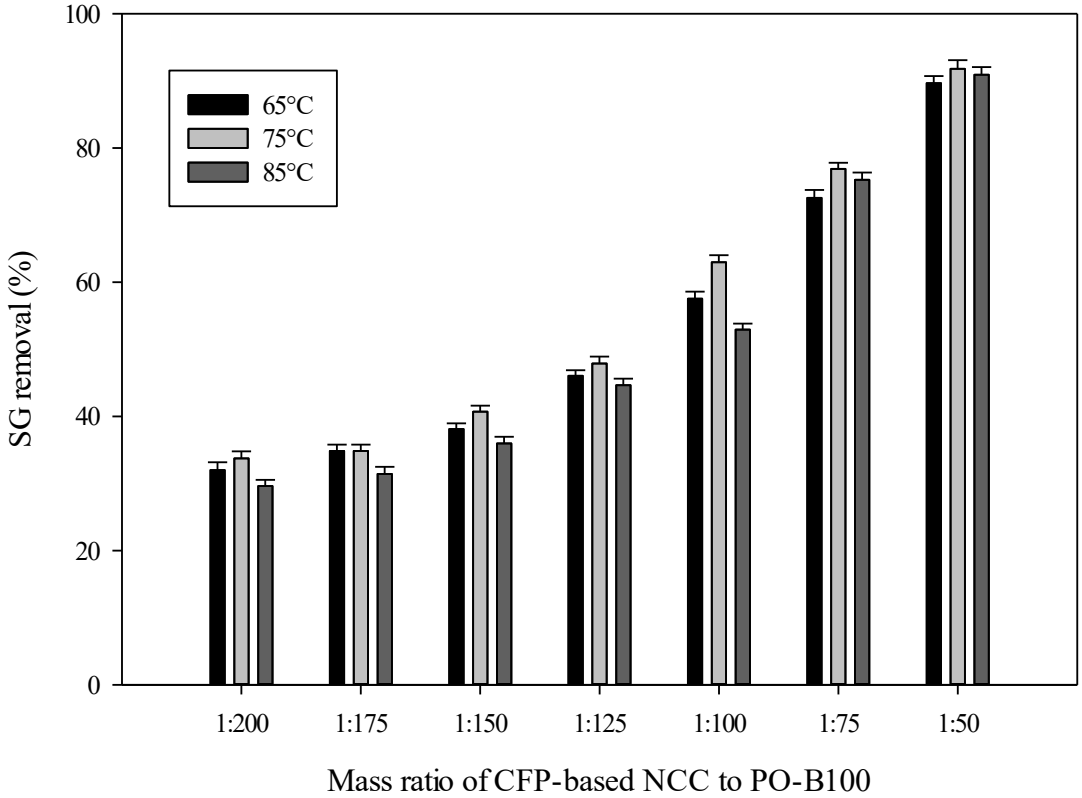

576
577
578

Figure 4

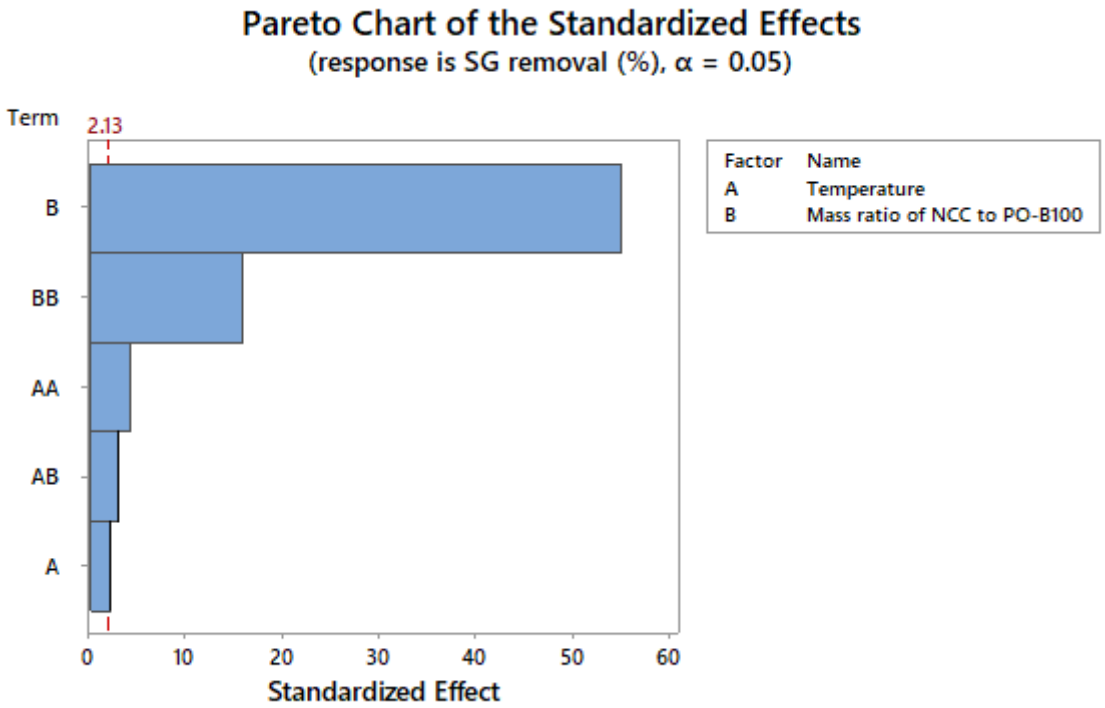
Pareto Chart of the Standardized Effects
(response is SG removal (%), α = 0.05)
Term
2.13
B
BB
AA
AB
A
0
10
20
30
40
50
60
Standardized Effect
Factor Name
A Temperature
B Mass ratio of NCC to PO-B100

Figure 5

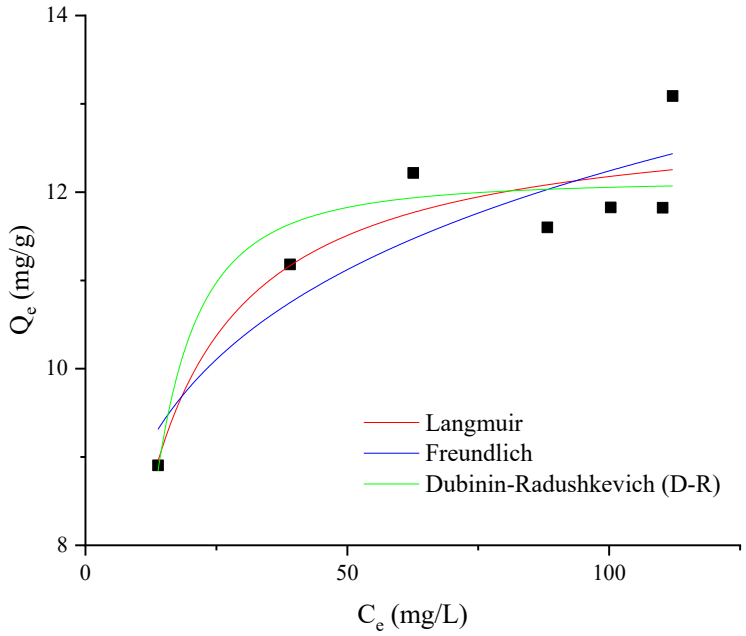
14
12
10
8
0
50
100
Q_e (mg/g)
C_e (mg/L)
Langmuir
Freundlich
Dubinin-Radushkevich (D-R)

Figure 6

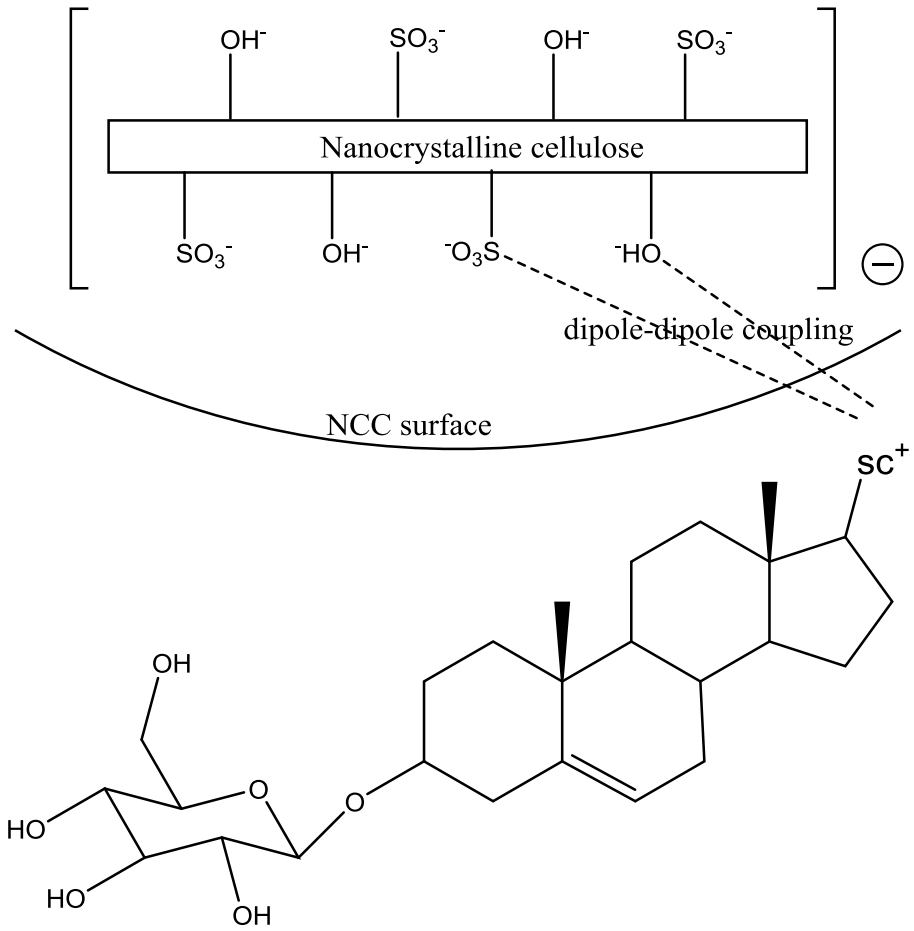
OH-
SO3-
OH-
SO3-
Nanocrystalline cellulose
SO3-
OH-
-O3S
-HO
dipole-dipole coupling
NCC surface
SC+
OH
O
O
HO
HO
OH

Figure 7

ABSTRACT

Increasing the content of biodiesel in the diesel fuel mixture faces some challenges due to the presence of steryl glucosides (SG) compounds, which causes the filter clogging and the reduction of engine power. In this study, coarse filter paper-based nanocrystalline cellulose (CFP-based NCC) with the crystallinity of 85.73 % is selected as a potential adsorbent to separate SG compounds in palm-based biodiesel (PO-B100). The adsorption experiments were carried out at various CFP-based NCC to PO-B100 mass ratio (1:50, 1:75, 1:100, 1:125, 1:150, 1:175, 1:200) and temperature (65, 75, 85 °C). The maximum SG removal was 91.81 %, obtained at 75 °C for CFP-based NCC to PO-B100 mass ratio of 1:50. The adsorption treatment also improves the cold stability of PO-B100 by reducing the cloud point from 13.2 °C to 11.5 °C. Langmuir isotherm model is best-fitted to the equilibrium adsorption data and thermodynamic studies suggested that the adsorption of SG onto the CFP-based NCC surface is spontaneous and endothermic. The isotherm and thermodynamic study showed that the mechanism governing the adsorption process may be driven by both dipole-dipole interactions and ion exchange. The adsorption results showed that CFP-based NCC has great affinity and selectivity to SG and can be considered as a promising adsorbent of SG.

Keywords: biodiesel; steryl glucosides removal; nanocrystalline cellulose; adsorption isotherm; adsorption mechanism; feasibility study

1. INTRODUCTION[1]

To date, petroleum diesel is used worldwide for transportation, manufacturing, power generation, construction and farming industries. However, disruption in crude market price and the long-term availability along with the nature deterioration due to its gas emission have become the major concerns for environmental sustainability [1]. Therefore, it is necessary to develop alternative fuels that are environmentally friendly, especially as a substitute for diesel fuel.

Of the several alternative fuels available, biodiesel is an alternative diesel fuel made from renewable biological resources [2]. Biodiesel is generally derived from transesterification of agricultural or animal lipids and short-chain alcohols in the presence of a catalyst. Conventional base-catalyzed transesterification in a batch stirred-tank reactor is the most common technique used to produce the commercially available biodiesel [3]. Several modifications on the conversion route as well as the reactor configuration and design have been performed in order to create, optimize and intensify the continuous production of biodiesel. The transesterification using catalyst-free subcritical [4–6] or supercritical alcohol [7,8], as well as heterogeneous [9] or enzymatic catalyst [9,10], gain wide attention in

[1] **Abbreviation**

SG	Steryl glucoside(s)
MG	Monoacylglyceride(s)
DG	Diacylglyceride(s)
TG	Triacylglyceride(s)
CFP	Coarse filter paper
NCC	Nanocrystalline cellulose
FAME	Fatty Acid Methyl Ester(s)
PO-B100	Palm-based biodiesel

41 improving the continuity of biodiesel production. Likozar et al. (2016) also introduced a
42 simple and robust design of a tubular reactor with a static mixer to intensify the mass transfer
43 rate between the reactants and increase the biodiesel conversion rate. Their work also studied
44 the chemical equilibrium and reaction kinetics at different operating parameters to optimize
45 the product yield [11].

46 While biodiesel is currently mass-produced and a large number of studies have been
47 carried out to improve its performance in various aspects, the white precipitates are still a
48 challenge for its manufacturers. Although biodiesel distributed around the country must
49 conform to the fuel property specifications as controlled by ASTM D6751, white precipitates
50 were often detected in biodiesel and its blends during storage [12]. Several cases even
51 showed that suspended particles in biodiesel have been found shortly after the production and
52 at a rather high temperature (slightly below 60 °C) [13]. The white precipitates may cause
53 filter plugging in engine systems [13,14]. This phenomenon was also observed in many
54 biodiesel plants and hence frequent maintenance and process modification are often essential
55 to maintain plant effectiveness and efficiency.

56 The presence of steryl glucosides (SG), which is one of the plant sterols, has been
57 identified as the major component of the white precipitates. It mostly presents in biodiesel
58 with a concentration of 35 ppm or higher [15]. The existence of this dispersed particles of SG
59 promotes the aggregation of other components in biodiesel, saturated monoacylglycerides
60 (MG) and diacylglycerides (DG), and subsequently affects the cold flow stability of fuel and
61 widespread use [16].

62 Several techniques have been conducted to minimize the SG content in the biodiesel
63 product, namely enzymatic hydrolysis [17,18], adsorption using magnesium silicate and
64 bleaching earth [16] and ultrafiltration [19]. SG removal by enzymatic hydrolysis resulted in
65 81 % removal efficiency with the addition of a synthetic codon-optimized version of the LacS

gene expressed from *E. coli* with the total operating time of 7 h [17]. Na-Ranong et al. (2015) reported that the conventional adsorption using magnesium silicate and bleaching earth in temperature of 65-80 °C yielded in 81.4-82.5 % removal efficiency of SG [16]. Tremblay and Montpetit (2017) stated that the highest separation for SG (86 %) by ultrafiltration was obtained when the biodiesel was transesterified using 0.7 % (w/w) catalyst and 4:1 methanol:soybean oil molar ratio [19]. Based on the removal efficiency and economic feasibility, the adsorption treatment is a potential method to reduce SG content as well as to improve the cold flow properties of the fuel in the industrial scale because it is found to be effective and facile, time-saving and energy-efficient.

The development of adsorbent for effective adsorption has been conducted using various types of materials. Currently, the development of cellulosic adsorbent received major interest because it is renewable, biodegradable, low cost, and non-toxic [20]. Cellulosic adsorbents have the ability to meet the requirement of being a biosorbent, as it is abundantly available as a natural biopolymer. Cellulose in the form of nanocrystalline cellulose (NCC) has been widely studied due to its extensive industrial application, namely enzyme immobilization, adsorption, catalysis, drug delivery, biosensors and bio-imaging [21]. NCC, with a large specific surface area and plenty of surface hydroxyl and anionic sulfate ester group for physical and chemical reactions [22–24], can be considered as a new promising adsorbent for SG removal.

As the Indonesian government plans to increase the use of biodiesel in diesel blend from B20 to B30 in the time span of 5 years, the use of NCC for SG removal and improvement of the cold stability is an interesting topic to be studied. The objective of this study is to observe the feasibility of coarse filter paper-based NCC (CFP-based NCC) as the adsorption agent for SG. Various operating parameters, namely temperature, and the mass

ratio of CFP-based NCC to palm-based biodiesel (PO-B100) will be monitored. The adsorption mechanism was also proposed based on the isotherm and thermodynamics study.

2. MATERIALS AND METHODS

2.1 Materials

PO-B100 was collected from a local palm oil manufacturer in Gresik, Indonesia, and stored for 3 days at room temperature prior to the adsorption experiment. Coarse filter paper (CFP) as the cellulosic material was obtained from a local supplier in Surabaya, Indonesia. Sulphuric acid, sodium hydroxide, ethyl acetate, and n-hexane were purchased from Merck, Germany. FAMEs standard 47885 U contains 37 components FAME mix and SG standard 1117 were procured from Supelco (Bellefonte, PA, USA) and Matreya (State College, PA, USA), respectively. Nitrogen gas (99.9 % purity) was purchased from Aneka Gas Industry Pty. Ltd., Surabaya. All reagents were of analytical grade and required no further purification.

2.2 Preparation of NCC

CFP was ground into fibrous powder before use. The non-cellulosic material of CFP was subsequently removed to obtain purified cellulose using the modified method of Putro et al. (2017) [25]: 12 grams of the CFP powder was delignified using 0.1 g/ml sodium hydroxide aqueous solution (40 ml). The delignified product was washed with distilled water and filtrated three times through a Whatman 1 (11 μm pore size) filter paper before being dried under vacuum at 80 °C for 12 hours.

CFP-based NCC was prepared by using acid hydrolysis following the procedure conducted by Putro et al. (2017) [25]. 1 gram of delignified cellulose was hydrolyzed with 20 ml sulphuric acid 64 % at 45 °C for 75 min under constant agitation. The reaction time was selected to ensure high reaction efficiency. After the specified duration, the reaction was

115 immediately quenched using 20-fold of cold distilled water. The suspension was centrifuged
116 at 4500 rpm for 10 min to remove the excess acid solution. The resulting precipitates were
117 dialyzed against distilled water until neutral pH was achieved. The colloidal suspension was
118 subjected to sonication treatment for 30 min in a cooling bath to avoid overheating and
119 subsequently subjected to vacuum drying at 80 °C for 6 h to obtain CFP-based NCC powder.
120

121 *2.3 Characterization of CFP-based NCC*

122 The surface morphologies of the CFP-based NCC particles were analyzed on a field
123 emission scanning electron microscope (FESEM) JEOL JSM-6500F (Jeol Ltd., Japan), with
124 an accelerating voltage of 5 – 10 kV and 9.5 – 9.6 mm working distance. The CFP-based
125 NCC powder was attached to a stub, sputtered and coated with gold prior to analysis. Fourier
126 Transform Infrared (FTIR) analysis was performed by an FTIR-8400S spectrophotometer
127 (Shimadzu, Japan) in the range of 400 – 4000 cm^{-1} at a 4 cm^{-1} scanning resolution. XRD
128 analysis was conducted by an X'PERT Panalytical Pro X-Ray diffractometer (Philips-FEI,
129 Netherlands) with monochromatic Cu $K\alpha_1$ radiation at wavelength (λ) = 0.154 nm, 40 kV of
130 voltage and 30 mA of tube current. The diffraction pattern was acquired in the range of 5° to
131 60° (2θ angle). The crystallinity index (CrI) was expressed according to the following
132 equation, as proposed by Segal et al. (1959) [26].

133 $$\mathrm{CrI}\ (\%) = \frac{(I_{200} - I_{am})}{I_{200}} x100 \quad (1)$$

134 Where I_{200} is the maximum intensity of the 200 lattice diffraction at 2θ around 22°,
135 I_{am} is the maximum intensity of the amorphous region at 2θ = 18°. The crystallite size (nm)
136 was calculated using the Scherrer analysis.
137

138 *2.4 Compositional study of SG in PO-B100 using GC-FID analysis*

The analysis of SG composition in PO-B100 was carried out using GC-17A (Shimadzu, Japan), completely equipped with a split/splitless injector and a flame ionization detector (FID). The separation was performed using nonpolar capillary column DB-5HT (5 %-phenyl)-methylpolysiloxane (15 m x 0.32 mm ID, Agilent Technology, CA). The column temperature was initially set at 80 °C, then subsequently ramped to 365 °C at the rate of 15 °C/min, and held constant for 19 min. The temperature of the injector and detector were adjusted constant at 370 °C. 100 mg of SG was dissolved in 1 ml ethyl acetate and subjected to filtration using polyvinylidene difluoride (PVDF) filter prior analysis. The prepared sample (1 µl) was injected into the GC with a split ratio of 1:50. The velocity of nitrogen (N_2, 99.9 %) as the carrier gas was fixed at 30 cm/s at 80 °C.

2.5 Removal of SG using adsorption

The adsorption of SG from PO-B100 was conducted in a batch mode according to the study conducted by Na-Ranong et al. (2015) with a few modifications [16]. A various mass ratio of CFP-based NCC to PO-B100 (1:50, 1:75, 1:100, 1:125, 1:150, 1:175, 1:200) was introduced into a series of beakers, where the mixture will be subjected to a 1-hour adsorption process at constant temperature and agitation speed (250 rpm). The selection of adsorption duration was based on the preliminary experiment conducted to find the equilibrium time. Several adsorption temperatures (65, 75 and 85 °C) were used to study the effect of temperature on the adsorption of SG. The solution was separated from the adsorbent by using centrifugation at the rotational speed of 4900 rpm for 10 min. The SG contents in PO-B100 before and after adsorption were analyzed using UV-mini 1240 spectrophotometer (Shimadzu, Japan) at 240 nm, according to the modified technique conducted by Moreau et al. (2008), Nyström (2007) and Araújo et al. (2013) [14,27,28]. The percentage of SG removal was determined by using the following equation.

$$SG\ removal\ (\%) = \frac{C_i - C_f}{C_i} x100 \quad (2)$$

Where C_i is the concentration of SG in untreated PO-B100 (mg/kg) and C_f is the concentration of SG in treated (after adsorption) PO-B100 (mg/kg). The results of SG removal were verified by using GC-FID analysis (see section 2.4) and its statistical approach was performed using Minitab software (version 18.1) to identify the significance order of the parameters affecting the adsorption.

2.6 Isotherm and thermodynamics study of the SG adsorption

The adsorption isotherm was conducted at the temperature of 65, 75 and 85 °C with various CFP-based NCC to PO-B100 mass ratio (1:50, 1:75, 1:100, 1:125, 1:150, 1:175, 1:200). It was performed using a similar procedure as previously mentioned in subsection 2.5. At the equilibrium condition, the amount of adsorbed SG per unit mass of CFP-based NCC as the adsorbent (Q_e) was calculated by the equation below.

$$Q_e \left(\frac{mg}{g}\right) = \frac{C_o - C_e}{m} x\ V \quad (3)$$

Where C_o and C_e are the initial and final (equilibrium) concentration of SG in PO-B100 (mg/L), respectively, m is the mass of adsorbent (g) and V is the volume of PO-B100 (L).

The equilibrium data obtained at various temperature were fitted to the three isotherm models, namely Langmuir, Freundlich and Dubinin-Radushkevich (D-R). Meanwhile, the thermodynamic parameters such as Gibbs free energy change (ΔG°), enthalpy (ΔH°) and entropy (ΔS°) were further determined from the results of isotherm study using equation (4) and (5).

$$\Delta G° = -RTln(K_L . M_{SG} . 10^3 . C^o) \quad (4)$$

$$\Delta G° = \Delta H° - T\Delta S° \quad (5)$$

188 Where R is the gas constant with the value of 8.314 J/mol.K, T is the absolute temperature in
189 Kelvin, K_L is Langmuir equilibrium constant in L/mg, M_{SG} is the molecular weight of SG in
190 g/mol and C^o is the reference concentration in standard state with the value of 1 mol/L.
191

192 **3. RESULTS AND DISCUSSIONS**

193 *3.1 Characterization of CFP-based NCC*

194 The X-ray diffraction pattern of the CFP and its NCC are shown in Figure 1, and the
195 corresponding crystallinity index is presented in Table 1. Both XRD patterns showed the
196 cellulose I characteristic peaks at 2θ around 15 – 17° (110 crystal plane) and 22 – 23° (200
197 crystal plane) [26,29]. The crystallinity index of CFP and its NCC were calculated using
198 equation (1) and recorded to have the corresponding value of 57.60 % and 85.73 %. The
199 change of crystallinity has occurred because of the progressive removal of amorphous
200 hemicellulose and lignin during acid hydrolysis. The highly crystalline product is more
201 efficient to improve the mechanical properties of the composite material, particularly as an
202 adsorbent, since crystallinity positively corresponds to the tensile strength of the material [30].

203 **Figure 1**

204 **Table 1**

205 The scanning electron micrograph in Figure 2 shows the shape and size of the CFP-
206 based NCC. The distribution of NCC products derived from CFP was estimated to have
207 approximately 200-400 nm in length (Figure 2). The prepared CFP-based NCC has a
208 homogenous needle-shaped with crystallite size in the range of 2 – 4 nm, obtained from the
209 combination of X-ray diffraction data and Scherrer analysis. The homogenous CFP-based
210 NCC particles are likely caused by the swollen of cellulose fibers due to NaOH
211 delignification pretreatment [25].

212 **Figure 2**

213 Figure 3 (a) – (b) illustrated the FTIR spectra of CFP-based NCC before and after
214 adsorption. As shown in Figure 3 (a), several peaks representing certain functional groups in
215 CFP-based NCC were found in the spectra. The broad band in the range of 3008 – 3459 cm^{-1}
216 represents the O-H stretching vibrations, while the peaks in the range of 2802 – 2925 cm^{-1}
217 correspond to C-H stretching vibrations. The absorption at 936 – 1137 cm^{-1} is related to the
218 functional group of C-O-C, and the peak at 1640 cm^{-1} indicates the presence of abundant
219 hydrophilic hydroxide group in the cellulose [31]. A peak at 1382 cm^{-1} represents the C-H
220 asymmetric deformations [32].

221 Meanwhile, Figure 3 (b) showed strong peaks in the wavenumbers of around 1019 –
222 1376 cm^{-1} and 2602 – 3160 cm^{-1}, which represent the C-O moiety, and CH_2 and CH_3
223 stretching vibrations. These two specific peaks are known as the fingerprint areas for SG.
224 Another peak at 1750 cm^{-1} corresponds to the typical C=O stretching band of the methyl ester,
225 while an O-H band around 3110 - 3700 cm^{-1} indicates the presence of hydroxyl groups in SG
226 and CFP-based NCC [33]. Therefore, based on the FTIR spectra, it can be concluded that SG
227 is the major component of the adsorbate on the surface of CFP-based NCC, which is
228 consistent with the GC-FID results discussed in section 3.2.

229 **Figure 3**

230

231 *3.2 Properties of PO-B100*

232 The properties of PO-B100 have been analyzed according to the standard method of
233 ASTM for its content of FAME, acid value (AV), MG, DG and triglycerides (TG). As
234 reported in Table 2, the purity of FAME in PO-B100 is 98.7 %, while the AV, MG, DG, and
235 TG values are 0.12 mg KOH/g, 0.23 %, 0.09 %, and 0.06 %, respectively. Furthermore, PO-

236 B100 feedstock contained 194.1 mg/kg of SG with the cloud point of 13.2 °C and a clear
237 initial appearance. Based on the GC-FID analysis, the SG profile in PO-B100 consists of
238 34.79 % of campesteryl glucoside, 23.73 % of stigmasteryl glucoside and 41.48 % of β-
239 sitosteryl glucoside. The results met the requirements of ASTM D6751 and SNI 7182:2015.
240 However, white precipitates could be found within a few hours after production.

241 **Table 2**

242 After the adsorption using the parameters giving the highest SG removal (1:50, 75 °C,
243 1 h; see section 3.3), the sample of treated PO-B100 was collected for the properties
244 measurement in order to monitor the effect of the adsorbent. According to the results, the
245 treated PO-B100 contained FAME with a purity of 98.8 % and AV value of 0.11 mg KOH/g.
246 The concentration of SG reduced significantly to 15.9 mg/kg with the composition of 24.81 %
247 campesteryl glucoside, 25.07 % stigmasteryl glucoside and 50.12 % β-sitosteryl glucoside,
248 while the other glycerides components, MG, DG, and TG, were slightly decreased to 0.22 %,
249 0.09 %, 0.05 %, respectively. The cloud point of the treated PO-B100 was also found to be
250 decreased to 11.5 °C. These results indicated that CFP-based NCC has selectivity to adsorb
251 SG, particularly campesteryl glucoside and stigmasteryl glucoside, as compared to the other
252 minor components, such as MG, DG, and TG. It also subsequently lowered the cloud point
253 significantly, which is advantageous for storage and transportation purposes [34].

254

255 *3.3 Adsorption of SG using CFP-based NCC*

256 Figure 4 summarized the SG removal rate at the various temperature and mass ratios
257 of CFP-based NCC to PO-B100. The highest value of the SG removal rate (91.81 %) was
258 obtained at the following conditions: 75 °C, CFP-based NCC to PO-B100 mass ratio of 1:50,
259 and 1 h adsorption time. Based on the results shown in Figure 4, the lowest removal rate of
260 SG in every adsorption temperature was seen at 1:200 of CFP-based NCC to PO-B100 mass

ratio. It was likely due to insufficient binding and active adsorption sites and the adsorption required more time to reach the equilibrium stage. The removal percentage of SG was observed to have amplified with the increase of CFP-based NCC to PO-B100 mass ratio from 1:200 to 1:50 at all temperatures in the tested range. Greater amounts of CFP-based NCC provide greater adsorption surface area and active sites in CFP-based NCC, leading to an adequate SG binding area and certainly, a higher percentage of SG removal [35]. It was also monitored that the SG removal rate exponentially increased when the CFP-based NCC to PO-B100 mass ratio was increased from 1:100 to 1:50 in the all adsorption temperature**.** The phenomenon indicated the good dispersion ability of CFP-based NCC in PO-B100, where constant diffusion path length of SG binding to CFP-based NCC surface was found regardless of the amount of adsorbent [36].

Figure 4

As depicted in Figure 4, temperature also remarkably affected the SG reduction. A temperature elevation from 65 °C to 75 °C improves the reduction of SG, regardless of CFP-based NCC to PO-B100 mass ratio. Chowdhury et al. (2011) stated that the adsorption enhancement along with the temperature increase may be associated with the increase of the number of active sites available for adsorption. The diffusion rate of the adsorbate across the external boundary layer also escalates with the rise in temperature, due to lower solution viscosity and enhancement in the mobility and kinetic energy of the adsorbate [37]. Therefore, the collision between particles intensifies with the temperature elevation so that the activation energy of the adsorption process is easier to achieve. As a result, the amount of the adsorbed SG enhances along with the temperature increase. However, it was also observed that the SG removal rate decreased when the temperature was further escalated from 75 °C to 85 °C. More (2018) mentioned that after reaching a certain temperature, excessive particle collision causes the removal of adsorbates from the adsorbent, leading to lower adsorption capacity

286 [38]. Lee et al. (2019) also stated that the NCC surface binding generally weakens along with
287 the temperature enhancement [36]. The fluctuations of the SG uptake observed with the
288 change in temperature suggests that the SG adsorption is governed by both physical attraction
289 and chemical bonding, indicating that the sorption of SG by CFP-based NCC is both driven
290 by physical and chemical sorption [37,39].

291 Figure 5 presented the Pareto chart of the standardized effect generated using
292 statistical analysis (Minitab version 18.1). The figure showed that both independent
293 parameters (temperature and the mass ratio of CFP-based NCC to PO-B100) were found to
294 be prominent with the significance order of the mass ratio of CFP-based NCC to PO-B100 >
295 temperature. The other quadratic and two-way interaction terms were also found to
296 significantly affect the SG removal rate.

297 **Figure 5**

298

299 *3.4 Study of adsorption isotherm and thermodynamic parameters*

300 In this study, three isotherm equations were fitted to the experimental equilibrium
301 data for SG at three temperature points (65 °C, 75 °C and 85 °C). The results are presented in
302 Table 3 and the isotherm models are plotted in Figure 6. The Langmuir isotherm constant, K_L
303 and maximum absorption capacity, $Q_{m(L)}$ were calculated from the nonlinear curve fitting
304 between Q_e and C_e. The value of $Q_{m(L)}$ was found to be increased from 12.50 mg/g at 65 °C to
305 12.93 mg/g at 75 °C before declining to 11.24 mg/g at the highest tested temperature (85 °C).
306 The $Q_{m(L)}$ results are quite comparable to the adsorption capacity of magnesium silicate and
307 bleaching earth on the SG (~13 mg/g) [16]. The Langmuir constant (K_L) also increases along
308 with the temperature, from 0.11 L/mg at the lowest temperature (65 °C) to 0.26 L/mg at the
309 highest temperature point (85 °C), indicating that the adsorption of SG to CFP-based NCC is
310 an endothermic process.

Table 3

Figure 6

The isotherm data were further analyzed by the Freundlich model. The Freundlich constant K_F and 1/n were obtained from the non-linear regression analysis. Table 3 showed that the values of 1/n are all under unity, ranging from 0.03 at 75 °C to 0.16 at 65 °C. The extent of 1/n represents the favorability degree of adsorption. The value of 1/n less than unity corresponds to favorable sorption. It was also observed that the Freundlich constant greatly escalates along with the temperature, implying that the adsorption was favorable at high temperature and the process is certainly endothermic. de Sá et al. (2017) mentioned that 1/n value between 0 and 1 is associated with a chemisorption process [40].

Another isotherm equation, the Dubinin-Radushkevich (D-R) model, was further applied to analyze the equilibrium data, particularly to determine the nature of SG adsorption onto CFP-based NCC surface. The D-R constant (β) gives an idea about the mean sorption energy, E, and their correlation can be expressed by the following equation:

$$E = \frac{1}{\sqrt{2\beta}} \quad (6)$$

where E represents sorption energy (kJ/mol) and β is the D-R constant ($mmol^2/J^2$). The value of sorption energy provides information to determine the type of adsorption mechanism, as chemical ion exchange or physical adsorption. Li et al. (2009) and Zhu et al. (2009) stated that if the sorption energy ranges from 8 to 16 kJ/mol, the sorption process is supposed to be chemisorption, while for energy value lower than 8 kJ/mol, the sorption is of physical nature [41,42]. Based on the results provided in Table 3, the adsorption mechanism is physical attraction since the E values for all tested temperatures are lower than 8 kJ/mol. The highest $Q_{m(D-R)}$ was found at 75 °C with a value of 12.13 mg/g, which was similar to the result obtained using Langmuir isotherm. The effect of temperature previously studied also

335 provides similar results where the temperature of 75 °C gives the highest SG removal rate
336 compared to the other tested temperatures.

337 The correlation coefficient (r^2) and chi-square (χ^2) values of the three isotherms are
338 also listed in Table 3. It could be concluded that the adsorption of SG onto the CFP-based
339 NCC surface is best fitted to the Langmuir isotherm equation under the temperature range
340 studied. Based on the three isotherm models studied, the adsorption mechanism is predicted
341 to be driven by both physical and chemical sorption due to its sorption energy value and
342 endothermic nature, respectively. The overall results of this study showed that NCC has a
343 particular affinity for SG and is an effective adsorbent for SG removal from PO-B100.

344 Table 4 listed the thermodynamics parameters of the SG adsorption onto the surface
345 of NCC, such as Gibbs free energy change (ΔG°), enthalpy (ΔH°) and entropy (ΔS°). The
346 values of Gibbs free energy (ΔG°) for the adsorption of SG were negative at all tested
347 temperatures. These values confirm the spontaneous nature of SG adsorption onto the CFP-
348 based NCC. Enhancement of the ΔG° value along with the increasing temperature implies
349 that the affinity of SG on CFP-based NCC was higher at high temperature. Positive ΔH°
350 value (42.90 kJ/mol) verifies that the adsorption is indeed an endothermic process, while the
351 absolute value of ΔS° (219.80 J/mol.K) reflects the increased randomness at the solid-
352 solution interface during the adsorption process [37,43].

353 **Table 4**

354

355 *3.5 Adsorption mechanism study*

356 The study of the adsorption mechanism was used to further illustrate the interaction
357 between SG and CFP-based NCC surface. Two important points have to be considered to
358 understand the mechanism, namely the surface properties of the adsorbent and the structure
359 of adsorbate. The NCC molecule was constructed by a substantial number of hydrogen bonds

between glucose units or glucose chains inside the molecule to form a very stable structure [44,45]. NCC contains the majority of oxygen functional groups such as hydroxyl, ether, and sulfonate. While the hydroxyl and ether groups are originally present in the cellulosic material, the sulfonate group existed due to the acid hydrolysis to produce NCC. On the other hand, SG was built by a steryl cation (SC^+) and a glucose unit, with a positive charge on the cationic steryl part.

According to the findings of this study, the adsorption was temperature-dependent and the isotherm modeling showed an equal contribution of physical attraction and chemical binding. Therefore, the mechanism of SG removal by adsorption on the CFP-based NCC surface may be presumed to involve these following steps:

- Migration of SG from the bulk of PO-B100 to the CFP-based NCC surface
- Diffusion of SG through the boundary layer to the CFP-based NCC surface
- Adsorption of SG on the surface of CFP-based NCC, which may be caused by physical interaction of dipole-dipole coupling between the positively charged SC^+ and the negatively charged NCC surface as suggested in Figure 7; and through a possible chemical binding mechanism of ion exchange as shown below:

  $NCC - OH \leftrightarrow NCC - O^- + H^+$

  $NCC - SO_3^- \leftrightarrow NCC - SO_3^-$

  $NCC - O^- + SC^+ \leftrightarrow NCC - O - SC$

  $NCC - SO_3^- + SC^+ \leftrightarrow NCC - O - SO_3$

- Intraparticle diffusion of SG into the pores of CFP-based NCC

Figure 7

4. CONCLUSIONS

CFP-based NCC was successfully used as an adsorbent for reducing SG in PO-B100. The content of SG was able to be reduced from 194.1 mg/kg to as low as 15.9 mg/kg (91.81 % removal rate) within 1 hour at the temperature of 75 °C using CFP-based NCC to PO-B100 mass ratio of 1:50. The study proved that CFP-based NCC has great affinity and selectivity to SG, particularly on the campesteryl glucoside and stigmasteryl glucoside. The adsorption treatment greatly improves the cold stability of PO-B100 by reducing the cloud point from 13.2 °C to 11.5 °C, while slightly affected the purity of FAME, AV and other minor components, such as MG, DG, and TG, which were still in the acceptable range according to ASTM D6751. The adsorption process was endothermic and may be driven by both physical attraction and chemical ion exchange. The adsorption treatment using CFP-based NCC should be a prospective method used to remove SG from PO-B100 since it possesses high efficiency, time-saving and energy-efficient.

ACKNOWLEDGMENT

This research did not receive any specific grant from funding agencies in the public, commercial or not-for-profit sectors.

REFERENCES

[1] N. Kumar, A. Sonthalia, H. S. Pali, Sidharth, Alternative Fuels for Diesel Engines: New Frontiers, Diesel Engines [Working Title]. (2018) 1–27. doi:10.5772/intechopen.80614.

[2] A.C. Pinto, L.L.N. Guarieiro, M.J.C. Rezende, N.M. Ribeiro, A. Ednildo, Biodiesel : An Overview, 16 (2005) 1313–1330.

[3] Z. Qiu, L. Zhao, L. Weatherley, Process intensification technologies in continuous biodiesel production, Chem. Eng. Process. Process Intensif. 49 (2010) 323–330. doi:10.1016/j.cep.2010.03.005.

[4] Y.H. Ju, L.H. Huynh, Y.A. Tsigie, Q.P. Ho, Synthesis of biodiesel in subcritical water and methanol, Fuel. 105 (2013) 266–271. doi:10.1016/j.fuel.2012.05.061.

[5] S. Thiruvenkadam, S. Izhar, Y. Hiroyuki, R. Harun, One-step microalgal biodiesel production from Chlorella pyrenoidosa using subcritical methanol extraction (SCM) technology, Biomass and Bioenergy. 120 (2019) 265–272. doi:10.1016/j.biombioe.2018.11.037.

[6] F.H. Santosa, L. Laysandra, F.E. Soetaredjo, S.P. Santoso, S. Ismadji, M. Yuliana, A facile noncatalytic methyl ester production from waste chicken tallow using single step subcritical methanol: Optimization study, Int. J. Energy Res. 43 (2019) 8852–8863. doi:10.1002/er.4844.

[7] M. Aghilinategh, M. Barati, M. Hamadanian, Supercritical methanol for one put biodiesel production from chlorella vulgaris microalgae in the presence of CaO/TiO 2 nano-photocatalyst and subcritical water, Biomass and Bioenergy. 123 (2019) 34–40. doi:10.1016/j.biombioe.2019.02.011.

[8] L.K. Ong, C. Effendi, A. Kurniawan, C.X. Lin, X.S. Zhao, S. Ismadji, Optimization of catalyst-free production of biodiesel from Ceiba pentandra (kapok) oil with high free fatty acid contents, Energy. 57 (2013) 615–623. doi:10.1016/j.energy.2013.05.069.

[9] M.K. Lam, K.T. Lee, A.R. Mohamed, Homogeneous, heterogeneous and enzymatic catalysis for transesterification of high free fatty acid oil (waste cooking oil) to biodiesel: A review, Biotechnol. Adv. 28 (2010) 500–518. doi:10.1016/j.biotechadv.2010.03.002.

427 [10] L.P. Christopher, Hemanathan Kumar, V.P. Zambare, Enzymatic biodiesel: Challenges
428 and opportunities, Appl. Energy. 119 (2014) 497–520.
429 doi:10.1016/j.apenergy.2014.01.017.

430 [11] B. Likozar, A. Pohar, J. Levec, Transesterification of oil to biodiesel in a continuous
431 tubular reactor with static mixers: Modelling reaction kinetics, mass transfer, scale-up
432 and optimization considering fatty acid composition, Fuel Process. Technol. 142 (2016)
433 326–336. doi:10.1016/j.fuproc.2015.10.035.

434 [12] I. Lee, L.M. Pfalzgraf, G.B. Poppe, E. Powers, T. Haines, The role of sterol glucosides
435 on filter plugging, Biodiesel Mag. 4. (2007) 105–112.

436 [13] V. Van Hoed, N. Zyaykina, W. De Greyt, J. Maes, R. Verhé, K. Demeestere,
437 Identification and occurrence of steryl glucosides in palm and soy biodiesel, JAOCS, J.
438 Am. Oil Chem. Soc. 85 (2008) 701–709. doi:10.1007/s11746-008-1263-5.

439 [14] R.A. Moreau, K.M. Scott, M.J. Haas, The identification and quantification of steryl
440 glucosides in precipitates from commercial biodiesel, JAOCS, J. Am. Oil Chem. Soc.
441 85 (2008) 761–770. doi:10.1007/s11746-008-1264-4.

442 [15] H. Tang, S.O. Salley, K.Y. Simon Ng, Fuel properties and precipitate formation at low
443 temperature in soy-, cottonseed-, and poultry fat-based biodiesel blends, Fuel. 87
444 (2008) 3006–3017. doi:10.1016/j.fuel.2008.04.030.

445 [16] D. Na-Ranong, P. Laungthaleongpong, S. Khambung, Removal of steryl glucosides in
446 palm oil based biodiesel using magnesium silicate and bleaching earth, Fuel. 143
447 (2015) 229–235. doi:10.1016/j.fuel.2014.11.049.

448 [17] A. Aguirre, S. Peiru, F. Eberhardt, L. Vetcher, R. Cabrera, H.G. Menzella, Enzymatic
449 hydrolysis of steryl glucosides, major contaminants of vegetable oil-derived biodiesel,

450 Appl. Microbiol. Biotechnol. 98 (2014) 4033–4040. doi:10.1007/s00253-013-5345-4.

451 [18] S. Peiru, A. Aguirre, F. Eberhardt, M. Braia, R. Cabrera, H.G. Menzella, An industrial
452 scale process for the enzymatic removal of steryl glucosides from biodiesel,
453 Biotechnol. Biofuels. 8 (2015). doi:10.1186/s13068-015-0405-x.

454 [19] A.Y. Tremblay, A. Montpetit, The in-process removal of sterol glycosides by
455 ultrafiltration in biodiesel production, Biofuel Res. J. 4 (2017) 559–564.
456 doi:10.18331/brj2017.4.1.6.

457 [20] M.Y. Chang, R.S. Juang, Adsorption of tannic acid, humic acid, and dyes from water
458 using the composite of chitosan and activated clay, J. Colloid Interface Sci. 278 (2004)
459 18–25. doi:10.1016/j.jcis.2004.05.029.

460 [21] A.G. Varghese, S.A. Paul, M.S. Latha, Green Adsorbents for Pollutant Removal, 2018.
461 doi:10.1007/978-3-319-92111-2.

462 [22] M. Börjesson, G. Westman, Crystalline Nanocellulose — Preparation, Modification,
463 and Properties, Cellul. - Fundam. Asp. Curr. Trends. (2015). doi:10.5772/61899.

464 [23] H. Voisin, L. Bergström, P. Liu, A. Mathew, Nanocellulose-Based Materials for Water
465 Purification, Nanomaterials. 7 (2017) 57. doi:10.3390/nano7030057.

466 [24] H. Liang, X. Hu, A quick review of the applications of nano crystalline cellulose in
467 wastewater treatment, J. Bioresour. Bioprod. 2016 (2016) 199–204.
468 www.Bioresources-Bioproducts.com.

469 [25] J.N. Putro, S.P. Santoso, S. Ismadji, Y.H. Ju, Investigation of heavy metal adsorption
470 in binary system by nanocrystalline cellulose – Bentonite nanocomposite:
471 Improvement on extended Langmuir isotherm model, Microporous Mesoporous Mater.
472 246 (2017) 166–177. doi:10.1016/j.micromeso.2017.03.032.

473 [26] L. Segal, J.J. Creely, A.E. Martin, C.M. Conrad, An Empirical Method for Estimating
474 the Degree of Crystallinity of Native Cellulose Using the X-Ray Diffractometer, Text.
475 Res. J. 29 (1959) 786–794. doi:10.1177/004051755902901003.

476 [27] L. Nyström, Occurrence and properties of steryl ferulates and glycosides in wheat and
477 rye, University of Helsinki, 2007.

478 [28] L.B.D.C. Araújo, S.L. Silva, M.A.M. Galvão, M.R.A. Ferreira, E.L. Araújo, K.P.
479 Randau, L.A.L. Soares, Total phytosterol content in drug materials and extracts from
480 roots of Acanthospermum hispidum by UV-VIS spectrophotometry, Brazilian J.
481 Pharmacogn. 23 (2013) 736–742. doi:10.1590/S0102-695X2013000500004.

482 [29] M.N.A.M. Taib, W.A. Yehye, N.M. Julkapli, Influence of Crosslinking Density on
483 Antioxidant Nanocellulose in Bio-degradation and Mechanical Properties of Nitrile
484 Rubber Composites, Fibers Polym. 20 (2019) 165–176. doi:10.1007/s12221-019-8575-
485 y.

486 [30] Y. Hu, L. Tang, Q. Lu, S. Wang, X. Chen, B. Huang, Preparation of cellulose
487 nanocrystals and carboxylated cellulose nanocrystals from borer powder of bamboo,
488 Cellulose. 21 (2014) 1611–1618. doi:10.1007/s10570-014-0236-0.

489 [31] A. Alemdar, M. Sain, Isolation and characterization of nanofibers from agricultural
490 residues - Wheat straw and soy hulls, Bioresour. Technol. 99 (2008) 1664–1671.
491 doi:10.1016/j.biortech.2007.04.029.

492 [32] X.F. Sun, F. Xu, R.C. Sun, P. Fowler, M.S. Baird, Characteristics of degraded
493 cellulose obtained from steam-exploded wheat straw, Carbohydr. Res. 340 (2005) 97–
494 106. doi:10.1016/j.carres.2004.10.022.

495 [33] H. Wang, H. Tang, S. Salley, K.Y. Simon Ng, Analysis of sterol glycosides in

496 biodiesel and biodiesel precipitates, JAOCS, J. Am. Oil Chem. Soc. 87 (2010) 215–
497 221. doi:10.1007/s11746-009-1489-x.

498 [34] N.A. Negm, M.T.H. Abou Kana, M.A. Youssif, M.Y. Mohamed, Biofuels from
499 vegetable oils as alternative fuels: Advantages and disadvantages, 2017.
500 doi:10.1201/b20780.

501 [35] A. Khodabandehloo, A. Rahbar-Kelishami, H. Shayesteh, Methylene blue removal
502 using Salix babylonica (Weeping willow) leaves powder as a low-cost biosorbent in
503 batch mode: Kinetic, equilibrium, and thermodynamic studies, J. Mol. Liq. 244 (2017)
504 540–548. doi:10.1016/j.molliq.2017.08.108.

505 [36] H.J. Lee, H.S. Lee, J. Seo, Y.H. Kang, W. Kim, T.H.K. Kang, State-of-the-art of
506 cellulose nanocrystals and optimal method for their dispersion for construction-related
507 applications, Appl. Sci. 9 (2019) 1–14. doi:10.3390/app9030426.

508 [37] S. Chowdhury, R. Mishra, P. Saha, P. Kushwaha, Adsorption thermodynamics,
509 kinetics and isosteric heat of adsorption of malachite green onto chemically modified
510 rice husk, Desalination. 265 (2011) 159–168. doi:10.1016/j.desal.2010.07.047.

511 [38] H. More, Factors Affecting Adsorption, (2018).
512 https://hemantmore.org.in/science/chemistry/factors-affecting-adsorption/13094/
513 (accessed May 5, 2019).

514 [39] M. Mohapatra, S. Khatun, S. Anand, Kinetics and thermodynamics of lead (II)
515 adsorption on lateritic nickel ores of Indian origin, Chem. Eng. J. 155 (2009) 184–190.
516 doi:10.1016/j.cej.2009.07.035.

517 [40] A. de Sá, A.S. Abreu, I. Moura, A.V. Machado, Polymeric materials for metal sorption
518 from hydric resources, Elsevier Inc., 2017. doi:10.1016/b978-0-12-804300-4.00008-3.

[41] C.S. Zhu, L.P. Wang, W. bin Chen, Removal of Cu(II) from aqueous solution by agricultural by-product: Peanut hull, J. Hazard. Mater. 168 (2009) 739–746. doi:10.1016/j.jhazmat.2009.02.085.

[42] Q. Li, L. Chai, Z. Yang, Q. Wang, Kinetics and thermodynamics of Pb(II) adsorption onto modified spent grain from aqueous solutions, Appl. Surf. Sci. 255 (2009) 4298–4303. doi:10.1016/j.apsusc.2008.11.024.

[43] Y. Liu, Y.J. Liu, Biosorption isotherms, kinetics and thermodynamics, Sep. Purif. Technol. 61 (2008) 229–242. doi:10.1016/j.seppur.2007.10.002.

[44] Y. Habibi, L.A. Lucia, O.J. Rojas, Cellulose nanocrystals: Chemistry, self-assembly, and applications, Chem. Rev. 110 (2010) 3479–3500. doi:10.1021/cr900339w.

[45] Y. Liu, D. Ying, L. Sanguansri, Y. Cai, X. Le, Adsorption of catechin onto cellulose and its mechanism study: Kinetic models, characterization and molecular simulation, Food Res. Int. 112 (2018) 225–232. doi:10.1016/j.foodres.2018.06.044.

534 **Figure captions.**

535 **Figure 1.** X-Ray Diffraction Patterns of (a) CFP, (b) CFP-based NCC

536 **Figure 2.** SEM image of the rod-like CFP-based NCC particles

537 **Figure 3.** FTIR spectrum of (a) CFP-based NCC before adsorption and (b) CFP-based NCC
538 after adsorption

539 **Figure 4.** SG removal rate varied with the mass ratio of CFP-based NCC to PO-B100 at three
540 different temperatures

541 **Figure 5.** The Pareto chart of the standardized effect showing the significance order of the
542 two independent variables (temperature and mass ratio of NCC to PO-B100) on the SG
543 removal, generated by ANOVA

544 **Figure 6.** The modelled isotherm profiles for the adsorption of SG to CFP-based NCC
545 surface (temperature = 75 °C, mass ratio of CFP-based NCC to PO-B100 = 1:50, time = 1 h,
546 agitation speed = 250 rpm)

547 **Figure 7.** Schematic representation of the proposed adsorption mechanism of SG onto CFP-
548 based NCC surface

549

550

551

552

553

554 **Table 1. The crystallinity index of CFP and CFP-based NCC**

Samples	2-theta (°)		Crystallinity (%)
	110 crystal plane	200 crystal plane	
CFP	15.44	22.63	57.60
CFP-based NCC	16.52	22.60	85.73

555

556

557 **Table 2. The properties of untreated and treated PO-B100 (1:50, 75 °C, 1 h), and the**
558 **comparison with ASTM D6751 and SNI 7182:2015**

Parameters	ASTM D6751	SNI 7182:2015	Untreated PO-B100	Treated PO-B100 (1:50, 75 °C, 1 h)
FAME (%)	≥ 96.5	≥ 96.5	98.7	98.8
AV (mg KOH/g)	≤ 0.50	≤ 0.50	0.12	0.11
MG (%)	≤ 0.80	≤ 0.80	0.23	0.22
DG (%)	≤ 0.20	-	0.09	0.09
TG (%)	≤ 0.20	-	0.06	0.05
SG (mg/kg)	N/A*	N/A*	194.1	15.9
Cloud point (°C)	-	18.0	13.2	11.5

559 * Not available

560

Table 3. Isotherm parameters of SG adsorption onto CFP-based NCC surface

Isotherm	Parameters	Temperature (K)		
		338	348	358
Langmuir	$Q_{m(L)}$ (mg/g)	12.50	12.93	11.24
	K_L (L/mg)	0.11	0.16	0.26
	r^2	0.8587	0.8580	0.7039
	χ^2	0.2329	0.2865	0.2487
Freundlich	K_F ((mg/g) $(L/mg)^{1/n}$)	5.59	6.48	7.31
	1/n	0.16	0.03	0.09
	r^2	0.8408	0.7986	0.6079
	χ^2	0.2624	0.4064	0.3293
Dubinin-Radushkevich	$Q_{m(D-R)}$ (mg/g)	11.58	12.13	10.86
	E (kJ/mol)	0.18	0.25	0.29
	r^2	0.8094	0.8387	0.7555
	χ^2	0.3147	0.3254	0.2053

564 **Table 4. Thermodynamic parameters of adsorption of SG onto CFP-based NCC surface**

Temperature (K)	Thermodynamic parameters		
	ΔG° (kJ/mol)	ΔH° (kJ/mol)	ΔS° (J/mol.K)
338	-31.44	42.90	219.80
348	-33.46		
358	-35.84		

565

566

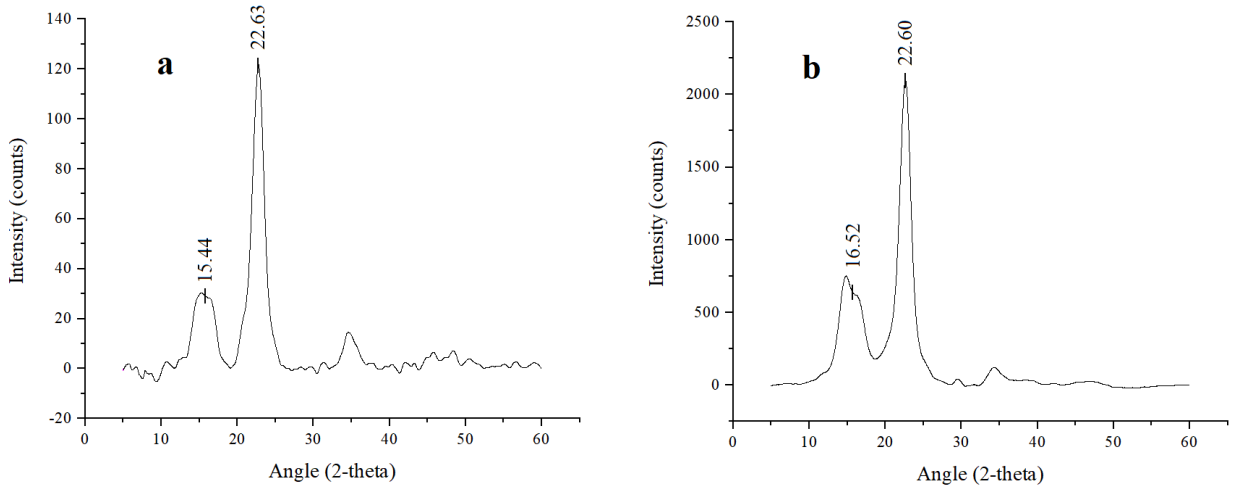
a
22.63
15.44
Intensity (counts)
Angle (2-theta)
b
22.60
16.52
Intensity (counts)
Angle (2-theta)

Figure 1

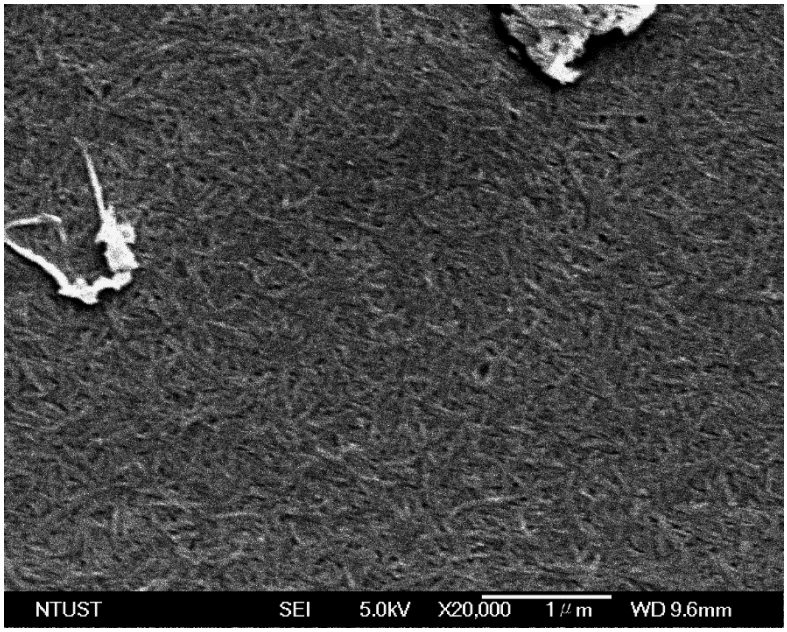

Figure 2

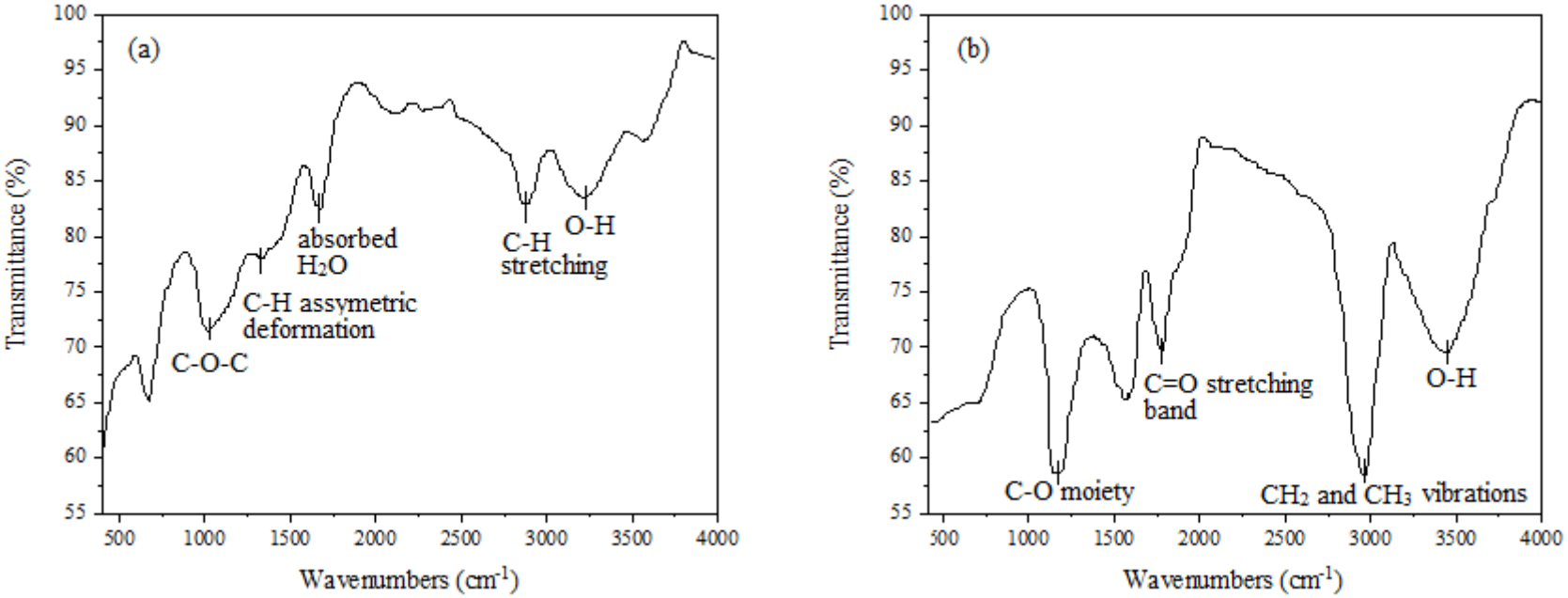
(a)
Transmittance (%)
Wavenumbers (cm-1)
C-O-C
C-H assymetric deformation
absorbed H2O
C-H stretching
O-H
(b)
Transmittance (%)
Wavenumbers (cm-1)
C-O moiety
C=O stretching band
CH2 and CH3 vibrations
O-H

Figure 3

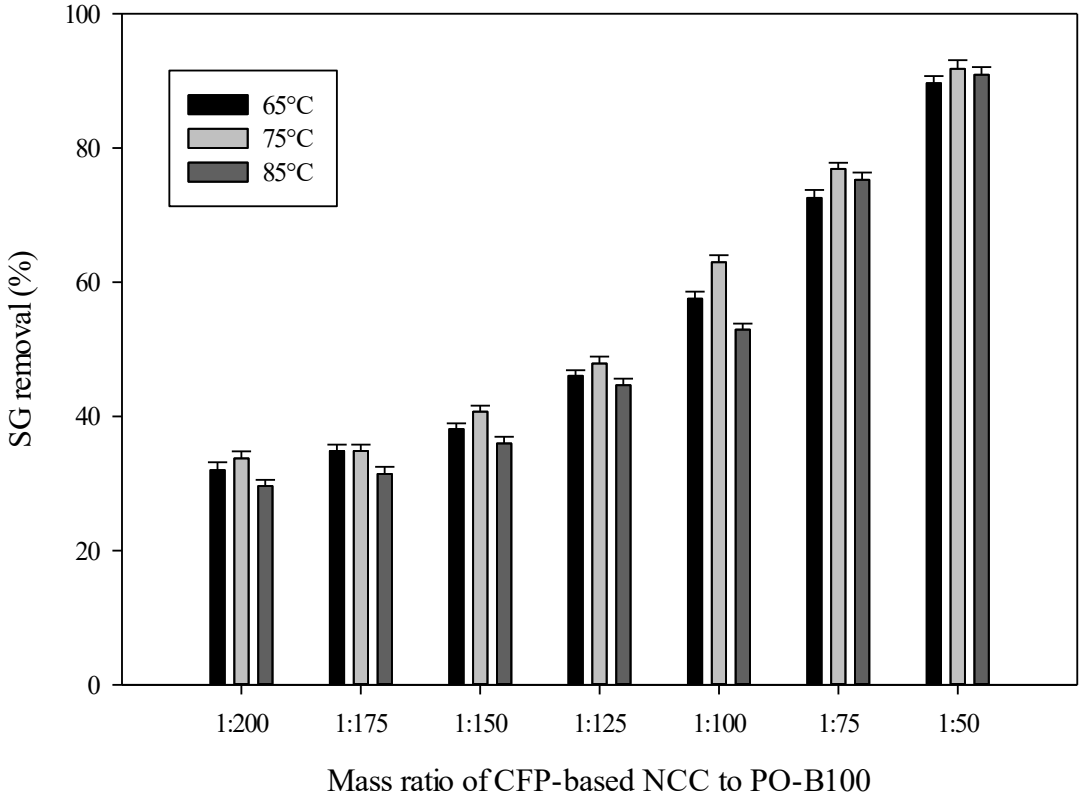

576
577 **Figure 4**
578

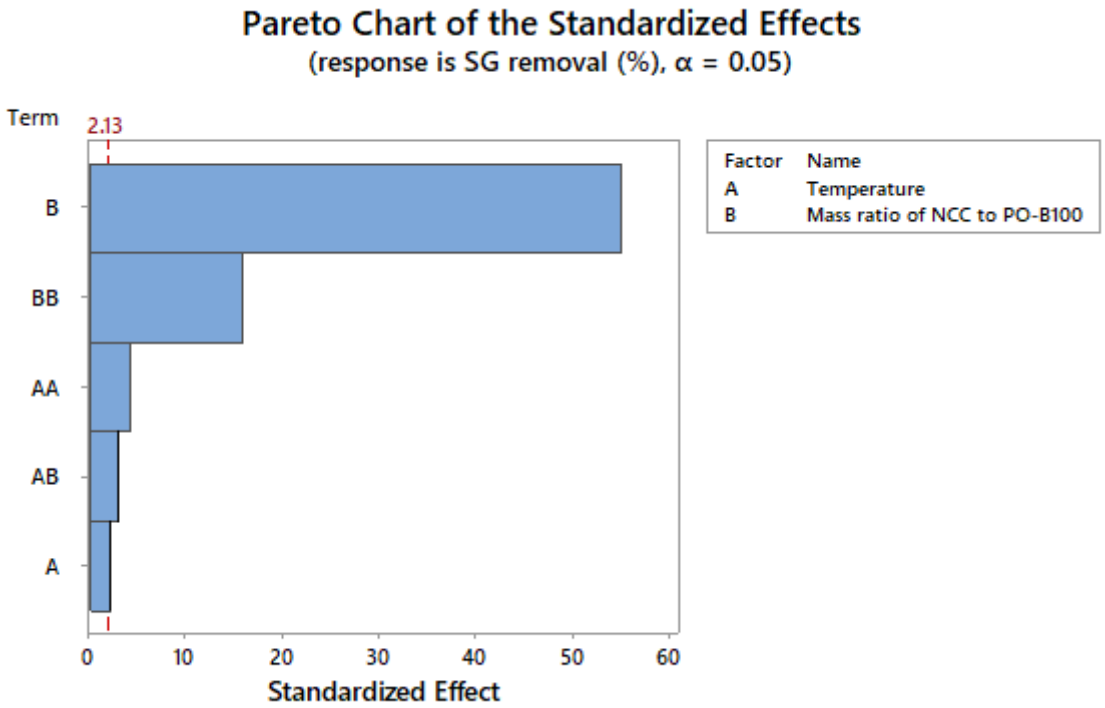
Pareto Chart of the Standardized Effects
(response is SG removal (%), α = 0.05)
Term
2.13
B
BB
AA
AB
A
0
10
20
30
40
50
60
Standardized Effect
Factor Name
A Temperature
B Mass ratio of NCC to PO-B100

Figure 5

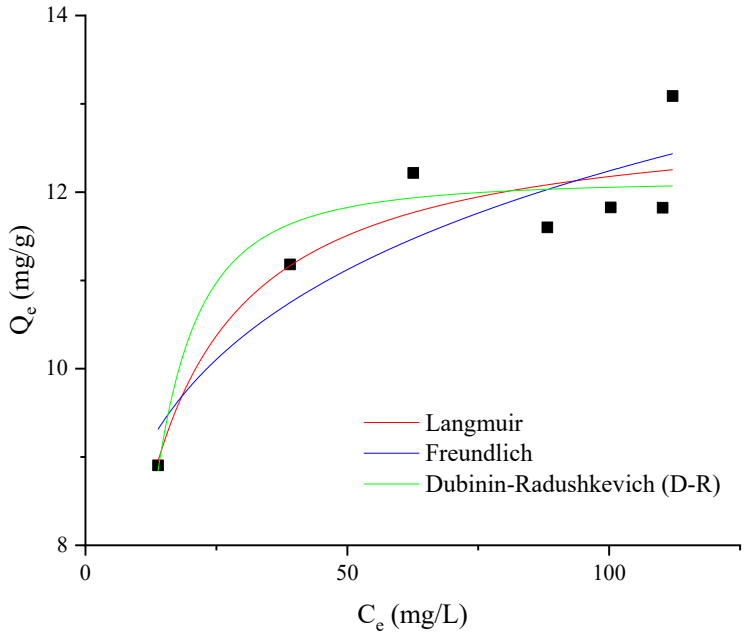
14
12
10
8
0
50
100
Qe (mg/g)
Ce (mg/L)
Langmuir
Freundlich
Dubinin-Radushkevich (D-R)

Figure 6

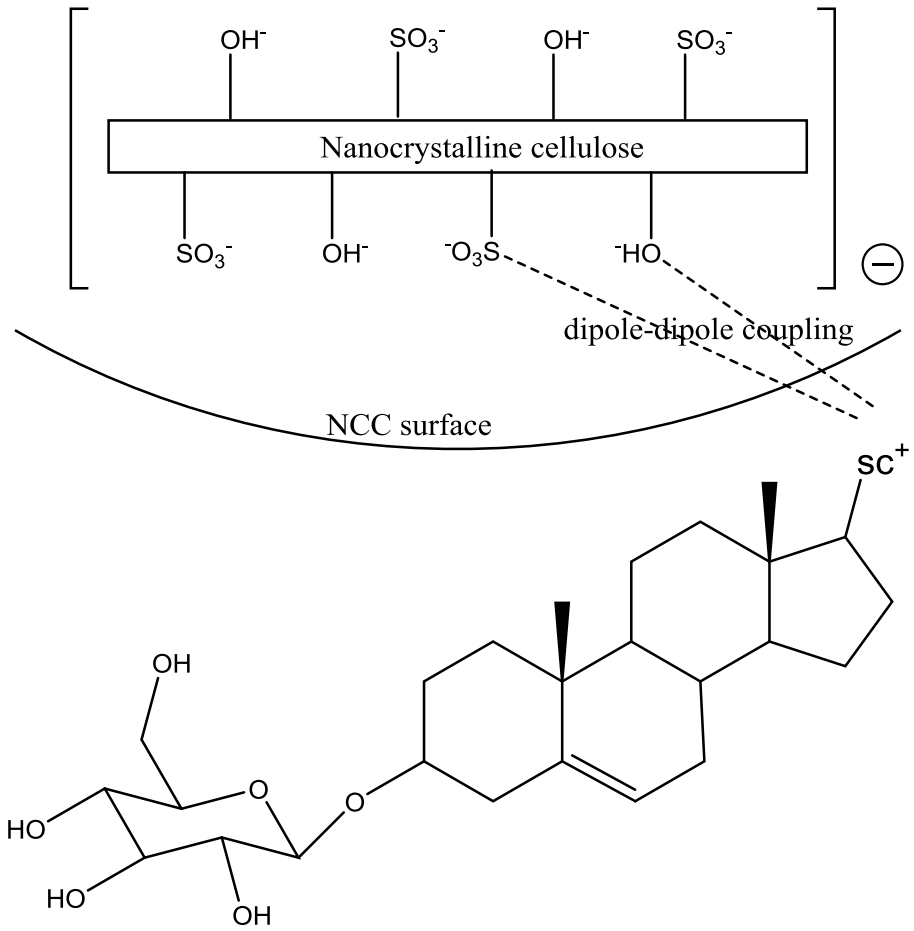
OH-
SO3-
OH-
SO3-
Nanocrystalline cellulose
SO3-
OH-
-O3S
-HO
dipole-dipole coupling
NCC surface
SC+
OH
O
O
HO
HO
OH

Figure 7

*Declaration of Interest Statement

Declaration of interests

☒ The authors declare that they have no known competing financial interests or personal relationships that could have appeared to influence the work reported in this paper.

☐The authors declare the following financial interests/personal relationships which may be considered as potential competing interests:

CREDIT AUTHOR STATEMENT

Liangna Widdyaningsih	-	Conceptualization, methodology, investigation, software, writing – original draft
Albert Setiawan	-	Conceptualization, methodology, investigation, software, writing – original draft
Shella Permatasari Santoso	-	Conceptualization, data curation, supervision
Felycia Edi Soetaredjo	-	Resources, visualization
Suryadi Ismadji	-	Resources, validation
Sandy Budi Hartono	-	Software, validation
Yi-Hsu Ju	-	Writing-review and editing
Tran-Nguyen Phuong Lan	-	Writing-review and editing
Maria Yuliana	-	Conceptualization, resources, visualization, writing-review and editing, supervision

Gmail

Maria Yuliana <mariayuliana@ukwms.ac.id>

Your Submission RENE-D-19-04543R1

1 message

Renewable Energy <eesserver@eesmail.elsevier.com> Sun, Mar 1, 2020 at 2:49 PM
Reply-To: Renewable Energy <rene@elsevier.com>
To: mariayuliana@ukwms.ac.id, maria_yuliana_liauw@yahoo.com
Cc: liangna16@gmail.com, albert.st12@gmail.com, shella_p5@yahoo.com, felyciae@yahoo.com, sandy@ukwms.ac.id, tnplan@ctu.edu.vn, suryadiismadji@yahoo.com, yhju@mail.ntust.edu.tw

Ms. Ref. No.: RENE-D-19-04543R1
Title: FEASIBILITY STUDY OF NANOCRYSTALLINE CELLULOSE AS ADSORBENT OF STERYL GLUCOSIDES FROM PALM-BASED BIODIESEL
Renewable Energy

Dear Dr. Yuliana,

I am pleased to inform you that your paper "FEASIBILITY STUDY OF NANOCRYSTALLINE CELLULOSE AS ADSORBENT OF STERYL GLUCOSIDES FROM PALM-BASED BIODIESEL" has been accepted for publication in Renewable Energy.

Your accepted manuscript will now be transferred to our production department and work will begin on creation of the proof. If we need any additional information to create the proof, we will let you know. If not, you will be contacted again in the next few days with a request to approve the proof and to complete a number of online forms that are required for publication.

Effective peer review is essential to uphold the quality and validity of individual articles, but also the overall integrity of the journal. We would like to remind you that for every article considered for publication, there are usually at least 2 reviews required for each review round, and it is critical that scientists wishing to publish their research also be willing to provide reviews to similarly enable the peer review of papers by other authors. Please accept any review assignment within your expertise area(s) we may address to you and undertake reviewing in the manner in which you would hope your own paper to be reviewed.

Thank you very much for expressing your interest in Renewable Energy.

Sincerely,
Soteris Kalogirou, D.Sc.
Editor-in-Chief
Renewable Energy

Renewable Energy 154 (2020) 99–106

Contents lists available at ScienceDirect

Renewable Energy

journal homepage: www.elsevier.com/locate/renene

Feasibility study of nanocrystalline cellulose as adsorbent of steryl glucosides from palm-based biodiesel

Liangna Widdyaningsih [a, 1], Albert Setiawan [a, 1], Shella Permatasari Santoso [a, b], Felycia Edi Soetaredjo [a, b], Suryadi Ismadji [a, b], Sandy Budi Hartono [a], Yi-Hsu Ju [b, c, d], Phuong Lan Tran-Nguyen [e], Maria Yuliana [a, *]

[a] Department of Chemical Engineering, Widya Mandala Catholic University Surabaya, Kalijudan 37, Surabaya, 60114, Indonesia
[b] Department of Chemical Engineering, National Taiwan University of Science and Technology, 43 Keelung Road, Sec 4, Taipei, 10607, Taiwan
[c] Graduate Institute of Applied Science and Technology, National Taiwan University of Science and Technology, 43 Keelung Road, Sec 4, Taipei, 10607, Taiwan
[d] Taiwan Building Technology Center, National Taiwan University of Science and Technology, 43 Keelung Road, Sec 4, Taipei, 10607, Taiwan
[e] Department of Mechanical Engineering, Can Tho University, 3-2 Street, Can Tho City, Viet Nam

ARTICLE INFO

Article history:
Received 16 October 2019
Received in revised form
3 February 2020
Accepted 1 March 2020
Available online 4 March 2020

Keywords:
Biodiesel
Steryl glucosides removal
Nanocrystalline cellulose
Adsorption isotherm
Adsorption mechanism
Feasibility study

ABSTRACT

Increasing the content of biodiesel in the diesel fuel mixture faces some challenges due to the presence of steryl glucosides (SG) compounds, which causes the filter clogging and the reduction of engine power. In this study, coarse filter paper-based nanocrystalline cellulose (CFP-based NCC) with the crystallinity of 85.73% is selected as a potential adsorbent to separate SG compounds in palm-based biodiesel (PO−B100). The adsorption experiments were carried out at various CFP-based NCC to PO-B100 mass ratio (1:50, 1:75, 1:100, 1:125, 1:150, 1:175, 1:200) and temperature (65, 75, 85 °C). The maximum SG removal was 91.81%, obtained at 75 °C for CFP-based NCC to PO-B100 mass ratio of 1:50. The adsorption treatment also improves the cold stability of PO-B100 by reducing the cloud point from 13.2 °C to 11.5 °C. Langmuir isotherm model is best-fitted to the equilibrium adsorption data and thermodynamic studies suggested that the adsorption of SG onto the CFP-based NCC surface is spontaneous and endothermic. The isotherm and thermodynamic study showed that the mechanism governing the adsorption process may be driven by both dipole-dipole interactions and ion exchange. The adsorption results showed that CFP-based NCC has great affinity and selectivity to SG and can be considered as a promising adsorbent of SG.

1. Introduction

To date, petroleum diesel is used worldwide for transportation, manufacturing, power generation, construction and farming industries. However, disruption in crude market price and the long-term availability along with the nature deterioration due to its gas emission have become the major concerns for environmental sustainability [1]. Therefore, it is necessary to develop alternative fuels that are environmentally friendly, especially as a substitute for diesel fuel.

Of the several alternative fuels available, biodiesel is an alternative diesel fuel made from renewable biological resources [2]. Biodiesel is generally derived from transesterification of agricultural or animal lipids and short-chain alcohols in the presence of a catalyst. Conventional base-catalyzed transesterification in a batch stirred-tank reactor is the most common technique used to produce the commercially available biodiesel [3]. Several modifications on the conversion route as well as the reactor configuration and design have been performed in order to create, optimize and intensify the continuous production of biodiesel. The transesterification using catalyst-free subcritical [4–6] or supercritical alcohol [7,8], as well as heterogeneous [9] or enzymatic catalyst [9,10], gain wide attention in improving the continuity of biodiesel production. Likozar et al. (2016) also introduced a simple and robust design of a tubular reactor with a static mixer to intensify the mass transfer rate between the reactants and increase the biodiesel conversion rate. Their work also studied the chemical equilibrium and reaction kinetics at different operating parameters to optimize the product

* Corresponding author.
E-mail address: mariayuliana@ukwms.ac.id (M. Yuliana).
[1] These authors contributed equally to this work.

https://doi.org/10.1016/j.renene.2020.03.001
0960-1481/

Abbreviation

SG	Steryl glucoside(s)
MG	Monoacylglyceride(s)
DG	Diacylglyceride(s)
TG	Triacylglyceride(s)
CFP	Coarse filter paper
NCC	Nanocrystalline cellulose
FAME	Fatty Acid Methyl Ester(s)
PO-B100	Palm-based biodiesel

yield [11].

While biodiesel is currently mass-produced and a large number of studies have been carried out to improve its performance in various aspects, the white precipitates are still a challenge for its manufacturers. Although biodiesel distributed around the country must conform to the fuel property specifications as controlled by ASTM D6751, white precipitates were often detected in biodiesel and its blends during storage [12]. Several cases even showed that suspended particles in biodiesel have been found shortly after the production and at a rather high temperature (slightly below 60 °C) [13]. The white precipitates may cause filter plugging in engine systems [13,14]. This phenomenon was also observed in many biodiesel plants and hence frequent maintenance and process modification are often essential to maintain plant effectiveness and efficiency.

The presence of steryl glucosides (SG), which is one of the plant sterols, has been identified as the major component of the white precipitates. It mostly presents in biodiesel with a concentration of 35 ppm or higher [15]. The existence of this dispersed particles of SG promotes the aggregation of other components in biodiesel, saturated monoacylglycerides (MG) and diacylglycerides (DG), and subsequently affects the cold flow stability of fuel and widespread use [16].

Several techniques have been conducted to minimize the SG content in the biodiesel product, namely enzymatic hydrolysis [17,18], adsorption using magnesium silicate and bleaching earth [16] and ultrafiltration [19]. SG removal by enzymatic hydrolysis resulted in 81% removal efficiency with the addition of a synthetic codon-optimized version of the LacS gene expressed from *E. coli* with the total operating time of 7 h [17]. Na-Ranong et al. (2015) reported that the conventional adsorption using magnesium silicate and bleaching earth in temperature of 65–80 °C yielded in 81.4–82.5% removal efficiency of SG [16]. Tremblay and Montpetit (2017) stated that the highest separation for SG (86%) by ultrafiltration was obtained when the biodiesel was transesterified using 0.7% (w/w) catalyst and 4:1 methanol:soybean oil molar ratio [19]. Based on the removal efficiency and economic feasibility, the adsorption treatment is a potential method to reduce SG content as well as to improve the cold flow properties of the fuel in the industrial scale because it is found to be effective and facile, time-saving and energy-efficient.

The development of adsorbent for effective adsorption has been conducted using various types of materials. Currently, the development of cellulosic adsorbent received major interest because it is renewable, biodegradable, low cost, and non-toxic [20]. Cellulosic adsorbents have the ability to meet the requirement of being a biosorbent, as it is abundantly available as a natural biopolymer. Cellulose in the form of nanocrystalline cellulose (NCC) has been widely studied due to its extensive industrial application, namely enzyme immobilization, adsorption, catalysis, drug delivery, biosensors and bio-imaging [21]. NCC, with a large specific surface area and plenty of surface hydroxyl and anionic sulfate ester group for physical and chemical reactions [22–24], can be considered as a new promising adsorbent for SG removal.

As the Indonesian government plans to increase the use of biodiesel in diesel blend from B20 to B30 in the time span of 5 years, the use of NCC for SG removal and improvement of the cold stability is an interesting topic to be studied. The objective of this study is to observe the feasibility of coarse filter paper-based NCC (CFP-based NCC) as the adsorption agent for SG. Various operating parameters, namely temperature, and the mass ratio of CFP-based NCC to palm-based biodiesel (PO–B100) will be monitored. The adsorption mechanism was also proposed based on the isotherm and thermodynamics study.

2. Materials and methods

2.1. Materials

PO-B100 was collected from a local palm oil manufacturer in Gresik, Indonesia, and stored for 3 days at room temperature prior to the adsorption experiment. Coarse filter paper (CFP) as the cellulosic material was obtained from a local supplier in Surabaya, Indonesia. Sulphuric acid, sodium hydroxide, ethyl acetate, and n-hexane were purchased from Merck, Germany. FAMEs standard 47885 U contains 37 components FAME mix and SG standard 1117 were procured from Supelco (Bellefonte, PA, USA) and Matreya (State College, PA, USA), respectively. Nitrogen gas (99.9% purity) was purchased from Aneka Gas Industry Pty. Ltd., Surabaya. All reagents were of analytical grade and required no further purification.

2.2. Preparation of NCC

CFP was ground into fibrous powder before use. The non-cellulosic material of CFP was subsequently removed to obtain purified cellulose using the modified method of Putro et al. (2017) [25]: 12 g of the CFP powder was delignified using 0.1 g/ml sodium hydroxide aqueous solution (40 ml). The delignified product was washed with distilled water and filtrated three times through a Whatman 1 (11 μm pore size) filter paper before being dried under vacuum at 80 °C for 12 h.

CFP-based NCC was prepared by using acid hydrolysis following the procedure conducted by Putro et al. (2017) [25]. 1 g of delignified cellulose was hydrolyzed with 20 ml sulphuric acid 64% at 45 °C for 75 min under constant agitation. The reaction time was selected to ensure high reaction efficiency. After the specified duration, the reaction was immediately quenched using 20-fold of cold distilled water. The suspension was centrifuged at 4500 rpm for 10 min to remove the excess acid solution. The resulting precipitates were dialyzed against distilled water until neutral pH was achieved. The colloidal suspension was subjected to sonication treatment for 30 min in a cooling bath to avoid overheating and subsequently subjected to vacuum drying at 80 °C for 6 h to obtain CFP-based NCC powder.

2.3. Characterization of CFP-based NCC

The surface morphologies of the CFP-based NCC particles were analyzed on a field emission scanning electron microscope (FESEM) JEOL JSM-6500F (Jeol Ltd., Japan), with an accelerating voltage of 5–10 kV and 9.5–9.6 mm working distance. The CFP-based NCC powder was attached to a stub, sputtered and coated with gold prior to analysis. Fourier Transform Infrared (FTIR) analysis was performed by an FTIR-8400S spectrophotometer (Shimadzu, Japan) in the range of 400–4000 cm^{-1} at a 4 cm^{-1} scanning resolution.

XRD analysis was conducted by an X'PERT Panalytical Pro X-Ray diffractometer (Philips-FEI, Netherlands) with monochromatic Cu $K\alpha_1$ radiation at wavelength (λ) = 0.154 nm, 40 kV of voltage and 30 mA of tube current. The diffraction pattern was acquired in the range of 5°–60° (2θ angle). The crystallinity index (CrI) was expressed according to the following equation, as proposed by Segal et al. (1959) [26].

$$\text{CrI}\ (\%) = \frac{(I_{200} - I_{am})}{I_{200}} x100 \quad (1)$$

Where I_{200} is the maximum intensity of the 200 lattice diffraction at 2θ around 22°, I_{am} is the maximum intensity of the amorphous region at 2θ = 18°. The crystallite size (nm) was calculated using the Scherrer analysis.

2.4. Compositional study of SG in PO-B100 using GC-FID analysis

The analysis of SG composition in PO-B100 was carried out using GC-17A (Shimadzu, Japan), completely equipped with a split/splitless injector and a flame ionization detector (FID). The separation was performed using nonpolar capillary column DB-5HT (5 %-phenyl)-methylpolysiloxane (15 m × 0.32 mm ID, Agilent Technology, CA). The column temperature was initially set at 80 °C, then subsequently ramped to 365 °C at the rate of 15 °C/min, and held constant for 19 min. The temperature of the injector and detector were adjusted constant at 370 °C 100 mg of SG was dissolved in 1 ml ethyl acetate and subjected to filtration using polyvinylidene difluoride (PVDF) filter prior analysis. The prepared sample (1 μl) was injected into the GC with a split ratio of 1:50. The velocity of nitrogen (N_2, 99.9%) as the carrier gas was fixed at 30 cm/s at 80 °C.

2.5. Removal of SG using adsorption

The adsorption of SG from PO-B100 was conducted in a batch mode according to the study conducted by Na-Ranong et al. (2015) with a few modifications [16]. A various mass ratio of CFP-based NCC to PO-B100 (1:50, 1:75, 1:100, 1:125, 1:150, 1:175, 1:200) was introduced into a series of beakers, where the mixture will be subjected to a 1-h adsorption process at constant temperature and agitation speed (250 rpm). The selection of adsorption duration was based on the preliminary experiment conducted to find the equilibrium time. Several adsorption temperatures (65, 75 and 85 °C) were used to study the effect of temperature on the adsorption of SG. The solution was separated from the adsorbent by using centrifugation at the rotational speed of 4900 rpm for 10 min. The SG contents in PO-B100 before and after adsorption were analyzed using UV-mini 1240 spectrophotometer (Shimadzu, Japan) at 240 nm, according to the modified technique conducted by Moreau et al. (2008), Nyström (2007) and Araújo et al. (2013) [14,27,28]. The percentage of SG removal was determined by using the following equation.

$$SG\ removal\ (\%) = \frac{C_i - C_f}{C_i} x100 \quad (2)$$

Where C_i is the concentration of SG in untreated PO-B100 (mg/kg) and C_f is the concentration of SG in treated (after adsorption) PO-B100 (mg/kg). The results of SG removal were verified by using GC-FID analysis (see section 2.4) and its statistical approach was performed using Minitab software (version 18.1) to identify the significance order of the parameters affecting the adsorption.

2.6. Isotherm and thermodynamics study of the SG adsorption

The adsorption isotherm was conducted at the temperature of 65, 75 and 85 °C with various CFP-based NCC to PO-B100 mass ratio (1:50, 1:75, 1:100, 1:125, 1:150, 1:175, 1:200). It was performed using a similar procedure as previously mentioned in subsection 2.5. At the equilibrium condition, the amount of adsorbed SG per unit mass of CFP-based NCC as the adsorbent (Q_e) was calculated by the equation below.

$$Q_e\left(\frac{mg}{g}\right) = \frac{C_o - C_e}{m} x\ V \quad (3)$$

Where C_o and C_e are the initial and final (equilibrium) concentration of SG in PO-B100 (mg/L), respectively, m is the mass of adsorbent (g) and V is the volume of PO-B100 (L).

The equilibrium data obtained at various temperature were fitted to the three isotherm models, namely Langmuir, Freundlich and Dubinin-Radushkevich (D-R). Meanwhile, the thermodynamic parameters such as Gibbs free energy change (ΔG°), enthalpy (ΔH°) and entropy (ΔS°) were further determined from the results of isotherm study using equations (4) and (5).

$$\Delta G^\circ = -RTln\left(K_L.M_{SG}.10^3.C^o\right) \quad (4)$$

$$\Delta G^\circ = \Delta H^\circ - T\Delta S^\circ \quad (5)$$

Where R is the gas constant with the value of 8.314 J/mol.K, T is the absolute temperature in Kelvin, K_L is Langmuir equilibrium constant in L/mg, M_{SG} is the molecular weight of SG in g/mol and C^o is the reference concentration in standard state with the value of 1 mol/L.

3. Results and discussions

3.1. Characterization of CFP-based NCC

The X-ray diffraction pattern of the CFP and its NCC are shown in Fig. 1, and the corresponding crystallinity index is presented in Table 1. Both XRD patterns showed the cellulose I characteristic peaks at 2θ around 15–17° (110 crystal plane) and 22–23° (200 crystal plane) [26,29]. The crystallinity index of CFP and its NCC were calculated using equation (1) and recorded to have the corresponding value of 57.60% and 85.73%. The change of crystallinity has occurred because of the progressive removal of amorphous hemicellulose and lignin during acid hydrolysis. The highly crystalline product is more efficient to improve the mechanical properties of the composite material, particularly as an adsorbent, since crystallinity positively corresponds to the tensile strength of the material [30].

The scanning electron micrograph in Fig. 2 shows the shape and size of the CFP-based NCC. The distribution of NCC products derived from CFP was estimated to have approximately 200–400 nm in length (Fig. 2). The prepared CFP-based NCC has a homogenous needle-shaped with crystallite size in the range of 2–4 nm, obtained from the combination of X-ray diffraction data and Scherrer analysis. The homogenous CFP-based NCC particles are likely caused by the swollen of cellulose fibers due to NaOH delignification pretreatment [25].

Fig. 3 (a) – (b) illustrated the FTIR spectra of CFP-based NCC before and after adsorption. As shown in Fig. 3 (a), several peaks representing certain functional groups in CFP-based NCC were found in the spectra. The broad band in the range of 3008–3459 cm^{-1} represents the O–H stretching vibrations, while

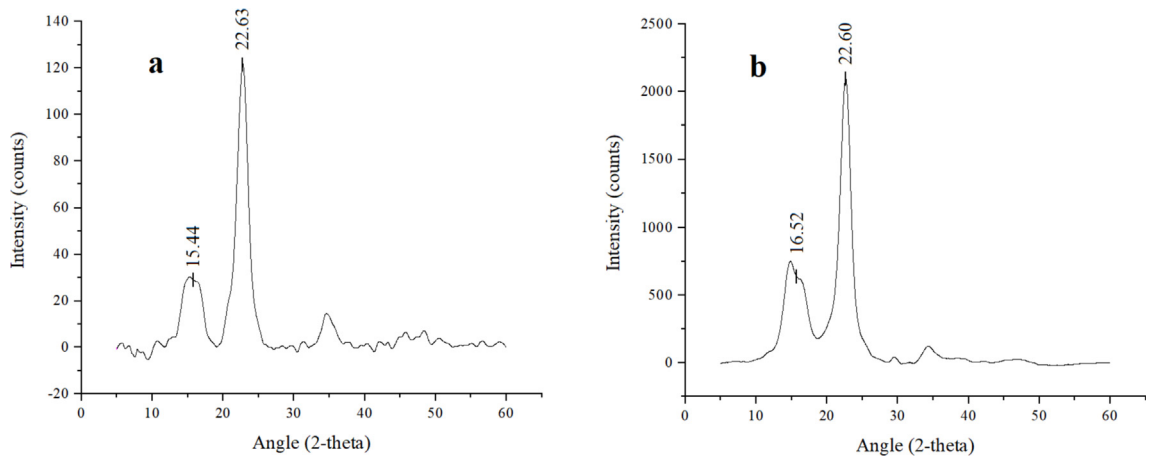

Fig. 1. X-ray diffraction patterns of (a) CFP, (b) CFP-based NCC.

Table 1
The crystallinity index of CFP and CFP-based NCC.

Samples	2-theta (°)		Crystallinity (%)
	110 crystal plane	200 crystal plane	
CFP	15.44	22.63	57.60
CFP-based NCC	16.52	22.60	85.73

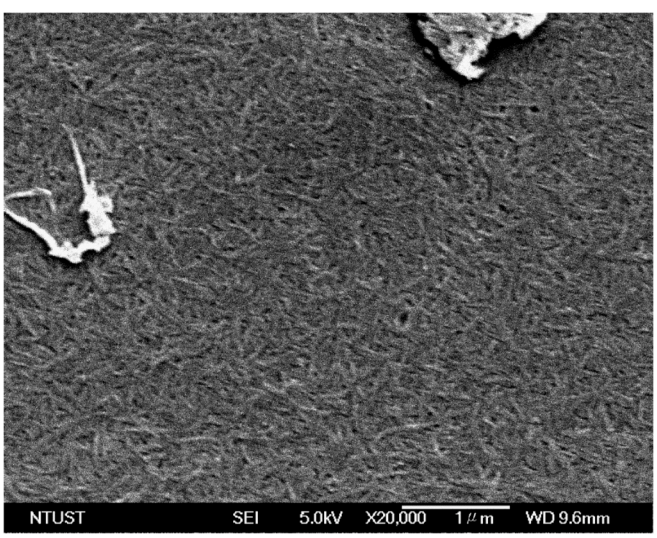

Fig. 2. SEM image of the rod-like CFP-based NCC particles.

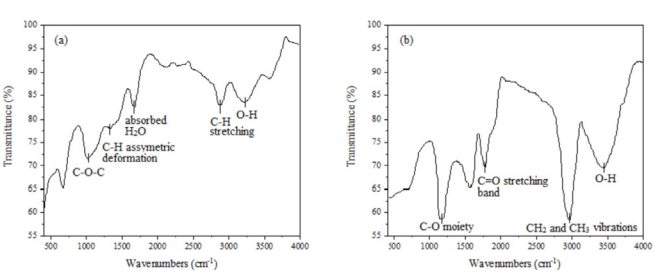

Fig. 3. FTIR spectrum of (a) CFP-based NCC before adsorption and (b) CFP-based NCC after adsorption.

the peaks in the range of 2802–2925 cm^{-1} correspond to C–H stretching vibrations. The absorption at 936–1137 cm^{-1} is related to the functional group of C–O–C, and the peak at 1640 cm^{-1} indicates the presence of abundant hydrophilic hydroxide group in the cellulose [31]. A peak at 1382 cm^{-1} represents the C–H asymmetric deformations [32].

Meanwhile, Fig. 3 (b) showed strong peaks in the wavenumbers of around 1019–1376 cm^{-1} and 2602–3160 cm^{-1}, which represent the C–O moiety, and CH_2 and CH_3 stretching vibrations. These two specific peaks are known as the fingerprint areas for SG. Another peak at 1750 cm^{-1} corresponds to the typical C=O stretching band of the methyl ester, while an O–H band around 3110 - 3700 cm^{-1} indicates the presence of hydroxyl groups in SG and CFP-based NCC [33]. Therefore, based on the FTIR spectra, it can be concluded that SG is the major component of the adsorbate on the surface of CFP-based NCC, which is consistent with the GC-FID results discussed in section 3.2.

3.2. Properties of PO-B100

The properties of PO-B100 have been analyzed according to the standard method of ASTM for its content of FAME, acid value (AV), MG, DG and triglycerides (TG). As reported in Table 2, the purity of FAME in PO-B100 is 98.7%, while the AV, MG, DG, and TG values are 0.12 mg KOH/g, 0.23%, 0.09%, and 0.06%, respectively. Furthermore, PO-B100 feedstock contained 194.1 mg/kg of SG with the cloud point of 13.2 °C and a clear initial appearance. Based on the GC-FID analysis, the SG profile in PO-B100 consists of 34.79% of campesteryl glucoside, 23.73% of stigmasteryl glucoside and 41.48% of β-sitosteryl glucoside. The results met the requirements of ASTM D6751 and SNI 7182:2015. However, white precipitates could be found within a few hours after production.

After the adsorption using the parameters giving the highest SG removal (1:50, 75 °C, 1 h; see section 3.3), the sample of treated PO-B100 was collected for the properties measurement in order to monitor the effect of the adsorbent. According to the results, the treated PO-B100 contained FAME with a purity of 98.8% and AV value of 0.11 mg KOH/g. The concentration of SG reduced significantly to 15.9 mg/kg with the composition of 24.81% campesteryl glucoside, 25.07% stigmasteryl glucoside and 50.12% β-sitosteryl glucoside, while the other glycerides components, MG, DG, and TG, were slightly decreased to 0.22%, 0.09%, 0.05%, respectively. The cloud point of the treated PO-B100 was also found to be decreased to 11.5 °C. These results indicated that CFP-based NCC has selectivity to adsorb SG, particularly campesteryl glucoside and

Table 2
The properties of untreated and treated PO-B100 (1:50, 75 °C, 1 h), and the comparison with ASTM D6751 and SNI 7182:2015.

Parameters	ASTM D6751	SNI 7182:2015	Untreated PO-B100	Treated PO-B100 (1:50, 75 °C, 1 h)
FAME (%)	≥96.5	≥96.5	98.7	98.8
AV (mg KOH/g)	≤0.50	≤0.50	0.12	0.11
MG (%)	≤0.80	≤0.80	0.23	0.22
DG (%)	≤0.20	–	0.09	0.09
TG (%)	≤0.20	–	0.06	0.05
SG (mg/kg)	N/A[a]	N/A[a]	194.1	15.9
Cloud point (°C)	–	18.0	13.2	11.5

[a] Not available.

stigmasteryl glucoside, as compared to the other minor components, such as MG, DG, and TG. It also subsequently lowered the cloud point significantly, which is advantageous for storage and transportation purposes [34].

3.3. Adsorption of SG using CFP-based NCC

Fig. 4 summarized the SG removal rate at the various temperature and mass ratios of CFP-based NCC to PO-B100. The highest value of the SG removal rate (91.81%) was obtained at the following conditions: 75 °C, CFP-based NCC to PO-B100 mass ratio of 1:50, and 1 h adsorption time. Based on the results shown in Fig. 4, the lowest removal rate of SG in every adsorption temperature was seen at 1:200 of CFP-based NCC to PO-B100 mass ratio. It was likely due to insufficient binding and active adsorption sites and the adsorption required more time to reach the equilibrium stage. The removal percentage of SG was observed to have amplified with the increase of CFP-based NCC to PO-B100 mass ratio from 1:200 to 1:50 at all temperatures in the tested range. Greater amounts of CFP-based NCC provide greater adsorption surface area and active sites in CFP-based NCC, leading to an adequate SG binding area and certainly, a higher percentage of SG removal [35]. It was also monitored that the SG removal rate exponentially increased when the CFP-based NCC to PO-B100 mass ratio was increased from 1:100 to 1:50 in the all adsorption temperature. The phenomenon indicated the good dispersion ability of CFP-based NCC in PO-B100, where constant diffusion path length of SG binding to CFP-based NCC surface was found regardless of the amount of adsorbent [36].

As depicted in Fig. 4, temperature also remarkably affected the SG reduction. A temperature elevation from 65 °C to 75 °C improves the reduction of SG, regardless of CFP-based NCC to PO-B100 mass ratio. Chowdhury et al. (2011) stated that the adsorption enhancement along with the temperature increase may be associated with the increase of the number of active sites available for adsorption. The diffusion rate of the adsorbate across the external boundary layer also escalates with the rise in temperature, due to lower solution viscosity and enhancement in the mobility and kinetic energy of the adsorbate [37]. Therefore, the collision between particles intensifies with the temperature elevation so that the activation energy of the adsorption process is easier to achieve. As a result, the amount of the adsorbed SG enhances along with the temperature increase. However, it was also observed that the SG removal rate decreased when the temperature was further escalated from 75 °C to 85 °C. More (2018) mentioned that after reaching a certain temperature, excessive particle collision causes the removal of adsorbates from the adsorbent, leading to lower adsorption capacity [38]. Lee et al. (2019) also stated that the NCC surface binding generally weakens along with the temperature enhancement [36]. The fluctuations of the SG uptake observed with the change in temperature suggests that the SG adsorption is governed by both physical attraction and chemical bonding, indicating that the sorption of SG by CFP-based NCC is both driven by physical and chemical sorption [37,39].

Fig. 5 presented the Pareto chart of the standardized effect generated using statistical analysis (Minitab version 18.1). The figure showed that both independent parameters (temperature and the mass ratio of CFP-based NCC to PO-B100) were found to be prominent with the significance order of the mass ratio of CFP-based NCC to PO-B100 > temperature. The other quadratic and two-way interaction terms were also found to significantly affect the SG removal rate.

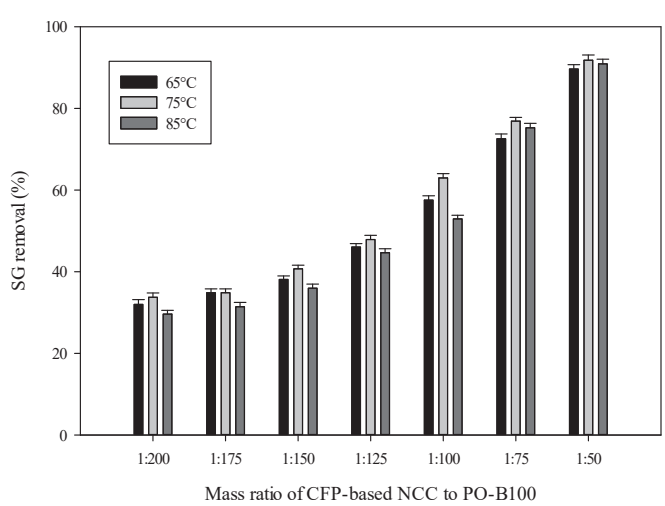

Fig. 4. SG removal rate varied with the mass ratio of CFP-based NCC to PO-B100 at three different temperatures.

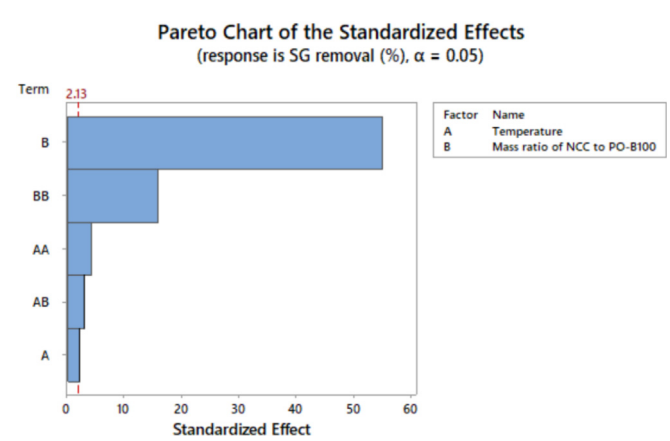

Fig. 5. The Pareto chart of the standardized effect showing the significance order of the two independent variables (temperature and mass ratio of NCC to PO-B100) on the SG removal, generated by ANOVA.

3.4. Study of adsorption isotherm and thermodynamic parameters

In this study, three isotherm equations were fitted to the experimental equilibrium data for SG at three temperature points (65 °C, 75 °C and 85 °C). The results are presented in Table 3 and the isotherm models are plotted in Fig. 6. The Langmuir isotherm constant, K_L and maximum absorption capacity, $Q_{m(L)}$ were calculated from the nonlinear curve fitting between Q_e and C_e. The value of $Q_{m(L)}$ was found to be increased from 12.50 mg/g at 65 °C to 12.93 mg/g at 75 °C before declining to 11.24 mg/g at the highest tested temperature (85 °C). The $Q_{m(L)}$ results are quite comparable to the adsorption capacity of magnesium silicate and bleaching earth on the SG (~13 mg/g) [16]. The Langmuir constant (K_L) also increases along with the temperature, from 0.11 L/mg at the lowest temperature (65 °C) to 0.26 L/mg at the highest temperature point (85 °C), indicating that the adsorption of SG to CFP-based NCC is an endothermic process.

The isotherm data were further analyzed by the Freundlich model. The Freundlich constant K_F and 1/n were obtained from the non-linear regression analysis. Table 3 showed that the values of 1/n are all under unity, ranging from 0.03 at 75 °C to 0.16 at 65 °C. The extent of 1/n represents the favorability degree of adsorption. The value of 1/n less than unity corresponds to favorable sorption. It was also observed that the Freundlich constant greatly escalates along with the temperature, implying that the adsorption was favorable at high temperature and the process is certainly endothermic. de Sá et al. (2017) mentioned that 1/n value between 0 and 1 is associated with a chemisorption process [40].

Another isotherm equation, the Dubinin-Radushkevich (D-R) model, was further applied to analyze the equilibrium data, particularly to determine the nature of SG adsorption onto CFP-based NCC surface. The D-R constant (β) gives an idea about the mean sorption energy, E, and their correlation can be expressed by the following equation:

$$E = \frac{1}{\sqrt{2\beta}} \tag{6}$$

where E represents sorption energy (kJ/mol) and β is the D-R constant ($mmol^2/J^2$). The value of sorption energy provides information to determine the type of adsorption mechanism, as chemical ion exchange or physical adsorption. Li et al. (2009) and Zhu et al. (2009) stated that if the sorption energy ranges from 8 to 16 kJ/mol, the sorption process is supposed to be chemisorption, while for energy value lower than 8 kJ/mol, the sorption is of physical nature [41,42]. Based on the results provided in Table 3, the adsorption mechanism is physical attraction since the E values for all tested temperatures are lower than 8 kJ/mol. The highest $Q_{m(D\text{-}R)}$ was found at 75 °C with a value of 12.13 mg/g, which was similar to the result obtained using Langmuir isotherm. The effect of temperature previously studied also provides similar results where the temperature of 75 °C gives the highest SG removal rate compared to the other tested temperatures.

Table 3
Isotherm parameters of SG adsorption onto CFP-based NCC surface.

Isotherm	Parameters	Temperature (K)		
		338	348	358
Langmuir	$Q_{m(L)}$ (mg/g)	12.50	12.93	11.24
	K_L (L/mg)	0.11	0.16	0.26
	r^2	0.8587	0.8580	0.7039
	χ^2	0.2329	0.2865	0.2487
Freundlich	K_F ((mg/g) $(L/mg)^{1/n}$)	5.59	6.48	7.31
	1/n	0.16	0.03	0.09
	r^2	0.8408	0.7986	0.6079
	χ^2	0.2624	0.4064	0.3293
Dubinin-Radushkevich	$Q_{m(D\text{-}R)}$ (mg/g)	11.58	12.13	10.86
	E (kJ/mol)	0.18	0.25	0.29
	r^2	0.8094	0.8387	0.7555
	χ^2	0.3147	0.3254	0.2053

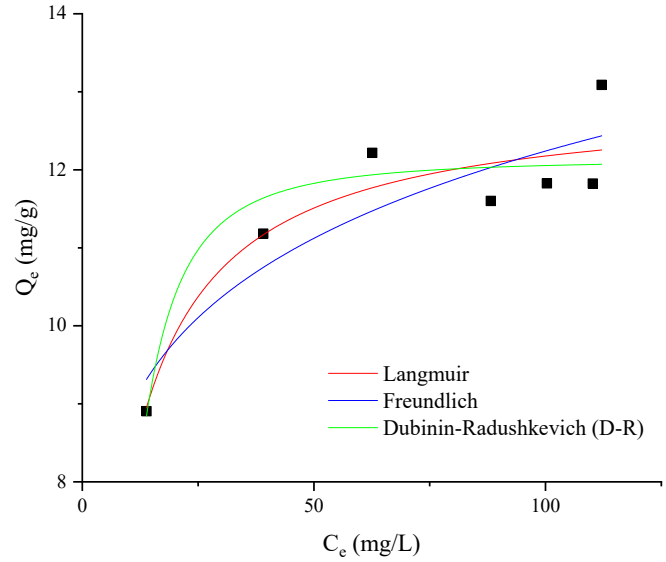

Fig. 6. The modelled isotherm profiles for the adsorption of SG to CFP-based NCC surface (temperature = 75 °C, mass ratio of CFP-based NCC to PO-B100 = 1:50, time = 1 h, agitation speed = 250 rpm).

The correlation coefficient (r^2) and chi-square (χ^2) values of the three isotherms are also listed in Table 3. It could be concluded that the adsorption of SG onto the CFP-based NCC surface is best fitted to the Langmuir isotherm equation under the temperature range studied. Based on the three isotherm models studied, the adsorption mechanism is predicted to be driven by both physical and chemical sorption due to its sorption energy value and endothermic nature, respectively. The overall results of this study showed that NCC has a particular affinity for SG and is an effective adsorbent for SG removal from PO-B100.

Table 4 listed the thermodynamics parameters of the SG adsorption onto the surface of NCC, such as Gibbs free energy change (ΔG°), enthalpy (ΔH°) and entropy (ΔS°). The values of Gibbs free energy (ΔG°) for the adsorption of SG were negative at all tested temperatures. These values confirm the spontaneous nature of SG adsorption onto the CFP-based NCC. Enhancement of the ΔG° value along with the increasing temperature implies that the affinity of SG on CFP-based NCC was higher at high temperature. Positive ΔH° value (42.90 kJ/mol) verifies that the adsorption is indeed an endothermic process, while the absolute value of ΔS° (219.80 J/mol.K) reflects the increased randomness at the solid-solution interface during the adsorption process [37,43].

3.5. Adsorption mechanism study

The study of the adsorption mechanism was used to further illustrate the interaction between SG and CFP-based NCC surface. Two important points have to be considered to understand the

Table 4
Thermodynamic parameters of adsorption of SG onto CFP-based NCC surface.

Temperature (K)	Thermodynamic parameters		
	ΔG° (kJ/mol)	ΔH° (kJ/mol)	ΔS° (J/mol.K)
338	−31.44	42.90	219.80
348	−33.46		
358	−35.84		

mechanism, namely the surface properties of the adsorbent and the structure of adsorbate. The NCC molecule was constructed by a substantial number of hydrogen bonds between glucose units or glucose chains inside the molecule to form a very stable structure [44,45]. NCC contains the majority of oxygen functional groups such as hydroxyl, ether, and sulfonate. While the hydroxyl and ether groups are originally present in the cellulosic material, the sulfonate group existed due to the acid hydrolysis to produce NCC. On the other hand, SG was built by a steryl cation (SC^+) and a glucose unit, with a positive charge on the cationic steryl part.

According to the findings of this study, the adsorption was temperature-dependent and the isotherm modeling showed an equal contribution of physical attraction and chemical binding. Therefore, the mechanism of SG removal by adsorption on the CFP-based NCC surface may be presumed to involve these following steps:

- Migration of SG from the bulk of PO-B100 to the CFP-based NCC surface
- Diffusion of SG through the boundary layer to the CFP-based NCC surface
- Adsorption of SG on the surface of CFP-based NCC, which may be caused by physical interaction of dipole-dipole coupling between the positively charged SC^+ and the negatively charged NCC surface as suggested in Fig. 7; and through a possible chemical binding mechanism of ion exchange as shown below:

$$NCC - OH \leftrightarrow NCC - O^- + H^+$$

$$NCC - SO_3^- \leftrightarrow NCC - SO_3^-$$

$$NCC - O^- + SC^+ \leftrightarrow NCC - O - SC$$

$$NCC - OH \leftrightarrow NCC - O^- + H^+$$

- Intraparticle diffusion of SG into the pores of CFP-based NCC

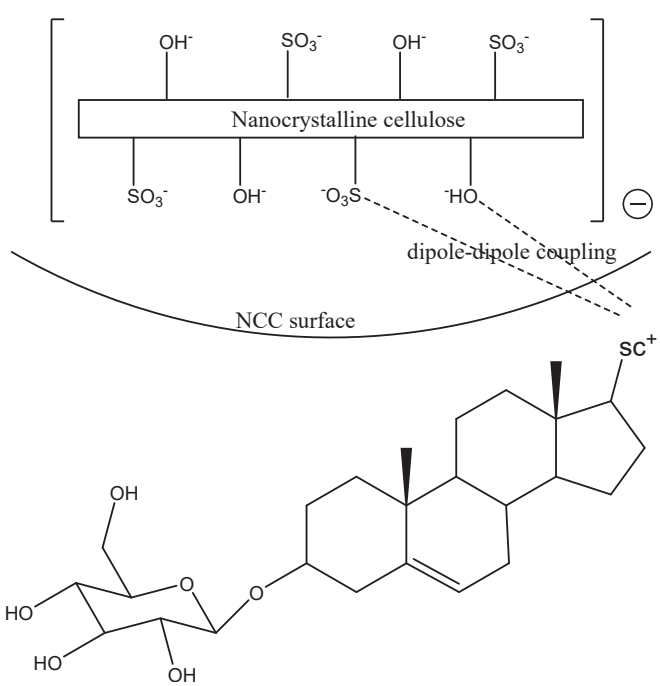

Fig. 7. Schematic representation of the proposed adsorption mechanism of SG onto CFP-based NCC surface.

4. Conclusions

CFP-based NCC was successfully used as an adsorbent for reducing SG in PO-B100. The content of SG was able to be reduced from 194.1 mg/kg to as low as 15.9 mg/kg (91.81% removal rate) within 1 h at the temperature of 75 °C using CFP-based NCC to PO-B100 mass ratio of 1:50. The study proved that CFP-based NCC has great affinity and selectivity to SG, particularly on the campesteryl glucoside and stigmasteryl glucoside. The adsorption treatment greatly improves the cold stability of PO-B100 by reducing the cloud point from 13.2 °C to 11.5 °C, while slightly affected the purity of FAME, AV and other minor components, such as MG, DG, and TG, which were still in the acceptable range according to ASTM D6751. The adsorption process was endothermic and may be driven by both physical attraction and chemical ion exchange. The adsorption treatment using CFP-based NCC should be a prospective method used to remove SG from PO-B100 since it possesses high efficiency, time-saving and energy-efficient.

Declaration of competing interest

The authors declare that they have no known competing financial interests or personal relationships that could have appeared to influence the work reported in this paper.

CRediT authorship contribution statement

Liangna Widdyaningsih: Conceptualization, Methodology, Investigation, Software, Writing - original draft. **Albert Setiawan:** Conceptualization, Methodology, Investigation, Software, Writing - original draft. **Shella Permatasari Santoso:** Conceptualization, Data curation, Supervision. **Felycia Edi Soetaredjo:** Resources, Visualization. **Suryadi Ismadji:** Resources, Validation. **Sandy Budi Hartono:** Software, Validation. **Yi-Hsu Ju:** Writing - review & editing. **Phuong Lan Tran-Nguyen:** Writing - review & editing. **Maria Yuliana:** Conceptualization, Resources, Visualization, Writing - review & editing, Supervision.

Acknowledgment

This work was supported by Widya Mandala Catholic University Surabaya, Indonesia, through research grant no. 0675/WM01/N/2019.

References

[1] N. Kumar, A. Sonthalia, H.S. Pali, Sidharth, Alternative Fuels for Diesel Engines: New Frontiers, Diesel Engines [Working Title], 2018, pp. 1–27, https://doi.org/10.5772/intechopen.80614.
[2] A.C. Pinto, L.L.N. Guarieiro, M.J.C. Rezende, N.M. Ribeiro, A. Ednildo, Biodiesel : An Overview, 16, 2005, pp. 1313–1330.
[3] Z. Qiu, L. Zhao, L. Weatherley, Process intensification technologies in continuous biodiesel production, Chem. Eng. Process. Process Intensif. 49 (2010) 323–330, https://doi.org/10.1016/j.cep.2010.03.005.
[4] Y.H. Ju, L.H. Huynh, Y.A. Tsigie, Q.P. Ho, Synthesis of biodiesel in subcritical water and methanol, Fuel 105 (2013) 266–271, https://doi.org/10.1016/j.fuel.2012.05.061.
[5] S. Thiruvenkadam, S. Izhar, Y. Hiroyuki, R. Harun, One-step microalgal biodiesel production from Chlorella pyrenoidosa using subcritical methanol extraction (SCM) technology, Biomass Bioenergy 120 (2019) 265–272, https://doi.org/10.1016/j.biombioe.2018.11.037.
[6] F.H. Santosa, L. Laysandra, F.E. Soetaredjo, S.P. Santoso, S. Ismadji, M. Yuliana, A facile noncatalytic methyl ester production from waste chicken tallow using single step subcritical methanol: optimization study, Int. J. Energy Res. 43 (2019) 8852–8863, https://doi.org/10.1002/er.4844.
[7] M. Aghilinategh, M. Barati, M. Hamadanian, Supercritical methanol for one put biodiesel production from chlorella vulgaris microalgae in the presence of CaO/TiO 2 nano-photocatalyst and subcritical water, Biomass Bioenergy 123 (2019) 34–40, https://doi.org/10.1016/j.biombioe.2019.02.011.
[8] L.K. Ong, C. Effendi, A. Kurniawan, C.X. Lin, X.S. Zhao, S. Ismadji, Optimization

of catalyst-free production of biodiesel from Ceiba pentandra (kapok) oil with high free fatty acid contents, Energy 57 (2013) 615–623, https://doi.org/10.1016/j.energy.2013.05.069.
[9] M.K. Lam, K.T. Lee, A.R. Mohamed, Homogeneous, heterogeneous and enzymatic catalysis for transesterification of high free fatty acid oil (waste cooking oil) to biodiesel: a review, Biotechnol. Adv. 28 (2010) 500–518, https://doi.org/10.1016/j.biotechadv.2010.03.002.
[10] L.P. Christopher, Hemanathan Kumar, V.P. Zambare, Enzymatic biodiesel: challenges and opportunities, Appl. Energy 119 (2014) 497–520, https://doi.org/10.1016/j.apenergy.2014.01.017.
[11] B. Likozar, A. Pohar, J. Levec, Transesterification of oil to biodiesel in a continuous tubular reactor with static mixers: modelling reaction kinetics, mass transfer, scale-up and optimization considering fatty acid composition, Fuel Process. Technol. 142 (2016) 326–336, https://doi.org/10.1016/j.fuproc.2015.10.035.
[12] I. Lee, L.M. Pfalzgraf, G.B. Poppe, E. Powers, T. Haines, The role of sterol glucosides on filter plugging, Biodiesel Mag 4 (2007) 105–112.
[13] V. Van Hoed, N. Zyaykina, W. De Greyt, J. Maes, R. Verhé, K. Demeestere, Identification and occurrence of steryl glucosides in palm and soy biodiesel, JAOCS, J. Am. Oil Chem. Soc. 85 (2008) 701–709, https://doi.org/10.1007/s11746-008-1263-5.
[14] R.A. Moreau, K.M. Scott, M.J. Haas, The identification and quantification of steryl glucosides in precipitates from commercial biodiesel, JAOCS, J. Am. Oil Chem. Soc. 85 (2008) 761–770, https://doi.org/10.1007/s11746-008-1264-4.
[15] H. Tang, S.O. Salley, K.Y. Simon Ng, Fuel properties and precipitate formation at low temperature in soy-, cottonseed-, and poultry fat-based biodiesel blends, Fuel 87 (2008) 3006–3017, https://doi.org/10.1016/j.fuel.2008.04.030.
[16] D. Na-Ranong, P. Laungthaleongpong, S. Khambung, Removal of steryl glucosides in palm oil based biodiesel using magnesium silicate and bleaching earth, Fuel 143 (2015) 229–235, https://doi.org/10.1016/j.fuel.2014.11.049.
[17] A. Aguirre, S. Peiru, F. Eberhardt, L. Vetcher, R. Cabrera, H.G. Menzella, Enzymatic hydrolysis of steryl glucosides, major contaminants of vegetable oil-derived biodiesel, Appl. Microbiol. Biotechnol. 98 (2014) 4033–4040, https://doi.org/10.1007/s00253-013-5345-4.
[18] S. Peiru, A. Aguirre, F. Eberhardt, M. Braia, R. Cabrera, H.G. Menzella, An industrial scale process for the enzymatic removal of steryl glucosides from biodiesel, Biotechnol. Biofuels 8 (2015), https://doi.org/10.1186/s13068-015-0405-x.
[19] A.Y. Tremblay, A. Montpetit, The in-process removal of sterol glycosides by ultrafiltration in biodiesel production, Biofuel Res. J. 4 (2017) 559–564, https://doi.org/10.18331/brj2017.4.1.6.
[20] M.Y. Chang, R.S. Juang, Adsorption of tannic acid, humic acid, and dyes from water using the composite of chitosan and activated clay, J. Colloid Interface Sci. 278 (2004) 18–25, https://doi.org/10.1016/j.jcis.2004.05.029.
[21] A.G. Varghese, S.A. Paul, M.S. Latha, Green Adsorbents for Pollutant Removal, 2018, https://doi.org/10.1007/978-3-319-92111-2.
[22] M. Börjesson, G. Westman, Crystalline nanocellulose — preparation, modification, and properties, Cellul. - Fundam. Asp. Curr. Trends. (2015), https://doi.org/10.5772/61899.
[23] H. Voisin, L. Bergström, P. Liu, A. Mathew, Nanocellulose-based materials for water purification, Nanomaterials 7 (2017) 57, https://doi.org/10.3390/nano7030057.
[24] H. Liang, X. Hu, A quick review of the applications of nano crystalline cellulose in wastewater treatment, J. Bioresour. Bioprod. (2016) 199–204, 2016, www.Bioresources-Bioproducts.com.
[25] J.N. Putro, S.P. Santoso, S. Ismadji, Y.H. Ju, Investigation of heavy metal adsorption in binary system by nanocrystalline cellulose – bentonite nanocomposite: improvement on extended Langmuir isotherm model, Microporous Mesoporous Mater. 246 (2017) 166–177, https://doi.org/10.1016/j.micromeso.2017.03.032.
[26] L. Segal, J.J. Creely, A.E. Martin, C.M. Conrad, An empirical method for estimating the degree of crystallinity of native cellulose using the X-ray diffractometer, Textil. Res. J. 29 (1959) 786–794, https://doi.org/10.1177/004051755902901003.
[27] L. Nyström, Occurrence and Properties of Steryl Ferulates and Glycosides in Wheat and Rye, University of Helsinki, 2007.
[28] L.B.D.C. Araújo, S.L. Silva, M.A.M. Galvão, M.R.A. Ferreira, E.L. Araújo, K.P. Randau, L.A.L. Soares, Total phytosterol content in drug materials and extracts from roots of Acanthospermum hispidum by UV-VIS spectrophotometry, Brazilian J. Pharmacogn. 23 (2013) 736–742, https://doi.org/10.1590/S0102-695X2013000500004.
[29] M.N.A.M. Taib, W.A. Yehye, N.M. Julkapli, Influence of crosslinking density on antioxidant nanocellulose in bio-degradation and mechanical properties of nitrile rubber composites, Fibers Polym. 20 (2019) 165–176, https://doi.org/10.1007/s12221-019-8575-y.
[30] Y. Hu, L. Tang, Q. Lu, S. Wang, X. Chen, B. Huang, Preparation of cellulose nanocrystals and carboxylated cellulose nanocrystals from borer powder of bamboo, Cellulose 21 (2014) 1611–1618, https://doi.org/10.1007/s10570-014-0236-0.
[31] A. Alemdar, M. Sain, Isolation and characterization of nanofibers from agricultural residues - wheat straw and soy hulls, Bioresour. Technol. 99 (2008) 1664–1671, https://doi.org/10.1016/j.biortech.2007.04.029.
[32] X.F. Sun, F. Xu, R.C. Sun, P. Fowler, M.S. Baird, Characteristics of degraded cellulose obtained from steam-exploded wheat straw, Carbohydr. Res. 340 (2005) 97–106, https://doi.org/10.1016/j.carres.2004.10.022.
[33] H. Wang, H. Tang, S. Salley, K.Y. Simon Ng, Analysis of sterol glycosides in biodiesel and biodiesel precipitates, JAOCS, J. Am. Oil Chem. Soc. 87 (2010) 215–221, https://doi.org/10.1007/s11746-009-1489-x.
[34] N.A. Negm, M.T.H. Abou Kana, M.A. Youssif, M.Y. Mohamed, Biofuels from Vegetable Oils as Alternative Fuels: Advantages and disadvantages, 2017, https://doi.org/10.1201/b20780.
[35] A. Khodabandehloo, A. Rahbar-Kelishami, H. Shayesteh, Methylene blue removal using Salix babylonica (Weeping willow) leaves powder as a low-cost biosorbent in batch mode: kinetic, equilibrium, and thermodynamic studies, J. Mol. Liq. 244 (2017) 540–548, https://doi.org/10.1016/j.molliq.2017.08.108.
[36] H.J. Lee, H.S. Lee, J. Seo, Y.H. Kang, W. Kim, T.H.K. Kang, State-of-the-art of cellulose nanocrystals and optimal method for their dispersion for construction-related applications, Appl. Sci. 9 (2019) 1–14, https://doi.org/10.3390/app9030426.
[37] S. Chowdhury, R. Mishra, P. Saha, P. Kushwaha, Adsorption thermodynamics, kinetics and isosteric heat of adsorption of malachite green onto chemically modified rice husk, Desalination 265 (2011) 159–168, https://doi.org/10.1016/j.desal.2010.07.047.
[38] H. More, Factors Affecting Adsorption. https://hemantmore.org.in/science/chemistry/factors-affecting-adsorption/13094/, 2018 accessed May 5, 2019.
[39] M. Mohapatra, S. Khatun, S. Anand, Kinetics and thermodynamics of lead (II) adsorption on lateritic nickel ores of Indian origin, Chem. Eng. J. 155 (2009) 184–190, https://doi.org/10.1016/j.cej.2009.07.035.
[40] A. de Sá, A.S. Abreu, I. Moura, A.V. Machado, Polymeric Materials for Metal Sorption from Hydric Resources, Elsevier Inc., 2017, https://doi.org/10.1016/b978-0-12-804300-4.00008-3.
[41] C.S. Zhu, L.P. Wang, W. bin Chen, Removal of Cu(II) from aqueous solution by agricultural by-product: peanut hull, J. Hazard Mater. 168 (2009) 739–746, https://doi.org/10.1016/j.jhazmat.2009.02.085.
[42] Q. Li, L. Chai, Z. Yang, Q. Wang, Kinetics and thermodynamics of Pb(II) adsorption onto modified spent grain from aqueous solutions, Appl. Surf. Sci. 255 (2009) 4298–4303, https://doi.org/10.1016/j.apsusc.2008.11.024.
[43] Y. Liu, Y.J. Liu, Biosorption isotherms, kinetics and thermodynamics, Separ. Purif. Technol. 61 (2008) 229–242, https://doi.org/10.1016/j.seppur.2007.10.002.
[44] Y. Habibi, L.A. Lucia, O.J. Rojas, Cellulose nanocrystals: chemistry, self-assembly, and applications, Chem. Rev. 110 (2010) 3479–3500, https://doi.org/10.1021/cr900339w.
[45] Y. Liu, D. Ying, L. Sanguansri, Y. Cai, X. Le, Adsorption of catechin onto cellulose and its mechanism study: kinetic models, characterization and molecular simulation, Food Res. Int. 112 (2018) 225–232, https://doi.org/10.1016/j.foodres.2018.06.044.